2013

Control by Vegetation Disturbance on Gully Rejuvenation Following Wildfire

Kevin Hyde
The University of Montana

CONTROL BY VEGETATION DISTURBANCE ON GULLY REJUVENATION FOLLOWING WILDFIRE

By

KEVIN DAVID HYDE

Master of Arts, The University of Montana, Missoula, MT, 2003
Bachelor of Arts, Bard College, Annandale-on-Hudson, NY, 1980

Dissertation

presented in partial fulfillment of the requirements
for the degree of

Doctor of Philosophy
in Forestry and Conservation, Ecosystem and Conservation Science

The University of Montana
Missoula, MT

June 2013

Approved by:

Sandy Ross, Associate Dean
The Graduate School

Ronald Wakimoto, Co-Chair
Department of Ecosystem and Conservation Science

Kelsey Jencso, Co-Chair
Department of Forest Management

Andrew Wilcox, Co-Chair
Department of Geosciences

Susan Cannon
US Geological Survey

Carl Seielstad
Department of Forest Management

ABSTRACT OF DISSERTATION

Hyde, Kevin D., Ph.D., Spring 2013 Forestry and Conservation

Control by Vegetation Disturbance on Gully Rejuvenation Following Wildfire

Co-Chairperson: Ronald Wakimoto

Co-Chairperson: Kelsey Jencso

Co-Chairperson: Andrew Wilcox

Gully rejuvenation (GR) following wildfire influences landform evolution and generates flooding and debris that alters aquatic habitat and threatens human activities. Fire severity, defined as the degree of vegetation loss by wildfire, is a hypothesized control on this erosion response. I investigated three related aspects of the relationship between fire severity and GR: The capacity of vegetation disturbance to explain the occurrence or non-occurrence of GR; the spatial structure of burn mosaics relative to post-fire erosion; and the relationship between fire severity and threshold conditions required for channel initiation. I surveyed 269 burned catchments and mapped 111 cases of GR across sites in Montana and Idaho. I created the Vegetation Disturbance Index (VDI) derived from LANDSAT images to quantify fire severity and implemented geospatial and statistical analysis to quantify relationships between VDI and post-fire erosion response. Vegetation disturbance strongly explained GR with additional influences from upslope geometry and pre-fire shrub cover. As fire severity increased, the percent of the catchment area covered by continuous patches of high severity burn increased non-linearly. Trends in patch structure defined a threshold of fire severity after which the probability of GR was strongly correlated with the development of large, continuous severely burned patches. Fire severity systematically influenced the relationship between source area and steepness. Threshold conditions for channel initiation, specifically source area steepness and curvature, decreased as vegetation disturbance increased. These results provide inferential evidence that vegetation disturbance exerts first-order controls over post-fire erosion processes. The results of the patch-pattern analysis suggest that progressive loss of vegetation due to wildfire leads to critical thresholds of hydrologic connectivity after which runoff and erosion accelerate. The source area analysis suggests that forces of convergent flow are not fully expressed until a significant proportion of vegetation has been consumed such that flow resistance is minimized. The VDI as a continuous metric of vegetation disturbance may contribute to improved quantitative analysis of landform evolution relative to vegetation disturbance, ecological effects of fire, and ecosystem response to climate change. The assessment methodology outlined herein provides a first step towards a systematic quantification of the potential for GR following wildfire.

ACKNOWLEDGEMENTS

A host of individuals made this work possible. My committee spurred my curiosity, forged my thinking, and challenged me to realize my potential as a researcher and scholar. I value the unique guidance each member provided and appreciate how everyone adapted to the unexpected. A private donor funded my fieldwork, a gift that also provided an unequivocal vote of confidence during a critical period of this journey. My grad school buddy, colleague, and spiritual sister, Karin Riley, and I wandered burned areas together, grew ideas and discussed papers over weekly breakfasts, and encouraged each other to see our degrees through. Jon Graham patiently provided advice on statistical analysis and generous discussion with Monica Turner improved the methods for the burn mosaic analysis. Countless personnel from the US Forest Service, many of them colleagues and friends, provided information about the post-fire events, helped me gain access into remote areas, and kept this research relevant. Special mention goes to Pete Robichaud for his insights and probing questions, Kevin Ryan for helping me understand the importance of research for the public good, and Dave Calkin for his indirect support in any ways. To a person, the Forest Service folks are among the finest individuals with whom I have worked throughout my career. My field assistants, Ian Hyde, Morgan Hyde, and Max Smith helped to keep me focused and safe as we bushwhacked through burned areas encountering warm bear sign, fresh cat tracks near camp, and the report of wolf pups in the areas we approached. They were troopers! The partnership and love of Virginia Clarke nurtured the personal resolve and internal focus through which this document emerged. For these contributions and many more I am deeply grateful. I carry your gifts forward as I look to the new challenge, to apply this degree with purpose.

DEDICATION

In memory of Scott Woods

and

To ET

Absence of proof is not proof of absence

TABLE OF CONTENTS

CHAPTER 1: INTRODUCTION

Gully rejuvenation commonly follows wildfire throughout the Western US (Cannon et al., 2003; Cannon et al., 2008; Gartner et al., 2008). The elemental importance of vegetation controls over erosion (Kirkby, 1995; Yetemen et al., 2010) and the role of vegetation disturbance in changing hydrogeomorphic response following fire are well recognized (Shakesby and Doerr, 2006; Moody et al., 2009; Cawson et al., 2012). However, the study of vegetation factors contributing to post-fire erosion is limited. Gully rejuvenation (GR) is the reactivation of channel incision some time after a gully forms and stabilizes (Hyde et al., 2007, sensu Horton, 1945). The term captures the cyclical nature of gully formation through channel initiation and incision processes and refill over time (Bull and Kirkby, 1997) driven by wildfire and other disturbance processes (Pierce et al., 2004). Debris flows and sediment laden-flows associated with GR scour ephemeral mountain channels and may transport large volumes of sediments including boulders and woody debris into valleys and streams systems downslope. The physical and ecological effects of hydrogeomorphic responses (including a spectrum of runoff to sediment-laden flows to debris flows) coupled with human vulnerability (Wisner et al., 2004) drive the need for understanding causal mechanisms and processes contributing to post-fire hydrogeomorphic responses and to incorporate these into predictive systems (Folke, 2006).

Fire severity, the degree of vegetation loss from wildfire (Keeley, 2009), is a critical determinant of the occurrence of erosion after wildfire (Lavee et al., 1995;

Shakesby and Doerr, 2006; Cannon et al., 2010; Parise and Cannon, 2011). Burned area reflectance classification (BARC) (RSAC, 2009) mapping can be used for broad-scale assessment of fire severity derived from remote-sensed imagery based on the differenced normalized burn ratio (dNBR) (Key and Benson, 2001). The dNBR algorithm has been shown to effectively measure fire severity and is most accurate when applied to forested areas (Epting et al., 2005; Chafer, 2008). The application of satellite imagery to assess fire effects holds untapped potential to study process relationships between vegetation disturbance and physical landscape response (Kremens and Smith, 2010; Reinhardt et al., 2010).

The spatial arrangement of burned areas exerts control over runoff response and influences post-fire geomorphic processes (Kutiel et al., 1995; Beeson et al., 2001; Hyde et al., 2007; Moody et al., 2007). The concept of hydrologic connectivity provides a framework for broad-scale integration of the patch-patterns resulting from wildfire and thresholds for hydrologic response within runoff dominated geomorphic systems (Pringle, 2003; Bracken and Croke, 2007; James and Roulet, 2007). Large, continuous patches without vegetation, such as those created by wildfire, present an opportunity for uninterrupted accumulation of overland flow, increasing the potential for rill formation and gully initiation (Lavee et al., 1995; Arnau-Rosalén et al., 2008). However, no studies have been conducted to quantify the spatial structure of burn mosaics relative to observed erosion response over broad scales. Interactions between vegetation and intense wildfire and other disturbance processes have been assumed to lead to non-

linear increases in connectivity of bare patches and are thought to lower the threshold conditions for accelerated erosion response (Davenport et al., 1998; Allen, 2007; Peters et al., 2007), although the basis for these assumptions is not clear.

The source area within first-order catchments is a region of elevated susceptibility to channel initiation (Sidle et al., 1985) where the typical concave form creates a zone of converging flow (Willgoose et al., 1991), focusing runoff into the catchment hollow. Source areas (to keep the nomenclature consistent) around gully heads are especially vulnerable to change in vegetative cover, and relatively minor changes in surface resistance may substantially alter threshold conditions that lead to channelization (Dietrich et al., 1992; Lesschen et al., 2007). The relationship between the severity of vegetation disturbance and threshold conditions for channel initiation within source areas is poorly understood.

Slope steepness and source areas above channel heads often exhibit an inverse relationship (Montgomery and Dietrich, 1988; Tarboton et al., 1992; Tucker and Bras, 1998) expressed in the form of a power function: $S = kA^{-\theta}$. The terms k and θ implicitly combine the effects of lithology, soils, climate, and vegetation on channel initiation processes (Yetemen et al., 2010). Although vegetation disturbance may destabilize or change the traditionally conceived slope-area relationship and channelization thresholds, vegetation is typically not considered in these analyses. However, the degree of vegetation removal may impact the either the slope or the area required for gully rejuvenation (Dietrich and Dunne, 1993; Vandekerckhove et al., 1998; Hancock and

Evans, 2006)., and sediment yield likely increases with decreasing cover (Hooke, 2000). Curvature, another factor influencing channel initiation, quantifies topographic convexity or concavity, where hillslope form either tends to concentrate or dissipate flow (Zevenbergen and Thorne, 1987; Schmidt et al., 2003; Gutiérrez-Jurado and Vivoni, 2013). Few studies have addressed curvature relative to channel initiation thresholds.

1.1 Study objectives

The research presented in this dissertation investigates the relationships between fire severity and post-fire erosion response. I pursued three primary objectives:

1. Quantify the capacity of vegetation disturbance to explain the occurrence or non-occurrence of GR following wildfire
2. Describe and quantify relationships between the spatial structure of burn mosaics and post-fire erosion
3. Evaluate relationships between fire severity and threshold conditions for channel initiation

To address the first objective I asked the question: Why does GR occur in some burned catchments and not others? I tested the hypothesis that the magnitude of vegetation disturbance is the dominant landscape variable explaining GR and demonstrated the integration of spatially continuous fire severity mapping with other continuous landscape metrics that quantify topography and extent of pre-fire vegetation.

Evaluation of the second objective consisted of three components; describe differences in the spatial structure of burn mosaics over a continuous range of fire severity; quantify the relationship between the spatial structure of burn mosaics and the probability of gully rejuvenation; and test for differences in the spatial structure of burn mosaics between catchments in which gully rejuvenation did and did not occur.

Addressing the third objective, I hypothesized that the level of fire severity affects the location of the channel head by reducing the threshold conditions that result in channel initiation. Specifically, I expected that the combination of source area and its steepness that control the location of the onset of channel incision decreases as vegetation disturbance increases. I also expect that GR occurs with lower source area curvature where fire consumed more vegetation.

1.2 Research overview

The approach for all three investigations within this dissertation combines field survey, geospatial and statistical analysis. I surveyed five burned areas in Montana and Idaho, inventoried 269 low-order catchments, and identified 111 cases of gully rejuvenation, and mapped 99 gully heads. Working in a GIS I compiled the field data, digital terrain models, pre-fire vegetation, and fire severity maps. I quantified fire severity using a metric derived from the BARC maps called the Vegetation Disturbance Index (VDI). To meet the first objective, I used binary logistic regression using the presence or absence of GR as the response variable regressed against fire severity and a select suite of landscape metrics chosen for their expected relevance to post-fire erosion.

Binary logistic regression analysis produced a probability of GR as a function of VDI, data that I carried over into the second phase of the investigation. In the second investigation I employed landscape pattern indices to quantify and compare the abundance and connectivity of patches at different fire severities within catchment burn mosaics. I evaluated these metrics against the probability of GR and compiled illustrations to describe and compare patterns of burn mosaics over the range of fire severity where GR occurred. Segmented plotting methods were used to identify potential process thresholds. In the third phase, I evaluated changes in the slope-area and curvature-area of the source areas above gully heads relative to progressive fire severity levels. LiDAR topographic data were used for the curvature analysis. I used multivariate analysis of variance (MANOVA) to I quantify the effects of fire severity on slope-area relationships.

This dissertation is organized around the three lines of inquiry described above with one chapter devoted to each investigation. The chapters are organized in the form of journal papers, each with separate sections describing background and relevant literature, methods, results, and discussion. All referenced material is compiled into single reference section. A series of appendices present data collected in the course of this research and other important supplementary materials.

CHAPTER 2: VEGETATION DISTURBANCE AS A FIRST-ORDER CONTROL OF GULLY REJUVENATION FOLLOWING FIRE[1]

Abstract

High intensity rainfall often causes gully rejuvenation (GR) following wildfire. Current research emphasizes that the effect of fire on soil physical properties is the primary control of post-fire erosion processes, while the effects of vegetation disturbance by fire on channel initiation thresholds remains largely unexplored. We conducted geospatial analysis combining satellite data of vegetation change and morphologic variables expected to influence channel stability and the occurrence of GR. We surveyed 269 first-order catchments at five Northern Rockies sites and identified 111 occurrences of GR. We quantified fire severity using the Vegetation Disturbance Index (VDI), a continuous metric based upon Burned Area Reflectance Classification (BARC) maps derived from satellite imagery. Binary logistic regression revealed stronger correlation between the occurrence of GR and vegetation disturbance than catchment morphology or pre-fire vegetation variables. However, addition of measures of catchment elongation and pre-fire shrub cover led to increased predictive power. A classification model built from these predictor variables produced statistically robust power to discriminate between catchments where GR did and did not occur (model accuracy = 0.74, AUC = 0.79). A model using VDI alone also discriminated very well (model accuracy = 0.71, AUC = 0.77) and we used the fitted regression model to predict the probability of GR

[1] The coauthors for the planned journal submission are Andrew Wilcox, Kelsey Jencso, and Scott Woods.

based solely on vegetation disturbance. Our findings demonstrate the role of vegetation change by fire as a first-order control of the occurrence of post-fire erosion. Further, our findings suggest that major erosion will occur in response to fire consumption of above ground biomass, and is relatively independent of fire effects on physical properties of soils. Other geologic and local conditions strongly influence the occurrence of GR and thus should be considered in assessments of severe erosion potential following fires. Additional work is needed to link remotely-sensed measures of vegetation disturbance to the specific physical processes controlling runoff generation and flow accumulation. The VDI as a spatially continuous metric of vegetation disturbance readily combines with other continuous landscape metrics and may contribute to improved quantitative analysis of landform evolution, ecological effects of fire, and ecosystem response to climate change.

2.1 Introduction

Extreme erosion in the form of gully rejuvenation following wildfire often generates debris flows and sediment-laden floods in mountainous terrain (Meyer et al., 2001; Conedera et al., 2003; McDaniel, 2007; Cannon et al., 2010). Fire related gully rejuvenation strongly influences landform evolution (Benda et al., 2003; Roering and Gerber, 2005; Shakesby and Doerr, 2006; Stock and Dietrich, 2006) and supplies the majority of sediment introduced into mountain stream systems of the Western United States (Pierce et al., 2004; Santi et al., 2008; Frechette and Meyer, 2009; Moody and Martin, 2009a). High energy sediment fluxes and floods alter channel morphology and

aquatic habitat (Gresswell, 1999; Zelt and Wohl, 2004; Burton, 2005) and threaten human activities. The physical and ecological effects of fire coupled with human vulnerability (Wisner et al., 2004) contribute to the need for improved understanding of the causal mechanisms and processes that contribute to post-fire debris flows and their incorporation within predictive models (Folke, 2006).

The term "gully rejuvenation" (GR), the reactivation of channel incision some time after a gully forms and stabilizes (Hyde et al., 2007, sensu Horton, 1945), captures the cyclical nature of gully formation and refill over time (Bull and Kirkby, 1997) driven by wildfire and other disturbance processes (Pierce et al., 2004). Gully erosion occurs where rainfall delivery exceeds infiltration capacity generating overland flow that concentrates and removes soil in a narrow path, often forming deep incisions (Poesen et al., 2003) (Figure 1). Major erosion events resulting from overland flow generally do not occur in stable forests with intact vegetation (Prosser and Williams, 1998; Moody and Martin, 2002; Wondzell and King, 2003; Jenkins et al., 2011). While elemental importance of vegetation controls over erosion (Kirkby, 1995; Yetemen et al., 2010) and the role of vegetation disturbance in changing hydrologic response following fire are well recognized (Shakesby and Doerr, 2006; Moody et al., 2009; Cawson et al., 2012), the primary cause of post-fire erosion is most commonly attributed to changes in soils properties caused by fire (e.g., Cerda and Robichaud, 2009; Doerr et al., 2009; Shakesby, 2011). A limited number of empirical studies evaluated vegetation factors directly contributing to post-fire erosion (Kutiel et al., 1995; Lavee et al., 1995; Benavides-Solorio

and MacDonald, 2001; Hanshaw et al., 2009; Larsen et al., 2009; Stoof et al., 2012). Further work is needed to understand and integrate multiple factors controlling GR following wildfire including vegetation disturbance, physical changes to soils, topography, rainfall drivers, and other factors (Bull and Kirkby, 1997; Hancock and Evans, 2010; Yetemen et al., 2010; Eustace et al., 2011; Luca et al., 2011). Such studies must be integrated over broad-scales in order to account for the interactions between transport processes as influenced by hillslope-channel linkages and the catchment connectivity (Wainwright et al., 2006). Identifying why gully erosion occurs in some burned catchments and not in others may lead to a process-based understanding of post-fire gully erosion processes. This knowledge may help develop predictive models of gully erosion that can be used in post-fire hazard assessment and prediction of erosion potential before fire occurs.

Scaling from plot level to landscape level analysis poses major challenges to post-fire erosion studies (Ebel et al., 2012). However, burned area reflectance classification (BARC) (RSAC, 2009) mapping provides broad-scale assessment of fire severity derived from remote-sensed imagery. The differenced normalized brightness range dNBR algorithm has been used to construct BARC maps (Key and Benson, 2006) and effectively measures fire effects and is considered to be most accurate in forested areas (Epting et al., 2005; Hudak et al., 2007; Chafer, 2008). BARC maps correlate strongly with fire-caused change in vegetation, especially forest canopy in Montana (Hudak et al.,

2007) and have been interpreted to measure vegetation change associated with post-fire debris flows (Gartner et al., 2008; Cannon et al., 2010).

The study presented here extends the work of Hyde et al. (2007) who limited their analysis of fire severity and gully rejuvenation to two areas (also used in this study) located 29km apart. This study adds three new areas representing other physiographic settings in Montana and Idaho and adds observations across a wider range of fire severities with intent to improve generalization of results across broader spatial scales. Further, this study utilizes the full-scale BARC with values from 0 to 255 to quantify fire severity whereas the prior study relied on modifications of BARC data classified into four bins.

The main purpose of this study was to evaluate the influences of vegetation disturbance, landscape morphology, and pre-fire vegetation on the occurrence of GR following fire. A second objective was to demonstrate the use of the full-scale measure of fire effects in the BARC maps with spatially and numerically continuous measures of other landscape characteristics as a means to conduct integrated broad-scale analysis. The primary research question was: Why does GR occur in some burned catchments and not others? We tested the hypothesis that the magnitude of vegetation disturbance is the dominant landscape variable explaining the occurrence of GR.

2.2 Regional Setting, Study Areas, and Rainfall Events

We studied five areas in Montana and Idaho in the Northern Rocky Mountains (Figure 2) that have experienced recent fire and post-fire GR events. The study areas

were defined by drainage divides and major stream channels within the broader burned areas. The Sleeping Child (SC) and Laird Creek (LC) study areas burned as part of the Bitterroot Complex Fire in 2000, Rooks Creek (RC) and Warm Springs (WS) within the Castle Rock Fire during 2007, and the Cascade (CS) area during the Cascade fire in 2008. Rainfall-triggered flooding and debris flows were reported in the SC and LC areas in July 2001 and during June and July 2009 in the CS, RC, and WS. We conducted field work in SC and LC during 2001-2003 and in CS, RC, and WS from 2009-2011.

The hydrology across the five study sites is primarily controlled by snowmelt runoff. Short-duration, high-intensity convective storms are common throughout the summer months. The average annual precipitation (1961-1990) for all sites is 700mm (WRCC, 2013) with influence from the plains rainfall regime from the east and sub-Pacific rainfall regime from the west (Moody and Martin, 2009a) (Figure 2). Mean elevation, parent geology, and soil texture vary between study areas (Table 1). All soils are friable loams or loamy sands with variable degrees of rocky materials. Prior to the fires, forest cover constituted the majority of the vegetation cover across all study areas and shrub cover occupied proportionally more landscape in LC, RC, and CS. Exposed, rocky areas account for 3% each of CS and WS (USDOI Geological Survey, 2009). Douglas fir (*Pseudotsuga menziesii)* covered over 60% of the forested landscapes in all but Cascade where lodgepole pine (*Pinus contorta*) and whitebark pine (*Pinus albicaulis*) were more common (45% and 31%, respectively).

2.2.1 Storm rainfall

Rainfall events associated with the GR events are reported here but not otherwise used directly in the analysis. Storm rainfall characteristics and distribution were assessed using local rain gage data and regional images from the Next Generation Radar (NEXRAD) weather system. The proximity to study areas of rain gages and NEXRAD stations varied substantially (Figure 3). The elevation of all gages fell below mean study area elevation (Table 1 and Table 3). Given expected rainfall increase with elevation from adiabatic cooling effects (Dingman, 2002) we expect that the gage data likely underestimates rainfall intensity at all sites. Three hour total precipitation data from the days surrounding the debris flow events were accessed through the Weather and Climate Toolkit (NOAA, 2012). While accuracy of NEXRAD rainfall intensity estimates depends on season, distance, and terrain (Smith et al., 1996), NEXRAD data have been deemed reliable confirmation of the spatial distribution of heavy rainfall events, especially for purposes of assessing landslide hazards (Wieczorek et al., 2001; Tiranti et al., 2008). We consider the NEXRAD data sufficient to verify general distribution and timing of rainfall events that triggered GR, although none of the rainfall data are sufficient to support conclusions about intensity levels relative to erosion thresholds (e.g. Cannon et al., 2008; Coe et al., 2008).

2.3 Methods

2.3.1 Catchment morphology, pre-fire vegetation, and fire severity

Boundaries of first-order catchments (Strahler, 1957) were manually delineated from 1:24K scale digital raster graphic, topographic maps and 10m resolution digital elevation models (DEM) (USDA, 2012) were processed to extract basin morphology metrics. We extracted the following morphometric and landscape summary variables for each catchment unit: area (hectares; HA), relief ratio (RR) (dimensionless), elongation ratio ER (dimensionless), pre-fire forest cover (FOR) (percent), and pre-fire shrub cover (SHB) (percent).

We calculated the RR, a measure of catchment steepness, as the ratio between source area relief (elevation difference between channel head and highest point in catchment) and length of longest catchment flow path. RR reflects advective processes associated with channel incision and development (Tarboton et al., 1992) and is similar to measuring local channel gradient (Montgomery and Dietrich, 1994). Cannon et al. (2001) used RR as the measure of source area slope in a study of slope-area thresholds for initiation of post-fire debris flows. The ER, a measure of catchment shape, was calculated as the ratio of the diameter of a circle with area equal to actual catchment area to the catchment length measured along the longest flow path. ER reflects dynamics of converging flows (Benda et al., 2004).

Pre-fire vegetation influences fire severity and post-fire erosion by controlling fire behavior and accumulation of erodible sediments since last fire (Jenkins et al., 2011).

To account for this potential variability we quantified pre-fire vegetation characteristics using 30m resolution GIS layers of existing vegetation cover (EVC) and existing vegetation type (EVT) (USDOI Geological Survey, 2009). The vegetation layers were resampled to 10m resolution using cubic interpolation to match the 10m DEM data.

We defined fire severity as the degree of vegetation loss from wildfire (Keeley, 2009) and measured severity using the vegetation disturbance index (VDI). The VDI metric use the full spectrum of values from the BARC image and increasing VDI values is interpreted to indicate increased vegetation loss. The VDI is calculated in the GIS as the mean BARC value, is interpreted as the mean spatial fire severity, and permits direct comparison of fire severity across source areas. The 30m resolution BARC 256 image (MTBS, 2012) was interpolated using cubic convolution to the 10m DEM data. We conducted sensitivity analysis to determine the effect of rescaling the BARC data found that the VDI values were virtually identical between the original 30m and the 10m re-sampled data ($R2 \geq 0.99$, ($p << 0.001$). Table 2 summarizes by study area the mean catchment value of the five metrics used in the analysis.

2.3.2 Field mapping of gully rejuvenation

To identify GR events, we surveyed valley bottoms for debris fans at the mouth of catchments and then surveyed catchment channels to locate gully heads. We define the occurrence of GR as a continuous incision (greater than 10m in length) into the soil B horizon originating at a gully head. Gully heads consistently occurred as a distinct transition from gentle u-shaped rill morphology with fine root hairs (< 2-3mm) to an

abrupt, vertical drop (Figure 1). The incision typically cut through all soil horizons to depths of tens of centimeters to over one meter, terminating in cobbles or boulders, often to bedrock. Only coarse roots greater than 1.5-2.0 cm remained within gully heads. We surveyed all catchments within the 5 areas, identified 269 study unit catchments, and recorded 111 cases of GR. The absence of vegetation growing on debris fans or within incised channels indicated that all cases of GR were recent and fire related. We mapped all field locations using a Trimble Juno SB global positioning system device (median horizontal precision of 2.9m). Inaccessible areas of SC were assessed through interpretation of geo-rectified 1:4200 scale aerial photography acquired in 2001. Three second-order catchments were accepted as study units in CS where first-order units could not be safely accessed due to bedrock exposures and highly steepened hillslopes.

2.3.3 Data analysis

We used binary logistic regression (BLR) (Hosmer and Lemeshow, 2000) to create classification models that test the explanatory power of the VDI, pre-fire vegetation, and morphometric variables for the occurrence of GR. The binary response variable was channel incision status, GR or NoGR. Our approach is similar to methods used by Luca et al. (2011) in determining susceptibility to gullying in South Italy. BLR analysis was implemented using the R statistical software (R Core Team, 2013), guided by code and methods developed by Rossiter and Loza (2011). First we tested for covariance between variables to identify possible covarying pairs which could lead to unstable model results and recognized that FOR and SHB (r=-0.90) could not be used in

the same BLR model (Hosmer and Lemeshow, 2000). We tested individual variables and then used the variable with the strongest explanatory power to compare response between study areas. Bi-directional, step-wise elimination was used to identify secondary metrics which were added to the base model if they significantly improved explanatory power. Finally, we developed models using minimal variables to reduce possibility of over-fitting models. We selected models based on the p-value of the z-score, Akaike information criterion (AIC) (Akaike, 1974), and McKelvey-Zavoina pseudo R^2 (McKelvey and Zavoina, 1975), as recommended by (DeMaris, 2002). We evaluated model goodness-of-fit guided by Hosmer and Lemeshow (2000) and Bradley (1997), using sensitivity (% GR correctly predicted), specificity (% NoGR correctly predicted), accuracy (% overall correct predictions), Matthew's correlation coefficient (MCC) (Matthews, 1975) and the receiver operator characteristics (ROC) curve with the associated area under curve (AUC) metric (Bradley, 1997). MCC ranges from -1 to +1; where +1 represents perfect predictive power, 0 indicates predictive power no better than random, and -1 indicates complete disagreement between predicted and observed. AUC expresses the probability that the classification model will correctly assign a higher probability of GR to randomly chosen cases of GR versus NoGR.

2.3.4 Analysis of classification exceptions

To further understand physical and process differences between GR and NoGR catchments, we used statistical tests and reviewed field and GIS observations to evaluate model classification errors. We used student's t-tests to assess false negative

classifications, where GR occurred but was not predicted, and false positive classifications, where the model predicted GR in catchments where no incision occurred. On review of observations we identified patterns associated with classification errors and grouped these by similar phenomena.

2.4 Results

2.4.1 GR relative to Fire severity

Highest overall fire severity occurred in SC (VDI = 193), with the lowest severity occurring in CS (VDI = 123). LC, RC, and WS experienced (VDI = 155, 155 and 162, respectively) (Figure 4). GR occurred in 111 (41%) of 269 catchments surveyed (Table 4). Relative to fire severity, a disproportionally high number of catchments experienced GR in CS (54%) with disproportionally fewer in RC (23%). Based on the gully head form (Figure 1, panel B) all observed gullies showed evidence of initiation by infiltration excess overland flow leading to concentrated runoff and erosion. We found no evidence of subsurface saturation induced failure in any catchment where the gully head was mapped. The frequency of GR generally increased with increasing VDI for all catchments and by individual study areas. All but eight cases of GR occurred where catchment VDI exceeded 135 (Figure 5 and Figure 6). One cases occurred in LC (VDI = 113) and seven occurred in CS (VDI 71-117).

2.4.2 Binary logistic regression model

For the full data set (N=269), fire severity (VDI) alone significantly explained the occurrence of GR (MZ $pR^2 = 0.28$, $p<<0.001$) and was positively correlated with increased

probability of GR. All other variables modeled individually provided no explanatory power (Table 5). Comparing between study areas, fire severity significantly explained GR in all study areas (MZ pR^2 from 0.40 to 0.57, $p \leq 0.01$) except CS. Fire severity alone provided weak explanation for GR events in CS (MZ $pR^2 = 0.14$, $p=0.07$). The results of forward selection regression guided a piecewise build of a final parsimonious model. The final model including fire severity, catchment elongation, and percent pre-fire shrub explained GR better than fire severity alone (MZ $pR^2 = 0.35$, $p<<0.001$; AIC = 305 using VDI alone dropping to AIC = 298 for the three variable model). The contribution of catchment elongation influenced GR more than pre-fire shrub cover ($p=0.009$ v. $p = 0.07$). Both catchment elongation and pre-fire shrub were negatively correlated with the probability of GR. The probability of GR derived from the BLR analysis increased non-linearly with increasing fire severity (Figure 6) and decreased somewhat with greater catchment roundness and to lesser degree with higher percentage of pre-fire shrub cover (Table 5).

The three models in the final model development provided comparable overall accuracy (0.71 to 0.74) and very good power to discriminate (Hosmer and Lemeshow, 2000) between cases of GR versus NoGR (AUC = 0.77 to <0.79) (Table 6 and Figure 7). All models more accurately identified stable catchments where GR did not occur than where GR did occur. Accounting for catchment elongation improved the ability of the model to correctly identify catchments where NoGR occurred (specificity increases from 0.80 to 0.84) and improved general predictive power (MCC from 0.39 to 0.43) with a

small improvement to discrimination power (AUC from 0.77 to 0.79). Accounting for percent shrub cover improved correct identification of catchments where GR occurred (sensitivity from 0.57 to 0.63) with reduced accuracy with identifying NoGR catchments. Predictive power including percent pre-fire shrub increased most strongly compared to other model configurations (MCC increased to 0.46) yet overall discrimination did not change compared to adding elongation alone. The equation for the predictive model using fire severity alone and including all data (N=269) is:

$$P(GR) = \frac{1}{1 + e^{-(-4.269 + 0.022\,\boldsymbol{VDI})}}$$

The equation for the final three variable model is:

$$P(GR) = \frac{1}{1 + e^{-(-2.375 + 0.024\,\boldsymbol{VDI} - 4.175\,\boldsymbol{ER} - 0.012\,\boldsymbol{SHB})}}$$

2.4.3 Exceptions to predictions rendered from classification model

The classification model produced 40 false positive predictions and 29 false negative predictions in the final model including elongation and percent shrub (Table 6). Visual assessment of catchment maps and review of field observations revealed distinct patterns associated with each group. Three landscape conditions were associated with false positive model predictions, cases of relatively high VDI with no GR. First, six un-gullied yet severely burned catchments (VDI from 203 – 255) where the model predicted GR were teardrop shaped. Anomalously narrow catchment heads tapered upslope to a sharp point in contrast to generally broader catchment heads common to most other catchments where high severity burn accompanied GR. Second, the spatial arrangement

of the burn mosaic also appeared to be a factor associated with false predictions in four catchments with moderate fire severity (VDI from 180 – 203). Areas of severe burn were concentrated low in the catchment. Third, in the channels of six catchments burned at high fire severity where no GR occurred (two in SC (VDI = 225, 255) and four in LC (VDI from 182 - 227)) we also observed dense riparian vegetation associated with mid-channel seeps.

We discovered two patterns with false negative cases. GR occurred in 20 of 29 catchments with overall lower fire severity (VDI from 151 – 193, mean = 175) where GR was not predicted but where areas of higher fire severity were concentrated in the upper catchment. Seven cases of GR were associated with evidence of fire-hose effect (Larsen et al., 2006; Coe et al., 2008) where gullying occurred very low in the catchment below bedrock nick points 3-5 meters high drained from areas with generally low to moderate fire effects (VDI from 96-137, mean = 121) (Figure 8). All but one of these cases were in CS. In general, throughout the CS study area we observed heavily armored headwaters with minimal exposed soil where trees grew through spaces between boulders and cobbles. In one sub-section of CS, no GR was associated with a forested area burned severely on steep, boulder-covered slopes above extensive paleo-landslide deposits.

T-tests for the difference of means of the five study variables revealed other common characteristics of misclassified catchments (Table 7). Where GR occurred but was not predicted (false negative cases) overall fire severity was lower and the catchments were steeper. Areas of false negative catchments were also significantly

smaller. Catchments with false positive predictions were somewhat less elongated than catchments where NoGR was correctly predicted.

2.5 Discussion

2.5.1 Vegetation and morphologic control of GR following wildfire

Our results suggest that vegetation disturbance exerts a first-order control over GR following wildfire. Aggregating all observations (N=269) and comparing between all study areas, the occurrence of GR increased with increasing fire severity and GR became less frequent under lower fire severity (Table 4 and Figure 5). This relationship was consistent across diverse landscape and catchment conditions (Table 1 and Table 2) and under uncertain rainfall intensities (Table 3 and Figure 3). The logistic regression analysis identified vegetation disturbance as the only variable to independently explain GR compared to using any other variable (Table 5). Fire effects on vegetation provided very good power to discriminate between where GR did and did not occur (AUC=0.77, Table 6). While adding two other variables, catchment elongation and percent pre-fire shrub, improved the predictive performance (AUC=0.79) but this increase in discrimination power was only improved by 2%. For the factors considered in our study, vegetation disturbance was the primary control over the occurrence of post-fire GR.

The logistic regression analysis generated an estimate of the probability of GR occurrence based on vegetation disturbance (Figure 6). The non-linear form of the probability curve suggests a process threshold consistent with the characterization of hydrogeomorphic response of burned forested presented by Moody and Martin (2009b),

who relate response thresholds to several factors including changes to vegetation density. Further, our finding of accelerated probability of GR with increased vegetation disturbance provides empirical support of Peters et al. (2004) and Phillips (2003); small perturbations in landscape conditions may amplify non-linearly across scales into very large, catastrophic system responses. Our findings may be related to prior indications that large runoff and erosion responses may cascade from changes in the vertical vegetation structure and patch-pattern relationships of vegetation mosaics in burned and unburned environments (Boer and Puigdefábregas, 2005; Ludwig et al., 2005; Lesschen et al., 2009). We suggest that the non-linear form of the probability curve in this study is consistent with the broader understanding of threshold behavior in gully initiation processes (Dietrich et al., 1992; Bull and Kirkby, 1997).

In addition to vegetation disturbance as a first-order control on GR, we also found that catchment elongation and percent pre-fire shrub cover can contribute to the occurrence or non-occurrence of GR. Evidence of these secondary factors highlights the complexity of these systems and need to identify local and regional patterns that influence post-fire erosion response. Improved model performance where considering catchment elongation (ER negatively correlated with occurrence of GR, Table 5) suggests that relatively rounder catchments are more likely to remain stable. We expect this to relate to the mechanics of converging flows in the upper catchment extent (Benda et al., 2004) (Figure 1) and exceedance conditions for channel incision though the processes of this phenomena are not clear and require further investigation. The negative correlation

between GR and pre-fire shrub abundance suggests that biophysical conditions associated with shrub environments inhibit the potential for gully incision relative to forested conditions. Shrub cover provides low overall erosion protection (Abrahams et al., 1994) and we suggest that this results in less material to erode following fire and conditions generally less prone to severe erosion response.

The combined results of the t-tests and review of GIS and field observations added five additional factors associated with the occurrence or non-occurrence of GR that were not accounted for in the statistical modeling; narrow catchment heads, location of severe burn within the catchment, mid-channel seeps, fire-hose effects, and catchment steepness. Narrow catchment heads were identified in six severely burned catchments where GR did not occur. The relationship between size of contributing area and channel initiation (Dietrich and Dunne, 1993) suggests that narrow catchment head morphology may not provide sufficient contributing area to initiate gully incision even under severe burn conditions.

The location of severely burned areas was associated with both false negative and false positive predictions but was more prevalent where GR occurred in overall low fire severity catchments and the severe burn was concentrated at the upper catchment extent. The sensitivity of source areas above channels to vegetation disturbance is well recognized (Dietrich et al., 1992; Lesschen et al., 2007; Collins and Bras, 2010) but we find no published empirical data to support these theories. The large number of cases (20 of 29) where false negative prediction was associated with high severity fire concentrated

in the upper catchments indicates the need for studies focusing on the sensitivity of runoff and sediment source areas (Dietrich and Dunne, 1993; Montgomery and Dietrich, 1994) to fire severity. The association between fire severity location and GR response raises the question of the relationship between structural connectivity (Bracken et al., 2013), patch-pattern processes (Turner, 1989; Ludwig et al., 2005; Puigdefábregas, 2005), and hydrologic connectivity (Pringle, 2003; Bracken and Croke, 2007) relative to burn mosaics. Pursuing these questions of spatial arrangement furthers previous work in linear relationships between fire effects and hillslope erosion (Moody et al., 2007) which also used BARC images to measure fire severity.

The unusual riparian conditions associated with severely burned areas where GR did not occur may reflect accelerated vegetation recovery that impeded overland flow continuity in a downslope direction. These conditions highlight the need to identify conditions that enhance vegetation recovery and increase thresholds for attenuating geomorphic response. All but one case (7 of 8) of GR associated with the fire-hose effect (Larsen et al., 2006; Coe et al., 2008) occurred in the CS study area in catchments with low overall fire severity where the model calculated very low probability of GR (<0.30). These cases correspond with other factors unique to CS; poor predictive power of vegetation disturbance in CS (Table 5), different dominant vegetation (Table 1), and heavily armored headwaters. We expect that the CS GR events associated with low fire severity occurred because fire reduced erosion thresholds that were already much lower due to prevalence of exposed bedrock and armored headwaters. These areas were

especially prone to severe erosion response under lower levels of vegetation disturbance. The fire-hose effect, in particular, was associated with especially steep drops near the valley floor (Figure 8) that fostered channel initiation. The anomalies of the CS study area emphasize the need to assess the influence of fire severity on erosion potential in the context of overall biophysical setting, especially local geology and underlying landform. Finally, false positive predictions in significantly steeper catchments (Table 7) suggest that gravity-driven increase in erosive forces were sufficient to overcome reduced flow resistance associated with lower vegetation disturbance, even in conjunction with smaller catchment areas.

The secondary factors identified in this study may be entirely local phenomena, however we expect many of these factors may be common across domains where severe erosion follows wildfire. It is likely that other important factors may be identified and warrant careful consideration where conducing assessments of the potential for GR after fire. Additionally, our analysis provides no clear indications of how any of these factors possibly interacted, though we expect interactions probably did occur at multiple spatial scales (Carlson and Doyle, 1999; Peters et al., 2004; Peters et al., 2007). The potential for interactions and probable relationship to non-linear geomorphic response (Phillips, 2003; Allen, 2007), specifically the non-linear probability of gully rejuvenation following fire (Figure 6), merits further study.

Given the inconsistent rainfall data available for this study (Figure 3), uncertainty about rainfall distribution and variability (Bracken et al., 2013) may provide

another reasonable explanation for false model predictions. Quite possibly, rainfall over severely burned catchments where no GR occurred was not sufficient to trigger GR. Conversely, exceptionally strong pockets of rainfall may have impacted catchments of lower overall severity where GR occurred. Uncertainty in rainfall duration and intensity may have introduced uncertainty in our analysis, yet the statistical robustness of our results between fire severity and GR lends confidence to our conclusions.

Our findings are consistent with Prosser and Williams (1998) who report that low to moderate severity burns produce minimal effect on erosion and that small, frequent storms produce large volumes of sediment only after the most severe fires. We attribute this accelerated erosion following high fire severity to loss of soil protection by ground vegetation and litter cover which substantially lowered the threshold conditions for sediment entrainment and transport by overland flow. Our findings also support the conclusion by Larsen et al. (2009) that vegetation disturbance may be a more significant predictor of severe erosion response than fire changes to soil. The evidence of secondary factors unrelated to soil properties that explain GR in our study areas supports findings of other studies of gully erosion not related to fire. Multiple factors, including morphology, lithology, vegetation, and rainfall regimes, more strongly predict potential for gully erosion than do soil conditions (Gutierrez et al., 2009; Eustace et al., 2011).

The findings of this study contradict Hancock and Evans (2010), who found no connection between gully morphology and chronic vegetation removal by fire in northern Australia. They postulate this reflects an equilibrium condition between fire

disturbance and erosion processes. Their study area experiences frequent fires and erosive rainfall with little time for sediment accumulation between fire events. Therefore the system may be supply limited. Jenkins et al. (2011) reinforce this explanation with their conclusion that the time elapsed since last fire erosion events influences the generation of post-fire debris flows. This reflects time for fuels to accumulate sufficiently to support a major fire and for sediments to build on hillslopes and accumulate in low-order channels under stable, vegetated conditions. Where fuel production outpaces sediment storage the conditions for severe erosion diminish. These relationships between vegetation development, fire frequency, and magnitude of post-fire erosion underscore the significance of interaction between biologic and physical controls on hydrogeomorphic response (Reinhardt et al., 2010) warrant further study.

2.5.2 Vegetation disturbance coupled to geomorphic response

We present a conceptual model of the sequence of events leading to overland flow and erosion following wildfire based upon the strong relationship between GR and vegetation disturbance by fire (Figure 9). Rainfall is the primary source of mass and energy input that drives the runoff and erosion response. Once rainfall occurs vegetation layers may intercept rainfall, attenuating energy and temporarily storing mass. At the ground surface the soil properties control bi-directional mass transfer and may further attenuate energy associated with rainfall delivery. When enough rainfall has accumulated due to infiltration excess overland flow may lead to surface erosion and the transport of water and sediment downslope. However, residual biomass may act to

attenuate overland flow energy and store some component of rainfall mass. As further illustrated in Figure 10, the loss of vegetation speeds the transfer of mass and energy to the soil surface, changing the time and force of rainfall delivery and the rates of mass and energy transfer once overland flow initiates. Depletion of sediment available for entrainment coupled with live vegetation losses reduces surface roughness and increases the rate at which additional unimpeded rainfall increases flow volume, further increasing runoff energy (Lavee et al., 1995; Prosser and Williams, 1998; Roering and Gerber, 2005).

Compared to this interpretation of vegetation controls, an emphasis on fire impacts to soils (e.g. Shakesby, 2011) only accounts for one component of this complex mass balance and energy transfer problem. Assuming uniform rainfall input, biomass loss alone may result in an accelerated rainfall delivery to the soil surface whereby a larger mass of rainfall impacts the soil surface over a shorter period of time, illustrated in the conceptual rainfall delivery hydrographs in Figure 10. Without a canopy, rainfall impacts the soil surface with greater energy and accumulates more rapidly. Emphasis on fire-induced changes to soils considers the fate of rainfall only once it reaches the soil surface and without explicitly quantifying how the consumption of vegetation by fire changes rainfall delivery rates and flow resistance once infiltration excess overland flow initiates.

We hypothesize that at some threshold of vegetation loss increases in rainfall delivery rates due to vegetation loss by fire overwhelm infiltration rates, independent of

changes to infiltration rates caused by fire. Findings from several studies lend support for this position. Larsen and others (2009) found that mechanical removal of ground cover produced runoff that was substantially the same as a slope of similar morphology where surface cover was removed by fire. In an unburned area, runoff generation occurred more rapidly with vegetation removal compared to removal of the "A" horizon where organic matter was expected to enhance infiltration and protect mineral soil below from erosion (Giordanengo et al., 2003). Hanshaw et al. (2009) compared rainfall delivery rates to the soil surface below unburned and burned chaparral canopy, and found that rainfall intensity and volume doubled or tripled under burned canopies. They did not relate the increase in rainfall intensities to local infiltration capacity. Work is needed to quantify timing and rainfall delivery changes associated with biomass consumption and to assess changes in rainfall delivery rates relative to changes in infiltration rates.

2.5.3 Implications of the VDI

We demonstrated use of the full scale BARC 256 image as a spatially continuous representation of wildfire disturbance. Further, we produced an estimate of the probability of GR (Figure 6) explicitly tied to an objective measure of fire severity using methods that can be systematically repeated in any environment and used to improve burned area assessments. Synoptic mapping of fire severity provides an effective framework through which to focus field surveys of burned areas and provides a spatial context with which to judge the significance of information acquired through ground

observation. Development and application of the VDI answers the need for implementation of a full scale fire severity metric (Kremens et al., 2010; Reinhardt et al., 2010). In the future the VDI metric may be integrated with other continuous scale landscapes metrics describing morphology, vegetation, geology, and other factors and potentially used to improve broad-scale, quantitative analysis within geographic information systems.

Realization of the potential for VDI applications will be contingent upon improved understanding of physical linkages between vegetation change and geomorphic process response. Additional effort is needed to refine understanding of physical vegetation attributes contained within the signal of BARC images (Hudak et al., 2007; Smith et al., 2007; De Santis et al., 2009). Work is also needed to understand the spatial structure of fire severity surfaces and burn mosaics within and between landscapes. This includes patterns within burn mosaics and gradients of change, both as functions of fire severity relative to fire and related processes (Smucker et al., 2005; Collins et al., 2007; Lozano et al., 2010). Finally, investigation of auto-correlations between fire severity measures with other biotic and abiotic landscape characteristics influencing fire severity, e.g. aspect (Marques and Mora, 1992; Holden et al., 2009) and dominant vegetation (Odion et al., 2004; Collins et al., 2007) may provide insight into process linkages between fire behavior and fire effects (Turner et al., 1994; Murray et al., 2008; Hyde et al., 2012).

As physical process linkages to satellite signals become better defined, the VDI as a metric of vegetation disturbance may help improve distributed, process models of hydrogeomorphic response and landscape evolution (e.g. Wigmosta et al., 1994; Collins et al., 2004; Istanbulluoglu and Bras, 2005a). These developments are especially important given the growing recognition of biologic controls in landscape evolution (Roering and Gerber, 2005; Marston, 2010; Reinhardt et al., 2010; Yetemen et al., 2010) in the context of need for better models of geomorphic transport processes and laws (Dietrich et al., 2003; Stock and Dietrich, 2006). The methods developed in this study to map fire severity may be useful for initial assessment of post-fire erosion potential where BARC or similar products are available immediately following wildfire. A GIS analyst can quantify fire severity across broad landscapes to prioritize a priori locations for risk assessment and field surveys. (Calkin et al., 2007; Calkin et al., 2011).

2.6 Conclusions

Fire severity measured by the continuous VDI metric strongly explains occurrence of GR following wildfire and supports the idea that vegetation disturbance exerts a first-order control on severe erosion following wildfire. Our predictions of GR occurrence improved with measures of catchment relief, elongation, and shrub cover. However, other geologic and local conditions strongly influence GR and need to be considered in post-fire assessments of severe erosion potential. Research is needed to quantify the role of biomass loss leading to accelerated runoff and erosion independent of fire effects on soil physical properties. Additional work is needed to link measures of

vegetation disturbance to physical processes including to refining the understanding of remote-sensed signals, analysis of fire severity patterns, and assessment spatial auto-correlation and covariance with other landscape metrics. The VDI as a continuous metric of vegetation disturbance may contribute to improved quantitative analysis and distributed modeling of landscape evolution and post-fire hazard assessment.

Tables

Table 1: Comparison between study areas of land area, elevation, parent geology, soil textures, and pre-fire existing vegetation types

Study Area	Area (ha)	Elevation Mean (m)	Parent Geology[1]	Soil texture[2] Primary / Secondary	Dominant Species[3] PSME[4]	PIAL[5]	PICO[6]
CS	150	2489	Cretaceous sedimentary Archean gneiss	extr. channery sandy loam gravelly sandy loam	13%	45%	31%
LC	2447	1812	Cretaceous granite	v. stony loamy sand gravelly sandy loam	63%	-	-
RC	464	2226	Paleozoic sedimentary	v. gravelly loam gravelly loam	69%	-	-
SC	1477	1801	mid-Proterozoic gneiss	stony loam extr. channery sandy loam	68%	-	15%
WS	173	2129	Paleozoic sedimentary	v. gravelly loam gravelly loam	76%	-	-

[1] Source: Reed Jr and Bush (2005); [2] Source: USDA NRCS Soil Survey Staff (); [3] Source: USDOI Geological Survey (2009), Existing vegetation type; [4] *Pseudotsuga menziesii* – Douglas-fir; [5] *Pinus albicaulis* – whitebark pine; [6] *Pinus contorta* – lodgepole pine

Table 2: Summary by study area of mean catchment value of the five metrics used in the binary linear regression analysis

Study Area	N	VDI	Area (ha)	Relief Ratio	Elongation Ratio	% Shrub Pre-fire
CS	35	131	25	0.42	0.50	19
LC	76	172	22	0.30	0.56	24
RC	44	157	7	0.38	0.53	33
SC	77	195	13	0.41	0.55	41
WS	37	157	3	0.49	0.48	12

Table 3: Summary of rainfall event data for each study area for known gully events

Study Area	Fire Year	Gully Event(s)	RAIN GAGE Max 1-hour Intensity mm h^{-1}	Gage Elevation (m)	NEXRAD Max 3hr Total Ppt mm
CS	2008	29 July 2009	28.7	1951	32.8
LC	2000	15, 20, 21 July 2001	8.0-14.0	1287 lower 1556 upper	5.1-31.8
RC	2007	June 2009 Multiple	10.2[a]	1795	1.2-5.1
SC	2000	15, 20, 21 July 2001	4.0-17.0	1417	12.7-19.1
WS	2007	June 2009 Multiple	10.2[a]	1795	2.5-12.7

[a] Recorded 20 Jun 2009 at Ketchum Ranger Station

Table 4: Summary of fire severity (VDI) and occurrence of GR by study area

Study Area	Overall VDI	VDI Range	Total Catchments	No GR	GR
CS	123	55-196	35	16 46%	19 54%
LC	155	64-250	76	50 66%	26 34%
RC	155	95-220	44	34 77%	10 23%
SC	193	63-255	77	37 48%	40 52%
WS	162	87-218	37	21 57%	16 43%
All	166	55- 255	269	158 59%	111 41%

Table 5: Summary of BLR results

Data	Variable	Est (β)	Exp(β)	Std.Err	z value	Pr(>|z|)	Sig	AIC	MZ pR^2
All Study Areas	*Int.*	-4.269	-	0.59	-7.18	<<0.001		305	0.284
	VDI	0.022	1.023	0.00	6.91	<<0.001	***		
	Int.	-0.245	-	0.16	0.16	0.131		367	0.007
	HA	-0.009	0.991	0.01	-1.14	0.253			
	Int.	-0.299	-	0.49	-0.60	0.546		368	0.000
	RR	-0.180	0.835	1.24	-0.15	0.884			
	Int.	0.782	-	0.73	1.08	0.281		365	0.013
	ER	-2.176	0.113	1.36	-1.60	0.109			
	Int.	-0.362	-	0.19	-1.93	0.054		368	0.000
	SHB	0.000	1.000	0.00	-0.04	0.966			
CS	*Int.*	-2.737	-	1.61	-1.70	0.089		NA	0.138
	VDI	0.022	1.023	0.01	1.84	0.066			
LC	*Int.*	-7.594	-	1.96	-3.87	<0.001		NA	0.574
	VDI	0.036	1.037	0.01	3.85	<0.001	***		
RC	*Int.*	-8.256	-	2.91	-2.83	0.005		NA	0.397
	VDI	0.042	1.043	0.02	2.57	0.010	*		
SC	*Int.*	-5.915	-	1.46	-4.04	<<0.001		NA	0.415
	VDI	0.030	1.030	0.01	4.20	<<0.001	***		
WS	*Int.*	-8.925	-	3.21	-2.78	0.006		NA	0.413
	VDI	0.054	1.056	0.02	2.74	0.006	**		
All Study Areas	*Int.*	-3.871		1.36	-2.85	0.004		299	0.366
	VDI	0.028	1.029	0.00	7.09	<<0.001	***		
	HA	0.012	1.012	0.01	1.29	0.198			
	RR	2.587	13.28	1.65	1.57	0.116			
	ER	-4.216	0.015	1.68	-2.50	0.012	*		
	SHB	0.012	1.012	0.01	-2.04	0.041	*		
Final Models	*Int.*	-4.269	-	0.59	-7.18	<<0.001		305	0.284
	VDI	0.022	1.023	0.00	6.91	<<0.001	***		
	Int.	-2.330	-	0.92	-2.53	0.011		299	0.326
	VDI	0.024	1.024	0.00	7.04	<<0.001	***		
	ER	-4.257	0.014	1.61	-2.64	0.008	**		
	Int.	-4.269	-	0.61	-7.04	<<0.001		303	0.309
	VDI	0.024	1.025	0.00	6.95	<<0.001	***		
	SHB	-0.012	0.988	0.01	-1.90	0.058	.		
	Int.	-2.375	-	0.92	-2.58	0.010		298	0.350
	VDI	0.026	1.026	0.00	7.08	<<0.001	***		
	ER	-4.175	0.015	1.60	-2.61	0.009	**		
	SHB	-0.012	0.988	0.01	-1.85	0.065	.		

[a] AIC is only relevant for comparison between models sing identical dependent variable data

Table 6: Summary of final models comparing classification accuracy and model discrimination power

Model	Observed		Predicted		TP	TN	FP	FN	Sens. (%TP)	Spec. (%TN)	Acc.	MCC	AUC
	GR	NoGR	GR	NoGR									
VDI	111	158	96	173	64	127	46	32	0.58	0.80	0.71	0.39	0.77
VDI ER	111	158	89	180	63	133	47	26	0.57	0.84	0.73	0.43	0.79
VDI ER SHB	111	158	99	170	70	130	40	29	0.63	0.82	0.74	0.46	0.79

Table 7: Summary of t-tests to evaluate differences in mean catchment characteristics between true and false predictions for catchments where GR occurred but was not predicted (FN) and where GR did not occur where predicted (FP)

	Metric	TP	FN	t Stat	p
GR	VDI	226	171	-11.9	<<0.001
	HA	14	9	-2.7	0.005
	RR	0.36	0.44	4.2	<<0.001
	ER	0.53	0.51	0.8	0.227
	FOR	64	69	0.9	0.186
	SHB	29	28	-0.34	0.369
		TN	**FP**		
NoGR	VDI	137	224	15.8	<<0.001
	HA	14	10	-1.6	0.054
	RR	0.39	0.36	-1.2	0.126
	ER	0.55	0.51	-2.0	0.025
	FOR	67	64	-0.5	0.298
	SHB	29	35	1.0	0.164

Figures

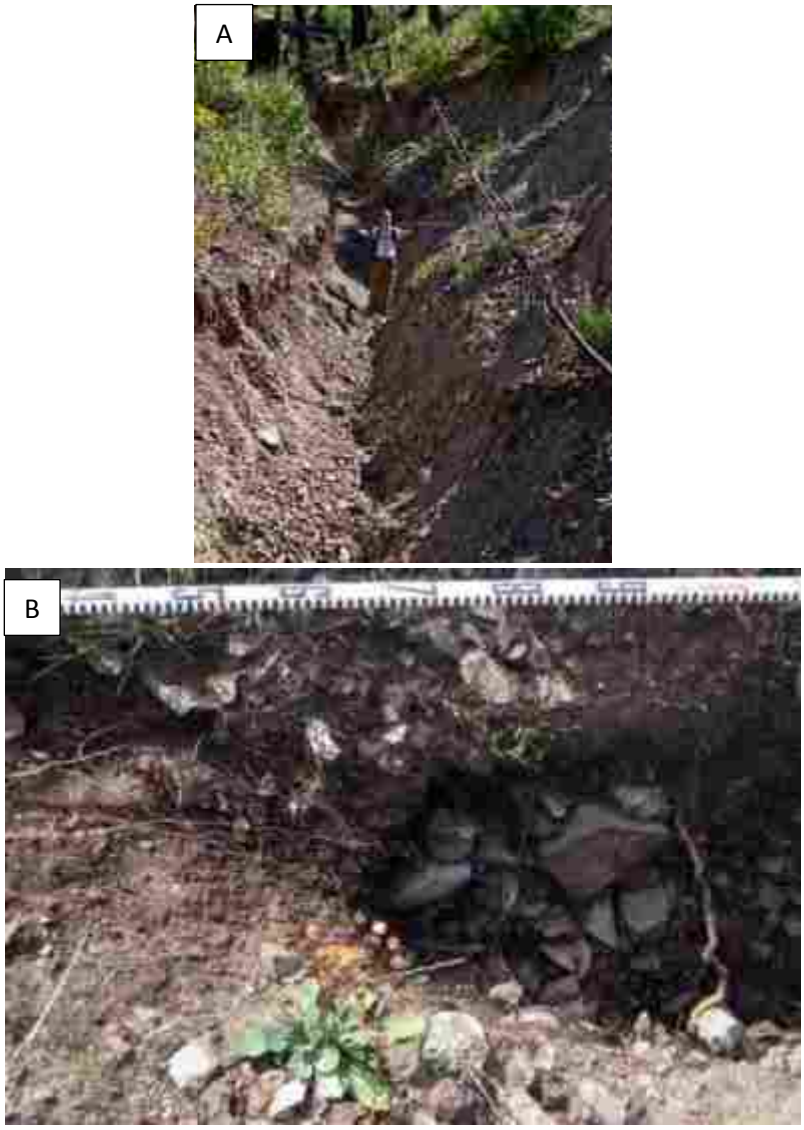

Figure 1: Panel A: Typical gully created by post-fire GR and debris flow with V-shape form and abrupt transition from hillslope to gully. Panel B: Typical gully head; arrow indicates direction of flow. Note fine root hairs in scoured rill above vertical incision into scoured area where only coarser roots remain.

Figure 2: Location of study areas within the Northern Rocky mountains – with precipitation regimes

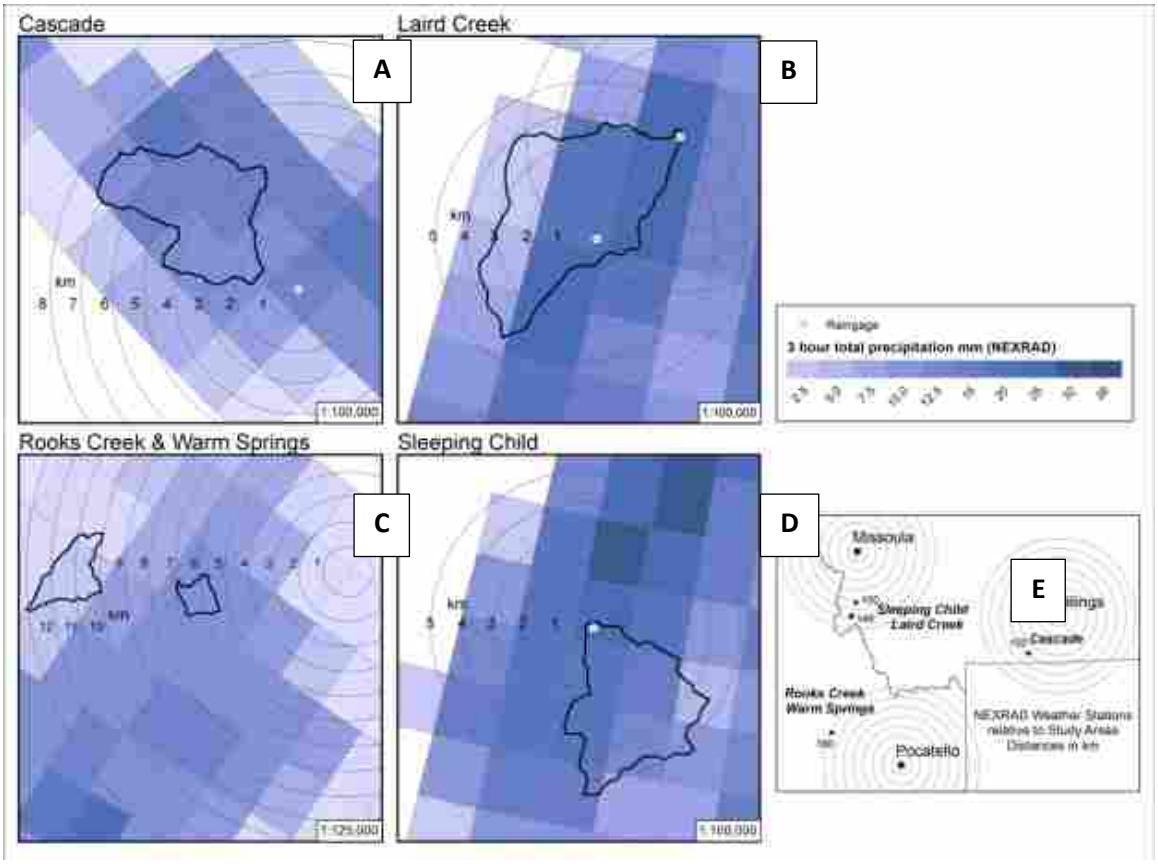

Figure 3: Panels A-D: Proximity of rain gages to study areas overlaid with NEXRAD storm rainfall images. Panel E: Proximity of NEXRAD stations to study areas

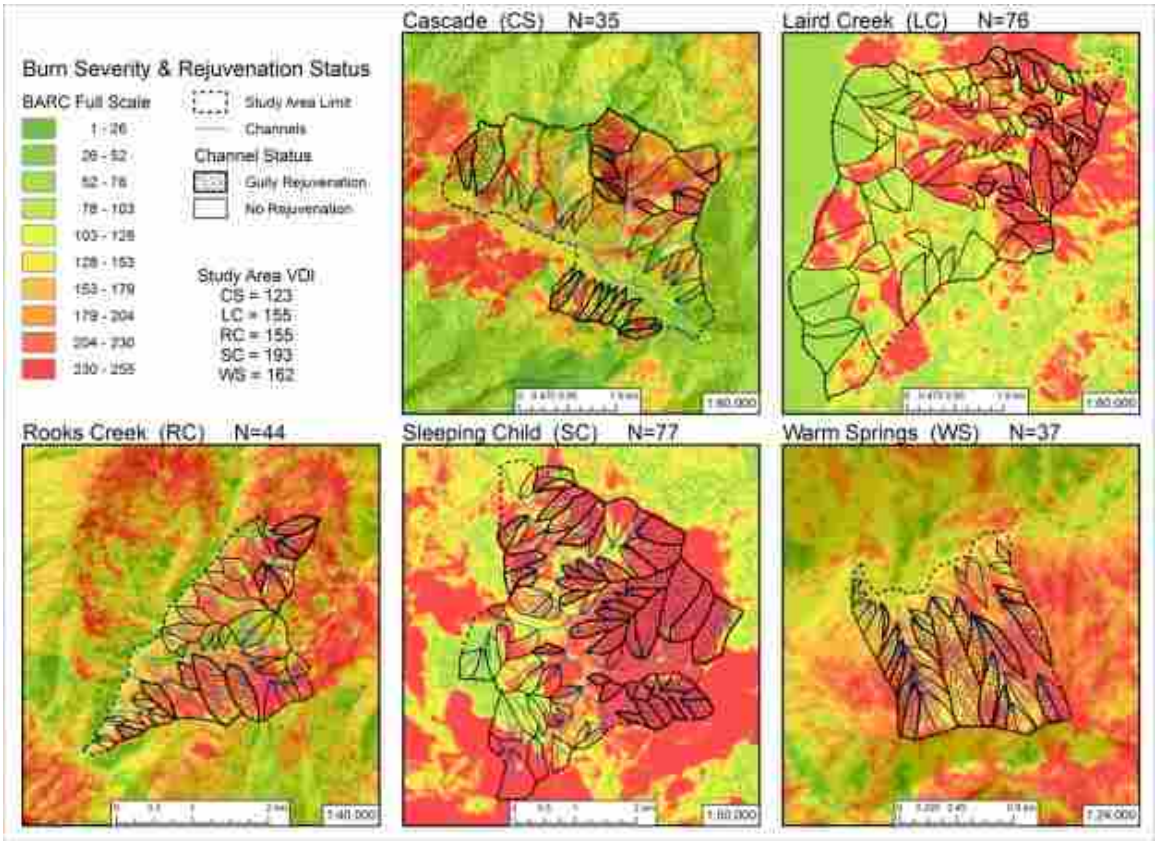

Figure 4: Maps of fire severity and overlay of study catchments with GR status for each study area

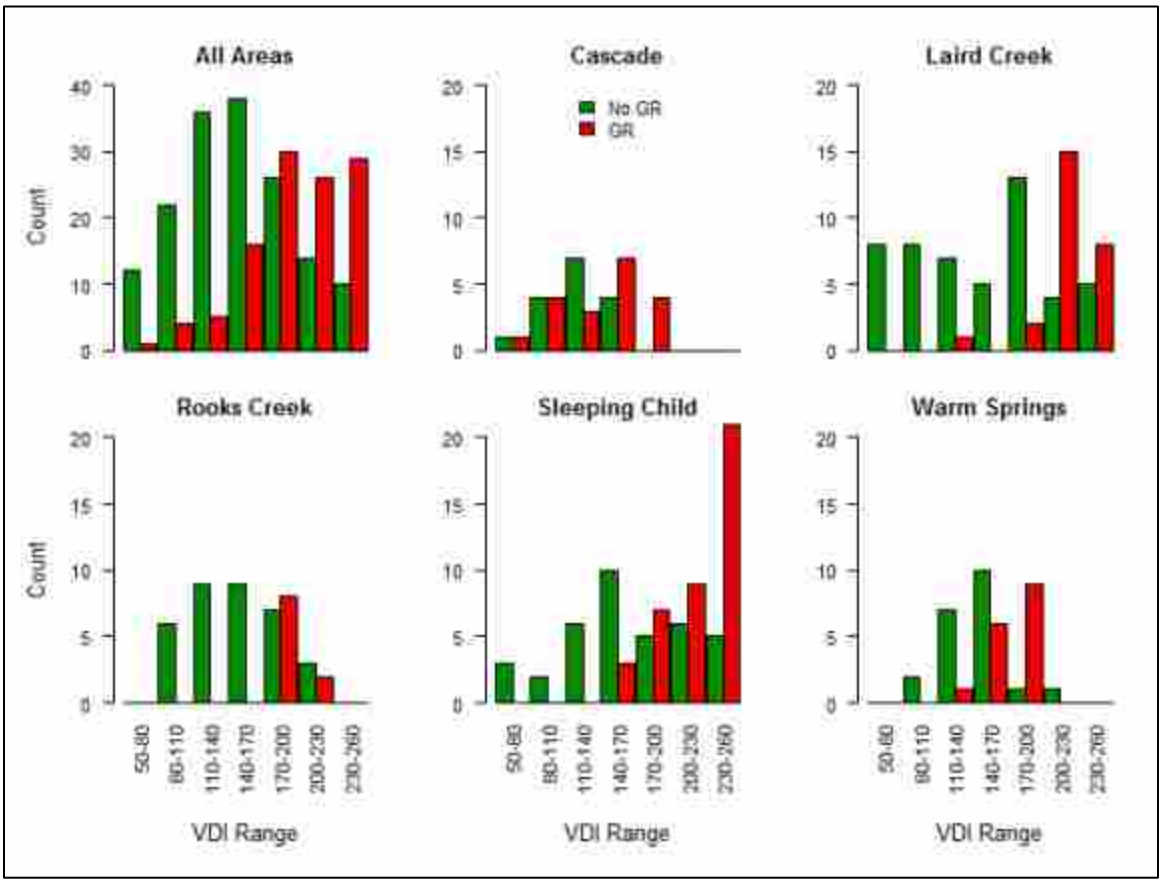

Figure 5: Bar charts showing cumulative frequency of GR versus GR as function of VDI for all catchments and each study area

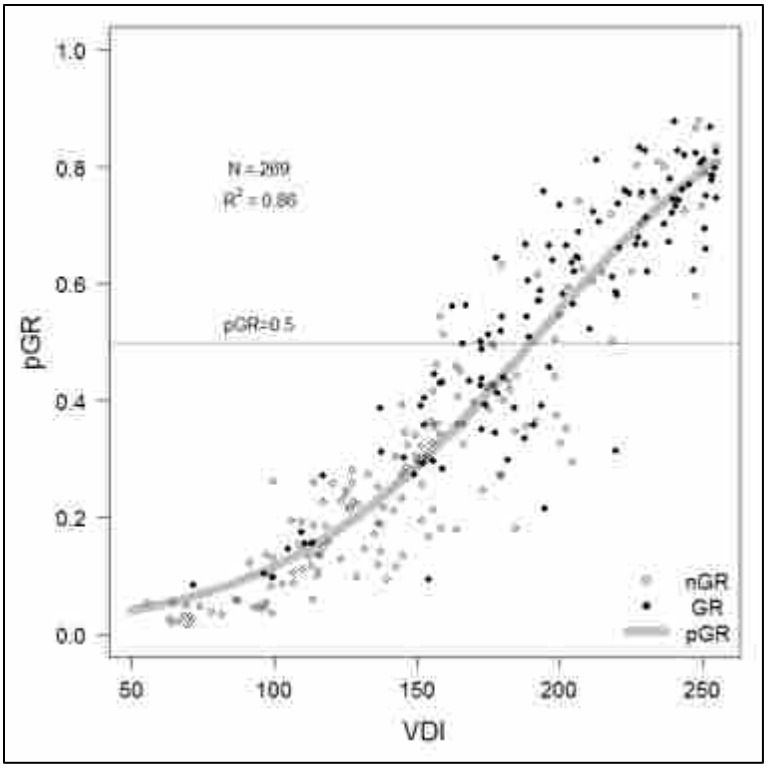

Figure 6: Plot illustrating non-linear increase in probability of GR occurrence (GR versus NoGR) as VDI increases. The s-shaped line shows the fitted probability of GR from BLR model using *only* VDI as the predictor variable. The scatter plotted points, P(GR) = *f*(VDI,ER,SHB), reflects the degree of unexplained variability after accounting for the effect of vegetation disturbance and before accounting for the effect of catchment elongation and pre-fire shrub in fitting the model.

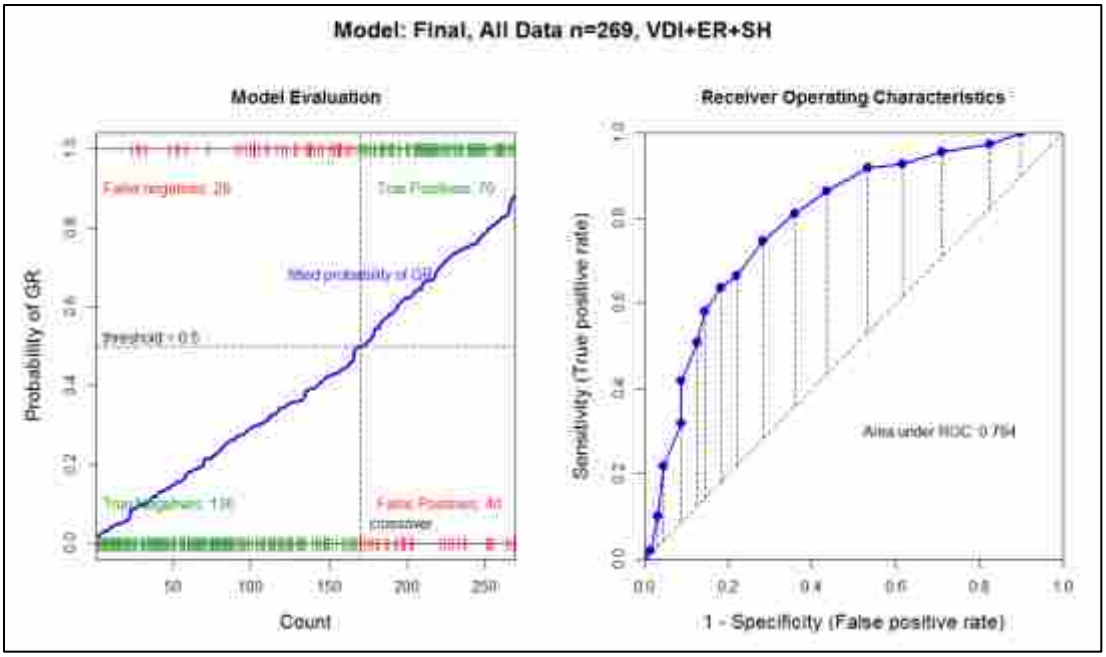

Figure 7: Evaluation and ROC curve for final, 3 variable model BLR model, P(GR) = *f*(VDI, ER, SHB), excluding CS catchments. Not that x-axis of "Model Evaluation" ordered count of observations and ***not*** VDI value. (Figure produced by logic and code from Rossiter and Loza (2011) with minimal modification)

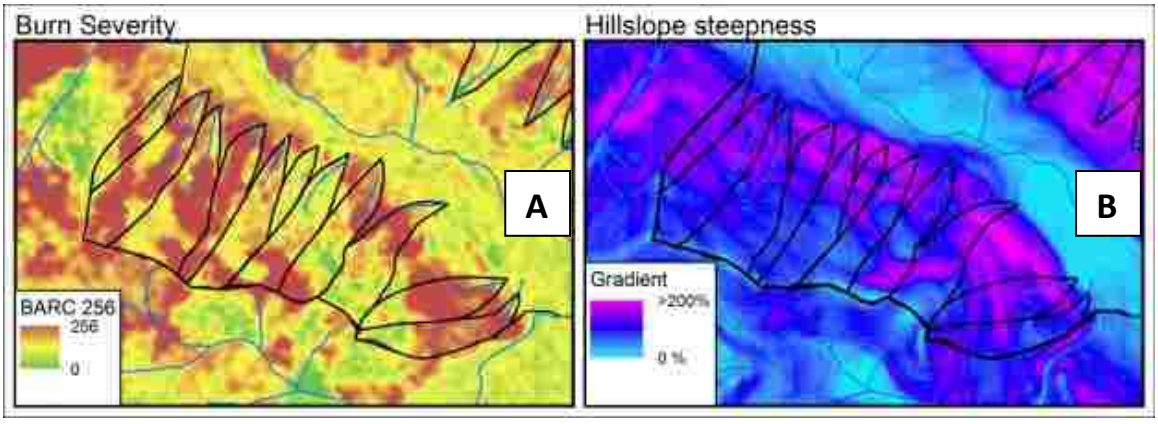

Figure 8: Catchments along south side of Cascade study area. Panel A illustrates highly variable fire severity above extreme slopes gradients (Panel B) at hillslope base where GR occurred apparently resulting from a fire-hose effect

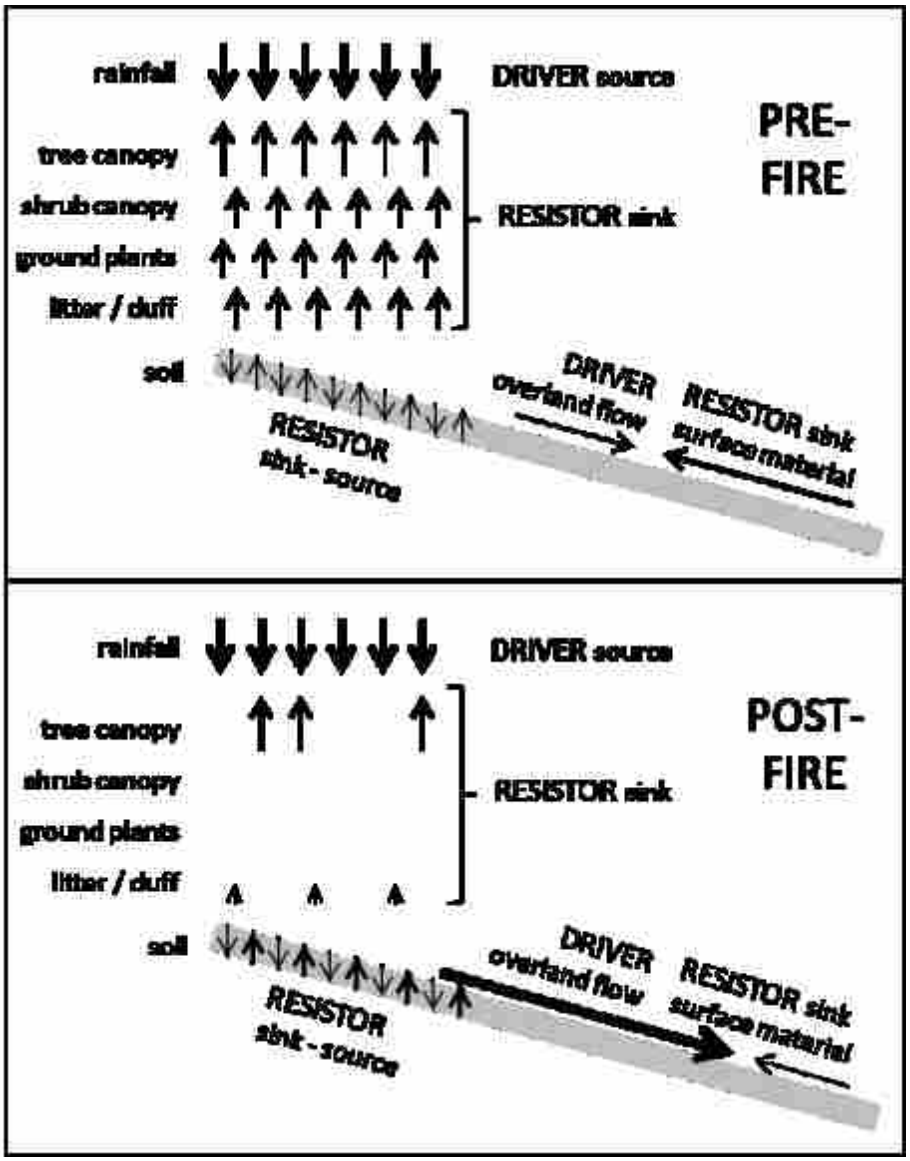

Figure 9: Conceptual model of driver-resistor relationships on forested hillslope before and after fire relative to rainfall delivery to soil surface and vegetation controls on attenuation of rainfall mass and energy

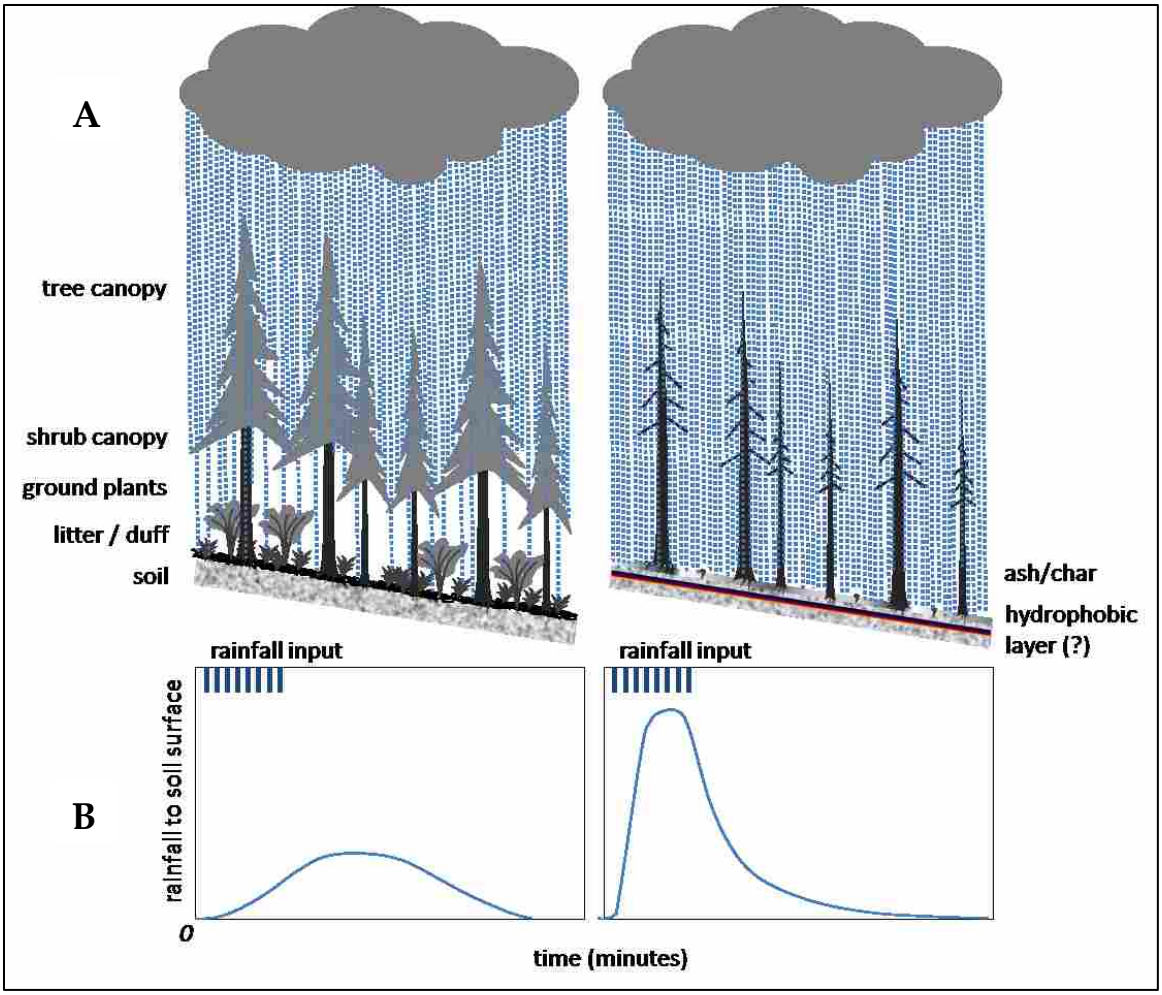

Figure 10: Relationship between above ground biomass structure and rainfall delivery to surface before and after wildfire. Panel A: Vertical vegetation structure comparing rainfall interception; B: Conceptualized rainfall delivery hydrographs

CHAPTER 3: THE INFLUENCE OF SPATIAL PATTERNS OF FIRE SEVERITY ON HYDROLOGIC CONNECTIVITY AND HILLSLOPE EROSION THRESHOLDS[2]

Abstract

Spatial configurations of burned and unburned vegetation patches influence post-fire overland flow response and the potential for erosion thresholds across hillslopes. However, the broad-scale relationships between fire severity, patterns of burn mosaics, and the hydrologic connectivity of overland flow pathways that lead to post fire erosion remain largely unexamined. We mapped 227 primarily first order catchments across four burned watersheds in the northern Rocky Mountains and identified 90 cases of channel incision that led to gully rejuvenation. We used landscape pattern indices derived from remotely sensed LANDSAT data to quantify the relationships between the spatial structure of burn mosaics and the probability of gully rejuvenation following wildfire. Generally, as the mean fire severity of a catchment increased, the percent of the landscape in high severity fire classes increased non-linearly, and large, connected, and more severely burned patches increasingly dominated the catchment area. Concomitantly, the probability of gully rejuvenation was positively correlated (R^2=0.93) with severely burned catchment areas. Statistical analysis revealed a threshold for erosion whereby a transition zone of high patch fragmentation precedes the threshold and after which progressively larger contiguous patches of severely burned areas and gully rejuvenation were observed. These observations suggest that progressive loss of vegetation due to wildfire leads to critical

[2] The coauthors for the planned journal submission are Kelsey Jencso and Karin Riley.

thresholds of structural connectivity that may enhance the hydrologic connectivity of overland flow pathways that lead to gully rejuvenation.

3.1 Introduction

Gully rejuvenation by post-fire runoff and erosion processes commonly follows wildfire throughout the western United States and has been cited as one of the leading forms of post-fire erosion response (Meyer and Wells, 1997; Roering and Gerber, 2005; Cannon et al., 2010). The term "gully rejuvenation", the reactivation of channel incision some time after a gully forms and stabilizes (Hyde et al., 2007, sensu Horton, 1945), captures the cyclical nature of gully formation and refill over time (Bull and Kirkby, 1997) which is driven by wildfire and other disturbance processes (Pierce et al., 2004). These geomorphic events influence landscape evolution (Pierce et al., 2004; Istanbulluoglu and Bras, 2005a; Roering and Gerber, 2005), alter aquatic habitats (Gresswell, 1999), impair water quality, damage infrastructure, and threaten human activities (Calkin et al., 2007; Parsons et al., 2010) at various time scales. Prior studies have suggested that spatial patterns of fire severity influence post-fire geomorphic response (Kutiel et al., 1995; Hyde et al., 2007; Moody et al., 2007; Hyde, 2013). However, little work has been done to quantify how the spatial structures of burn mosaics influence erosion response over broad scales.

Wildfire consumes, to varying degrees, standing vegetation and organic matter above and below the mineral soil surface. The pre-fire spatial arrangement of live and dead vegetation and variation in fire behavior combine to form burn mosaics often

composed of patches of varying size and fire severity (Lentile et al., 2006; Parr and Andersen, 2006; Keeley, 2009). Fire severity describes the degree to which a fire consumes biomass and reflects the relative proportion of residual unburned or incompletely burned biomass versus biomass completely reduced to ash and char (Chafer, 2008; Keeley, 2009). The magnitude of fire severity is a critical determinant of the occurrence of overland flow (Shakesby and Doerr, 2006) and erosion following wildfire (Lavee et al., 1995; Shakesby and Doerr, 2006; Cannon et al., 2010; Parise and Cannon, 2011). However, it remains unclear how the spatial arrangement of burned areas influences runoff response (Moody et al., 2007) and the propensity for erosion across differing landscape positions.

The propagation of geomorphic process responses in a catchment, whether driven by natural events or human activity, depends on spatial connections of hillslope and channel elements (Harvey, 2007). The concept of hydrologic connectivity provides a framework for broad-scale integration of the patch-patterns resulting from wildfire and thresholds for hydrologic response within run-off dominated geomorphic systems (Bracken and Croke, 2007; James and Roulet, 2007). Hydrologic connectivity is generally defined as the water-mediated transfer of matter and energy within or between elements of the hydrologic cycle (Pringle, 2003) and, more specifically, refers to interactions of hydrologic processes with the physical environment (Turnbull et al., 2008). Structural connectivity refers to the spatial patterns of landscape elements and the extent to which they are physically linked or contiguous with one another (Turnbull et al., 2008; Bracken

et al., 2013). The structural connectivity of bare patches of mineral soil with low surface roughness may enhance the functional or process-based hydrologic connectivity (Bracken et al., 2013) of overland flow pathways directed downslope and may provide a critical context for assessing the controls on hydrogeomorphic processes and runoff and erosion potential (Darboux et al., 2002; Kirkby et al., 2002; Lexartza-Artza and Wainwright, 2009).

In semi-arid landscapes, a common domain for wildfires throughout the western US (Arno, 2000), variations in how vegetation is organized affects runoff and erosion processes (Gutiérrez-Jurado and Vivoni, 2013). In general, the spatial arrangement, connectivity, and size of burned ground versus vegetated patches (including living and dead biomass and layers of litter and duff) may determine run-on/run-off, source-sink sequences that control the hillslope and catchment response to erosive forces (Cammeraat, 2004; Boer and Puigdefábregas, 2005; Arnau-Rosalén et al., 2008). Large, continuous burned patches without vegetation may facilitate the accumulation of overland flow, increasing potential for rill formation and gully initiation (Lavee et al., 1995; Allen, 2007; Arnau-Rosalén et al., 2008). Conversely, bare patches of undisturbed vegetation upslope may produce overland flow and sediment transport only to have the water absorbed and sediment deposited as it enters a vegetated patch (Puigdefábregas, 2005; Lesschen et al., 2008). It follows that the propensity for hydrologic connectivity and the transport of water and sediment in a downslope direction may be influenced by the contiguous nature of burn patterns.

The purpose of this study was to quantify relationships between the spatial structure of burn mosaics and post-fire erosion to better understand how physical changes from fire and resulting landscape patterns influence geomorphic processes. There were three objectives for this study. First, we sought to describe differences in the spatial structure of burn mosaics over a range of fire severity from mostly unburned to completely burned catchments. Next, we aimed to quantify the relationship between the spatial structure of burn mosaics as a proxy for hydrologic connectivity and the probability of gully rejuvenation following wildfire. The final purpose was to test for differences in the spatial structure of burn mosaics between catchments in which gully rejuvenation did and did not occur.

3.2 Study Areas

We completed our analysis using four areas located in the Northern Rocky Mountains of the US (Figure 1, Panel 1). Extensive wildfires (Bitterroot Complex Fires) occurred across the Sleeping Child and Laird Creek areas in the summer of 2000. Following the wildfires a series of convective summer thunderstorms and intense rainfall generated overland flow (Figure 2) and triggered sediment-laden flooding and debris flows in July 2001. The Castle Rock Fire burned the Rooks Creek and Warm Springs area in 2008. Convective summer thunderstorms generated flooding and debris flows in June and July of 2009. The climate across all four sites is dominated by Pacific maritime weather from the northwest and a continental plains climate influence from the southeast (Moody and Martin, 2009a). Snow is the dominant form of precipitation

and isolated high-intensity, short-duration storms are common during the summer months. The average annual precipitation (1961-1990) for all sites is 700mm (WRCC, 2013). Soils in the catchments are classified as sandy loams that are 0.2 to 1m deep and which overlay bedrock dominated by granitic and sedimentary parent materials (Reed Jr and Bush, 2005). Mixed conifer forests primarily composed (>60%) of Douglas-fir (***Pseudotsuga menziesii***) covered the pre-fire landscape (USDOI Geological Survey, 2009).

3.3 Methods

3.3.1 Field study – GR, gully head definitions

We conducted field surveys to determine the presence or absence of gully rejuvenation following wildfire. Prior to field work the first-order catchments were manually mapped in a Geographic Information System guided by 10m digital elevation models and 1:24000 scale digital topographic maps (USDA, 2012). Delineation began at the catchment outlet and proceeded upslope perpendicular to the contour lines to the drainage divide. We searched primary valley bottoms to locate fresh flood and debris fans, and then systematically surveyed catchment channels to locate gully heads using the mapped catchments as a guide. We judged that gully rejuvenation occurred where continuous incision (greater than 10m in length) into the soil B horizon originated at a gully head. Gully heads were consistently identified as a distinct transition from gentle u-shaped rill morphology with fine root hairs (< 2-3mm) to an abrupt, vertical drop (Figure 3). The gully head incision typically cut through all soil horizons to depths of

tens of centimeters to over one meter, terminating in cobbles or boulders, often to bedrock. Only coarse roots greater than 1.5-2.0 cm remained within the gully heads. We interpret the finger-shaped gully head form to indicate channel initiation by erosion initiated through concentration of overland flow (Dietrich and Dunne, 1993) in accordance with the interpretations of (Gabet and Bookter, 2008) in their study of nine of the same Sleeping Child catchments included in our study. Absence of vegetation growing on debris fans or within incised channels indicated that all cases of gully rejuvenation occurred in response to recent storms following the fires. We surveyed the full population of catchments within the 4 areas and present burn mosaic pattern analysis for 227 catchments, accounting for 90 cases of gully rejuvenation and 137 ungullied catchments.

3.3.2 Measuring and classifying fire severity

We defined fire severity as the degree of vegetation loss from wildfire (Keeley, 2009). We quantified fire severity on a continuous scale (0 to 255) using LANDSAT satellite derived raster images (MTBS, 2012). The burned area reflectance classification (BARC) images were calculated using the differenced normalized burn ratio (dNBR) (Key and Benson, 2006). Fire severity maps produced using the dNBR effectively quantify relative changes to forest canopy compared to other measures of fire effects. (Epting et al., 2005; Hudak et al., 2007; Chafer, 2008). Correlations between the dNBR maps and loss of vegetation cover were determined to be especially strong in Western Montana (Hudak et al., 2007). The spatially continuous fire severity metric produces a

vegetation disturbance index (VDI) that can be used to compare the mean fire severity between areas (Hyde, 2013).

The 30-m LANDSAT derived image was interpolated using cubic convolution to 10-m resolution to produce finer-scale distinction between burned areas. The finer-scale data more accurately matched the patch-pattern unit boundaries within each first-order catchment surveyed. Further, the fine-scale data more accurately matched burned gradients based on field observations and visual inspection of aerial photography. We conducted sensitivity analysis to determine the effect of rescaling the data on the VD. The analysis confirmed that VDI values were strongly and significantly correlated between the 30m and 10m data ($R^2 \geq 0.94$, ($p < 0.001$).

We classified the VDI into seven equal interval fire severity levels for comparison to the landscape pattern metrics (described below). Hyde (2013) used binary logistic regression to evaluate the occurrence of gully rejuvenation as a function of vegetation disturbance, pre-fire vegetation, and catchment morphology. Using the values of the fitted regression model they determined that the probability of gully rejuvenations (pGR) increases non-linearly with increasing fire severity as measured by the VDI scale (Figure 4). To avoid arbitrary class breaks, we examined the distribution of VDI values in the context of the probability of gully rejuvenation for the 227 catchment in this study and reviewed field observations for physically meaningful breaks in the distributions of VDI values to identify classification breaks. Classification of fire severity began by identifying at the 50% probability crossover (pGR = 0.5, VDI ≅ 200). Only one case of

gully rejuvenation was observed where VDI was approximately less than 140. Based on these two points, seven equal interval fire severity levels (A-G) were defined at 30 unit increments: A = <80; B = 80, <110; C = 110, < 140; D = 140, < 170; E = 170, <200; F = 200, <230; G = 230+. Figure illustrates the geographic distribution of these fire severity classes across the study areas.

We used catchment boundaries to extract the burn mosaic data. First we calculated the VDI for each catchment and assigned the corresponding fire severity class to permit comparison of patch pattern characteristics between groups of catchments at increasing severity levels. Table summarizes the distribution of catchments by study area, GR status, and fire severity level. Erosion status indicates whether gully rejuvenation did (GR) or did not (NoGR) occur and was used to test for differences in patch patterns. GR was not observed below a mean catchment fire severity value of VDI = 137. Comparison by erosion status was made only between catchments above this value, resulting in 89 cases of GR and 79 cases of NoGR. After assigning catchment fire severity levels we reclassified the BARC values within each catchment to assign the fire severity level to each raster cell.

3.3.3 Measurement and analysis of patch patterns

Characteristics of fire severity patches within and between catchments were analyzed using landscape pattern indices (LPI) metrics described generally by Gustafson (1998) and implemented in FRAGSTATS, a tool developed to quantify and characterize landscape organization for ecosystem studies (McGarigal et al., 2012). LPI metrics have

been used in erosion, run-off, and wildfire studies to investigate the influence of patterns of vegetated and bare patches on vegetation recovery following land abandonment (Lesschen et al., 2008), to examine the impact of prescribed fire on wildfire patterns (Boer et al., 2009), to characterize pre- and post-fire changes in landscape composition and structure relative to burn severity (Hayes and Robeson, 2009), and for cross-scale assessment of the spatial variability of soil hydrophobicity following wildfire (Woods et al., 2007).

We defined patches in Fragstats using the eight adjacent cells option. Landscape level patch-pattern relationships are defined in multiple ways using patch characteristics within and between patches, for example, patch size, shape, and number and distribution of patch types (Cushman et al., 2008). We chose two LPI metrics that characterized the configuration of burn mosaics across different fire severity levels and believed to be relevant (Cushman et al., 2008; Kupfer, 2012) to post-fire erosion processes (Gartner et al., 2008; Parsons et al., 2010). The contagion (CONT) metric measures patch topology and connectivity, specifically aggregation (large, continuous patches of like fire severity) and interspersion (small, scattered patches of like fire severity). The value of CONT ranges from 0 to 100, approaching 0 when all patch types are maximally fragmented and evenly interspersed and approaching 100 where a continuous patch at a single fire severity level extends throughout the catchment. The second metric, percent landscape (PLAND) calculates the proportional area at each fire severity level within each catchment and provides means to compare the relative

composition and dominance of fire severity level types between catchments without regard to patch arrangement. Patches at each severity could be fragmented or continuous. To aid visualization we present maps of burn mosaics for 4 catchments at progressively higher fire severity VDI, with corresponding fire severity level and patch pattern metrics (Figure 4).

We compared the outputs of the patch-pattern analyses through graphical displays and by statistical analysis using R software (R Core Team, 2013). Non-monotonic trends in the both CONT and PLAND data necessitated the use segmented linear regression (Worsley, 1983; Toms and Lesperance, 2003) to assess relationships between patch-pattern metrics, VDI, and the probability of GR. The LPI metrics were compared by fire severity group between erosion status (GR v NoGR) using the two sample t-tests to evaluate the effects of the spatial structure of burn mosaics on erosion response.

3.4 Results

3.4.1 Change in burn mosaic structure and composition with increasing fire severity

The catchment level contagion generally followed a hyperbolic trend across the range of fire severities (Figure 6, Panel 1) with a strong correlation to the VDI ($R^2 = 0.76$, $p<0.001$). The high contagion value at the lowest fire severity level indicates that burn mosaics were strongly aggregated into a few dominant patches of lower fire severity (Table 4). Burn mosaics exhibited decreasing contagion over the mid-range of fire severity (severity groups B-E, contagion dropped from 46 to 39) signaling increased

fragmentation, interspersion, and heterogeneity among patch types. While fragmentation over this range was not correlated with VDI within each fire severity group, the variability of fragmentation consistently decreased (s.d. dropped from 10.5 to 5.9) indicating a trend of smaller patch size with increasing severity. The contagion trend reversed and showed a non-linear increase at the highest severity level groups, F and G. Here, catchments displayed increased levels of patch aggregation with increasing consolidation and homogeneity of burn mosaics. At the highest severity level, group G, increased aggregation was strongly correlated to increasing magnitudes of the VDI (R^2 = 0.81, $p<0.001$).

Catchments at each fire severity level were composed of patches across the range of all fire severity levels (Figure 7 and Figure 8). The dominant patch type in each fire severity group tended to match the group level (e.g. the patches at fire severity level C typically covered the largest proportion of area in group C fire severity catchments). The proportional abundance of patches at the other severity levels declined progressively relative to the dominant patch type within each catchment, except in three cases in three cases one fire severity type, level G, fully covered group G catchments. Catchments classified at the mid-severity range were composed of a mixture between two to all seven consecutive fire severity levels.

The proportional composition of burn mosaics corresponded to the fragmentation and consolidation trend indicated by the contagion metric (Figure 6, Panel 1, and Figure 7). The strong patch aggregation within the catchments at the lowest

and highest fire severity levels, A and G, also averaged over 80% of the land area burned at the corresponding fire severity level. The variability of proportions of area burned within each fire severity group paralleled the fragmentation of the burn mosaics across the intermediate range of fire severity.

Segmented regression of contagion as a function of VDI defined a significant breakpoint in contagion relative to fire severity at VDI = 195.3 (SE = 2.2; Figure 6, Panel 1). Initially, fragmentation increased and became more constant as VDI approached 195. In the second phase a strong linear increase in patch aggregation occurred across the burn mosaics and this corresponded with higher fire severities. It is important to note the proximity of the CONT breakpoint value to the class division for severity level F, VDI >200 and the probability of GR becoming greater than 0.50 (Figure 4). To evaluate this relationship further we combined the proportions of each catchment burned at levels F+G (hereafter referred to as % F+G) to determine how these higher severity classes might lead to greater erosion potential for landscape positions downslope (Calkin et al., 2007; Parsons et al., 2010).

Segmented regression of % F+G as a function of VDI defined a breakpoint at VDI = 155.3 (SE = 2.1) (Figure, Panel 2). The % F+G of the 80 catchments burned at severities below this point varied widely (range 0 to 36%) but was low overall (mean = 4) and in half of these catchments no area was burned at the highest severity levels. The area burned at % F+G increased strongly and steeply after the breakpoint. The variability was greatest through the VDI range from 110-170 (groups C and D) and corresponds to the

severity range where the landscape was generally most fragmented and patch types were most uniformly distributed (Figure 6, Panel 2). Initially burn mosaic structures were more heterogeneous and then became organized into connected patches of areas burned at higher fire severity.

3.4.2 Burn mosaic structure and probability of gully rejuvenation

Across the range of fire severity where GR was observed (VDI>137), the increase in catchment area burned at high fire severity (% F+G) correlated strongly with the increasing probability of GR (R^2=0.93, p<0.001) (Figure 9, Panel 1). Coincidentally, the breakpoint for the segmented regression for contagion intersects the GR probability curve at the 50% probability cross-over. Below this point within the observed GR range (VDI from 137-195) CONT was uncorrelated with the probability of GR (R^2<0.01, p=0.38). Thereafter, a strong positive correlation occurred (R^2<0.78, p<0.001).

3.4.3 Burn mosaic structure where GR did and did not occur

Only 4% of GR cases and the majority of stable catchments (NoGR) were observed below VDIs less than 155 (Table 4). This corresponds with very low abundance of patches burned at moderate to high severity, very mixed levels of patch aggregation and fragmentation, and probability of GR below 20%. Between the breakpoints (155 to 195) GR status was mixed with somewhat more cases of stable catchments (36) than gullied (29), yet with 32% of the cases of GR. Burn mosaics over this severity range exhibited variable degrees of fragmentation (CONT from 27 to 61, mean = 39) and were not correlated with the probability of GR while the percentage of area severely burned

was positively correlated with the probability of GR ($R2 = 0.61$, $p<0.001$). Sixty-three percent (63%) of all GR cases occurred where VDI exceeded 195 as patch aggregation, area covered by high severity burn, and probability of GR all increased (Figure 9, Panel 1).

Our comparison of catchments where GR did and did not occur revealed differences in burn mosaic structure only within fire severity group E (VDI from 170 to 200) (Table 5). Contagion was significantly higher in catchments where GR occurred ($p=0.010$) while area burned at the highest severity levels (%F+G) was lower with marginal significance ($p=0.064$). However, within severity group E, area burned at severity level E was significantly greater ($p<0.001$, Table 5) with a large absolute difference where GR occurred (36% of area at fire severity level E where GR occurred v. 21% for nGR).

3.5 Discussion

3.5.1 Structural connectivity of burn mosaic and gully rejuvenation

Our results demonstrate that with increasing fire severity, progressively larger and more connected patches of severely burned area compose burn mosaics (Figure 9). The strong correlations of landscape vegetation burn patterns and the probability of gully rejuvenation indicate that the burn mosaic patterns systematically and over broad scales influence post-fire erosion. Further, the statistically defined break-points followed by dramatic, non-linear change in landscape pattern trends also indicate a response

threshold that can be quantified using satellite imagery and simple patch-pattern analysis (Figure 6).

Visualization of burn mosaics in progressive severity steps explicitly illustrates development of continuous expanses of severely burned areas and conceptually links the metrics used in this study – fire severity, spatial structure, and erosion probability – with burn mosaic forms (Figure 9). The full color images in Figure 9, Panel 2 shows progressive expansion of areas burned at higher severity levels over the severity range. Also, gradients of fire severity patch patterns not revealed by statistical analysis are evident in the images.

At the lowest severity level example (VDI=118, Group C) expanses of lightly burned areas surround islands of severely burned patches. The next severity example characterizes the chaotic structure of burn patches in the severity range we identified as the transition zone. While larger than in the less severely burned landscape, the areas of severe burn remain highly fragmented (VDI=167, Group D). With increased overall severity the patterns reverses; connected and more severely burned areas burned area surround fragmented patches of lower fire severity (VDI=206, Group F). Finally, in the highest severity example (VDI=236, Group G) fully connected expanses of severely burned area surround small, fragmented islands of lower fire severity.

The black and white panels (Figure, Panel 3) emphasize development of the most severely burned areas showing the progression from islands to connected patches to landscapes where severely burned areas form the primary landscape matrix. These

illustrations also visually link the development of severely burned areas with corresponding probability of gully rejuvenation. In the example where high severity patches covered nearly a third of the landscape (VDI=206) the interspersion of areas burned at lesser severity levels resulted in a relatively fragmented landscape (CONT=44) and probability of gully rejuvenation is only somewhat stronger than random (pGR=0.58). The development of a cohesive matrix of high severity burn increased measured aggregation (CONT=68) and associated with a probability of gully rejuvenation near certainty (pGR=0.98).

3.5.2 Patch-patterns, hydrologic connectivity, and erosion thresholds

The analysis of burn mosaic patterns relative to fire severity and erosion response provides insight into how wildfire influences hydrologic and geomorphic processes. Davenport et al. (1998) extended percolation theory to thresholds of erosion response through the idea of the catastrophe cusp (Davenport et al., 1998) as defined by rapid acceleration of erosion after a threshold of vegetation loss. We suggest a modified version of this concept based on the findings of this study (Figure 10). Continuous vegetation limits runoff driven erosion (Horton, 1933; Horton, 1945) and major erosion events resulting from overland flow generally do not occur in stable forests with intact vegetation (Prosser and Williams, 1998; Wondzell and King, 2003; Jenkins et al., 2011). Following fire, erosion rates potential may increase as the size and number of bare patches increases with increasing fire severity. Non-linear erosion response and gully rejuvenation occur after a threshold of severely burned patch connectivity is exceeded

(Allen, 2007) and may enhance the probability that landscape becomes hydrologically connected (Bautista et al., 2007; Lesschen et al., 2009).

This study provides empirical evidence of the link between spatial patterns of vegetation disturbance by fire and the probable occurrence of gully rejuvenation following fire. We suggest that increased fire severity and the increasing structural connectivity of severely burned patches may lead to hydrologic connectivity of overland flow pathways when precipitation occurs. We speculate on the linkage between structural connectivity, hydrologic connectivity, and the occurrence of gully rejuvenation through the following this causal chain of biophysical interactions related to the erosivity of runoff and resistivity of vegetation (Collins and Bras, 2010). Infiltration-excess runoff occurs primarily in arid, semi-arid, or disturbed landscapes where the effective rainfall rate exceeds infiltration capacity and excess rainfall accumulates and flows downslope (Horton, 1933; Montgomery et al., 1997). The vertical structure of the intact canopy and groundcover can attenuate the timing and force of rainfall delivered to the ground surface (Dunne et al., 1991). Infiltration rates are controlled by soil surface conditions, soil structure, and resulting porosity. Vegetation and the mineral ground surface impose surface roughness that resists flow accumulation, increases surface water residence time, limits flow velocity and depth, and therefore reduces runoff erosivity (Dunne and Dietrich, 1980; Julien, 1998).

Fire may impact the runoff – erosion relationships along three primary mechanisms; canopy loss, altered soils properties, and changes in surface roughness.

Fire consumes canopy, increasing throughfall which can result in localized increases in rainfall intensity that are proportional to the volume of canopy lost (Hanshaw et al., 2009; Stoof et al., 2012). The heat produced by fire breaks disaggregates soil structure, fractures minerals and produces ash and char that may clog pores (Woods and Balfour, 2008; Woods and Balfour, 2010), and may enhance, decrease, or not change soil water repellency (Shakesby and Doerr, 2006). Consumption of surface biomass exposes the soil surface to pore clogging from raindrop impact (Swanson, 1978; Meyer and Wells, 1997), and decreases surface roughness and flow resistance, (Kutiel et al., 1995; Lavee et al., 1995; Larsen et al., 2009). In composite, vegetation loss leads to structural changes that result in more rapid accumulation of rainfall mass and energy and subsequent increases in overland flow and erosion and may lower thresholds for gully rejuvenation.

This study puts these probable hydrologic process changes associated with wildfire in a spatial context at the catchment level. Across our study sites we interpret the formation of large, continuous patches of severely burned vegetation patches to indicate development of a high degree of structural connectivity of areas relatively devoid of vegetation and surface biomass. These areas provide opportunity for minimal rainfall attenuation and maximum accumulation of overland flow relative to less severely burned or unburned areas. The correlation between this structural connectivity and the probability of gully rejuvenation suggests that fire created conditions for enhanced hydrologic connectivity of overland flow pathways (Figure 2) that exceeded a critical threshold and triggered gully rejuvenation downslope (Figure 3).

3.5.3 Study implications

Our results provide a framework for testing this conceptual model and further assessment of interactions between burn mosaics and hydrologic processes that lead to gully rejuvenation. We did not explicitly test spatial patterns of hydrologic connectivity. However, we provide first steps toward quantifying patch patterns resulting from fire or other disturbance processes relative to erosion controls mediated by structural connectivity that may have a significant influence of the degree of landscape hydrologic connectivity. The findings of Hyde (2013) support need for spatially-explicit analysis of the location of severe burn in catchments where a classification model falsely predicted that erosion would not occur. Specifically, gully rejuvenation occurred in 20 catchments with low overall fire severity (VDI from 151 – 193, mean = 175 – within the transition zone identified in this study) where severe burn was concentrated in the upper catchment extent. These observations highlight the need to evaluate burn mosaics within source areas above channel heads, land surfaces areas in catchments that control channel initiation processes (Dietrich and Dunne, 1993)and that are very sensitive to even minor changes in surface cover (Dietrich et al., 1992; Lesschen et al., 2007).

Future work should investigate spatially explicit configurations of patch patterns relative to hillslope steepness and terrain curvature and extend emerging understanding of topographic controls on hydrologic connectivity (Jencso and McGlynn, 2011). Our results suggest that it is important to evaluate the direction of potential overland flow relative to fire severity sequences and account for potential convergence (flow

accumulation), divergence (flow dispersion) and parallel flow (no flow change relative to surface form). Further observations and theoretical work should focus on the influence of burn configurations across broad-scales, their impacts on canopy loss and throughfall (Hanshaw et al., 2009; Stoof et al., 2012; Bracken et al., 2013), changes in flow accumulation with changes in surface roughness (Kutiel et al., 1995; Lavee et al., 1995), and fire induced changes to infiltration (Woods et al., 2007; Shakesby, 2011).

Conclusions

This study provides a first insight into the fundamental relationships between the spatial structure of burn mosaics, vegetation disturbance, and erosion response. We identify links between satellite measures of vegetation change (Hudak et al., 2007), the burn mosaic configurations, and the probability of the occurrence of GR following . Our observations support the emerging idea that vegetation loss plays an important role in the hydrologic connectivity thresholds leading to post-fire hydrogeomorphic response. Much remains to be learned about broader process and mechanistic relationships between spatial patterns of landform, vegetation, and disturbance processes in the context of ecohydrology (Vivoni, 2012) and biogeomorphology. We suggest that significant progress will be made in biogeomorphology where research focuses on the interactions between spatial patterns of vegetation and hydrogeomorphic processes (after Turner, 2005).

Tables

Table 1: Summary of study catchments by study area, erosion status, and fire severity level. No GR occurred below catchment VDI > 137 and all but 1 of 90 cases of GR occurred at VDI = 140 or greater, fire severity levels D –G.

		Fire Severity Level with VDI Range									
Study Area	**Erosion Status**	**A** <80	**B** 80 < 110	**C** 110 < 140	**D** 140 < 170	**E** 170 < 200	**F** 200 < 230	**G** 230 +	**Totals**		**% GR**
Laird Creek	GR	-		-	-	2	14	9	25	71	35%
	No_GR	8	8	7	5	11	2	5	46		
Rooks Creek	GR	-	-	-	-	8	2	-	10	44	23%
	No_GR	-	6	9	9	6	4	-	34		
Sleeping Child	GR	-	-	-	3	7	8	21	39	75	52%
	No_GR	3	2	6	10	5	6	4	36		
Warm Springs	GR	-	-	1	6	9	-	-	16	37	43%
	No_GR	-	2	7	10	1	1	-	21		
Totals	GR	-	-	1	9	26	24	30	90	227	40%
	No_GR	11	18	29	34	23	13	9	137		
		11	18	30	43	49	37	39	227		

Table 2: Summary of catchment level burn mosaic contagion with linear models, CONT = *f* (VDI) by fire severity group

Fire Severity Group	N	Mean	s.d	Term	Est.	Std.Err	t-val	p-val	Sig[1]	R^2
A	11	70	8.0	*Intercept*	148.51	32.66	4.55	0.001	*	0.39
				VDI	-1.14	0.47	-2.40	0.040		
B	18	46	10.5	*Intercept*	72.59	31.75	2.29	0.036		0.04
				VDI	-0.27	0.32	-0.83	0.419		
C	30	42	8.3	*Intercept*	46.55	21.97	2.12	0.043		0.00
				VDI	-0.03	0.17	-0.19	0.847		
D	43	40	6.6	*Intercept*	35.66	21.01	1.70	0.097		0.00
				VDI	0.03	0.14	0.22	0.829		
E	49	39	5.9	*Intercept*	25.12	17.79	1.41	0.165		0.01
				VDI	0.08	0.10	0.80	0.427		
F	37	49	8.6	*Intercept*	-60.45	26.23	-2.30	0.027	***	0.33
				VDI	0.51	0.12	4.18	<0.001		
G	39	79	14.6	*Intercept*	-348.68	33.30	-10.47	<<0.001	***	0.81
				VDI	1.74	0.14	12.76	<<0.001		

[1] Significance: ' *** ' <0.001, ' ** ' < 0.01, ' * ' <0.05, ' .' <0.10

Table 3: Erosion status over ranges defined by breakpoints from segmented regression

Break	VDI Range	NoGR	%	GR	%
% F+G	< 155	76	55%	4	4%
	155 to 195	36	26%	29	32%
CONT	>195	25	18%	57	63%
Totals		137		90	

Table 4: Results of t-tests for differences in landscape pattern indices between catchments where GR did and did not occur.

Factor	Level	Count		Mean		t-value	p-value	Sig
		GR	nGR	GR	nGR			
CONT	D	9	34	41.0	40.0	0.423	0.679	
	E	***26***	***23***	***41.3***	***37.1***	***2.705***	***0.010***	*
	F	24	13	48.6	49.9	-0.469	0.642	
	G	30	9	77.2	72.7	0.824	0.424	
% F+G	D	9	34	9.7	10.6	-0.227	0.825	
	E	***26***	***23***	***32.6***	***40.2***	***-1.896***	***0.064***	**.**
	F	24	13	70.6	69.7	0.237	0.815	
	G	30	9	94.1	95.2	-0.532	0.602	

Table 5: Differences in proportional abundance (PLAND) by fire severity levels within severity group E

Level	Mean		t-value	p-value	Sig
	GR	nGR			
A	0.9	1.6	-1.055	0.297	
B	2.6	8.1	-3.717	<0.001	***
C	8.7	12.0	-2.186	0.034	*
D	19.3	16.8	1.100	0.277	
E	36.0	21.2	3.860	<0.001	***
F	22.2	19.5	0.997	0.324	
G	10.4	20.7	-2.593	0.013	*

Figures

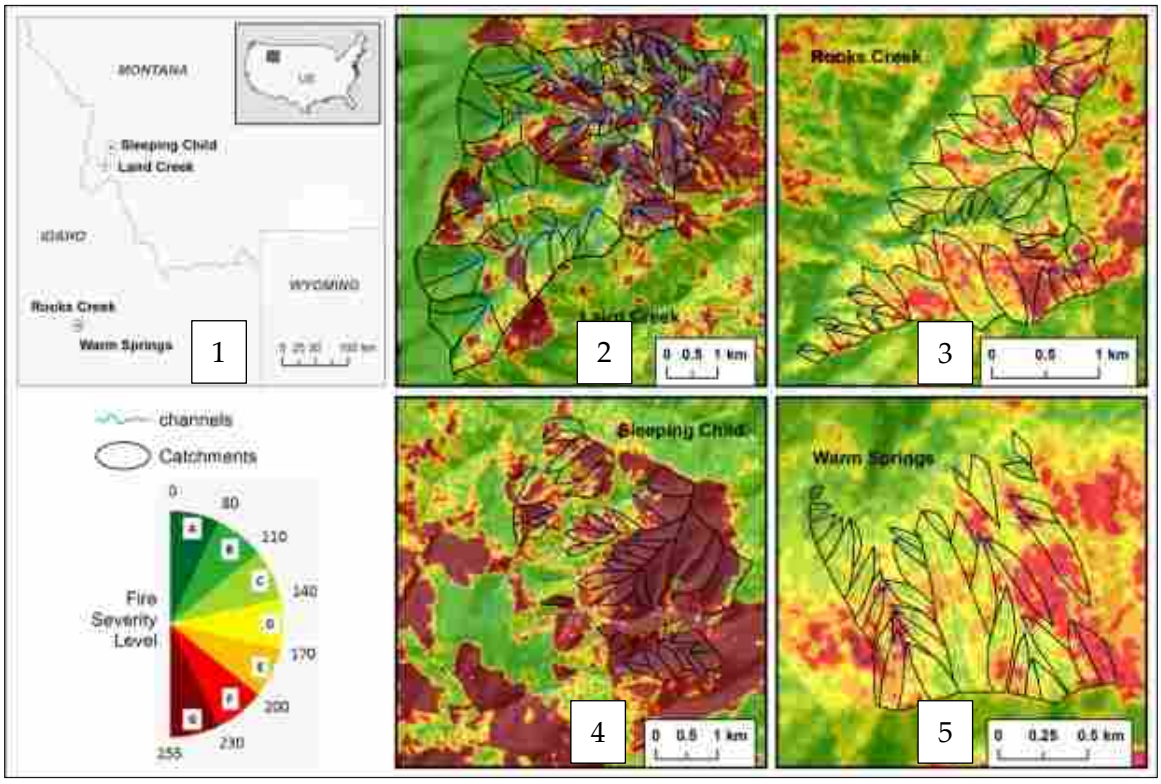

Figure 1: Panel 1 – Location of study areas within western US. Panels 2-5 – Study catchments within burn mosaics classified into 7 fire severity levels, A-G.

Figure 2: Focused overland flow within Laird Creek study area observed 10 minutes after the onset of intense rainfall on 20 July 2001. Photograph courtesy of the Bitterroot National Forest.

Figure 3: Characteristic gully head where rill lined with fine root hairs abruptly transitions a sharply defined finger-shaped form. Arrow points downslope.

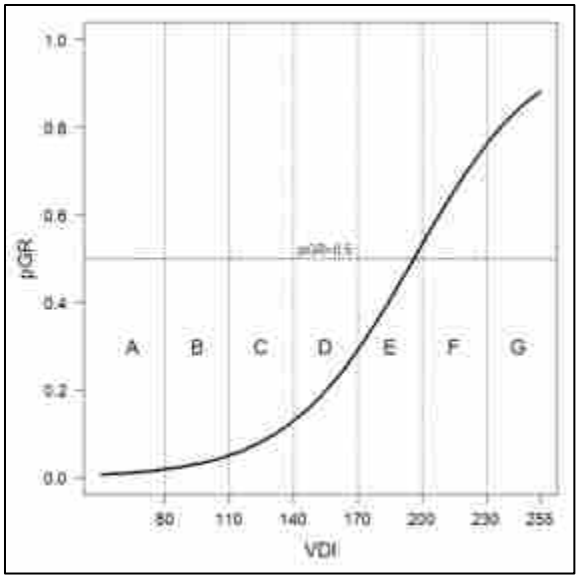

Figure 4: Probability of gully rejuvenation (No GR versus GR) following wildfire as a function of fire severity measured by the vegetation disturbance index (VDI). Fire severity levels, A-G, indicate the class breaks used in this study and explained in section 3.2. The curve is the fitted probability of GR from binary logistic regression using only VDI as the independent variable (classification accuracy, 0.74, AUC = 0.79).

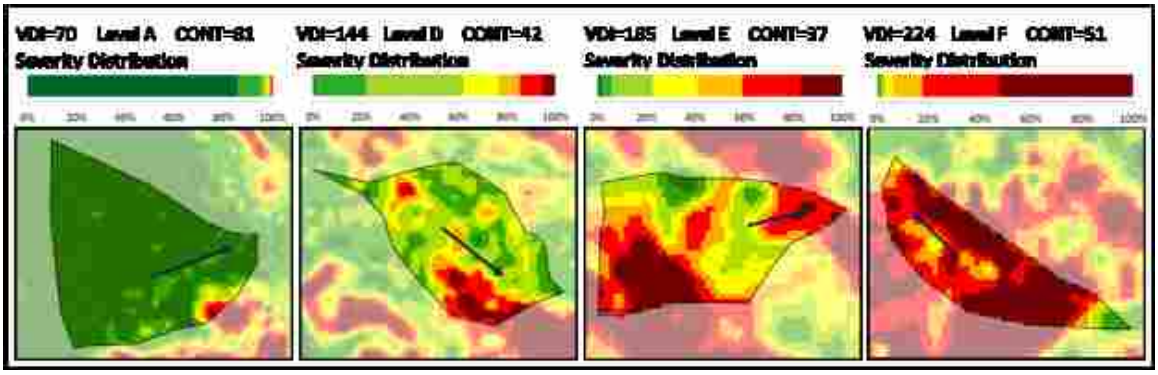

Figure 5: Examples of burn mosaics for catchments of different mean fire severity (VDI), catchment summary of contagion (CONT), and visual display of proportional distribution (PLAND) of fire severity levels. The black arrow indicates downslope direction. The 10 meter elevation contours provide an impression of catchment morphology.

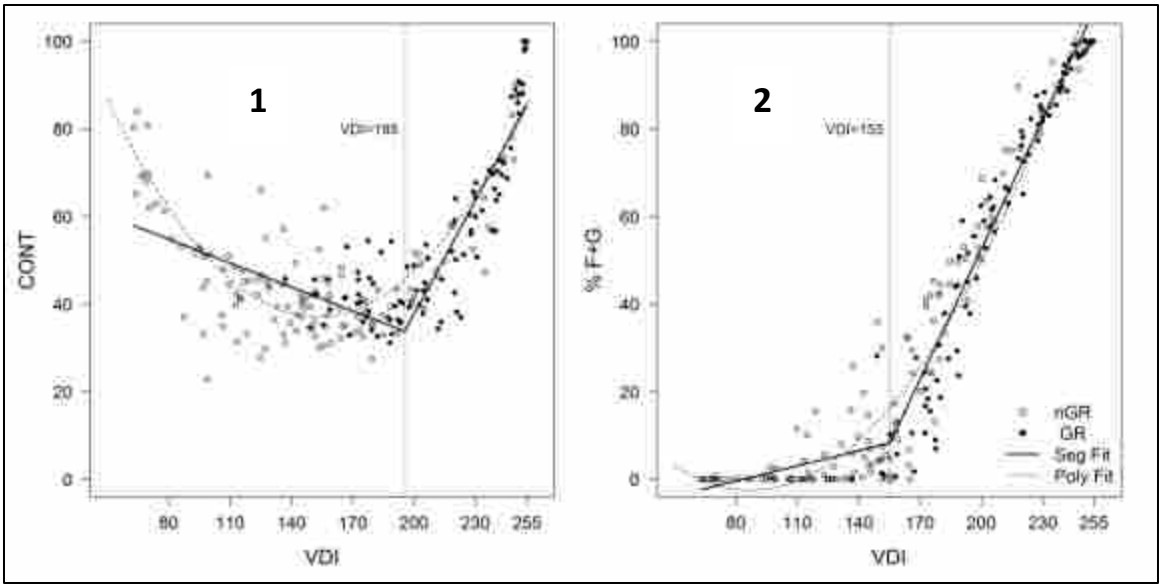

Figure 6: Plots showing trend of increasing patch aggregation and increasing catchment area burned at highest severity levels (% F+G) with increasing fire severity. Panel 1: Contagion as a function of VDI (Segmented fit: $R^2 = 0.73$, $p<<0.001$; breakpoint, VDI =195.3, SE = 2.2). Panel 2: Percent severely burned catchment area (%F+G) as a function of VDI (Segmented fit: $R^2 = 0.95$, $p<<0.001$; breakpoint, VDI =155.3, SE = 2.1). The vertical dotted lines mark the breakpoints in the segmented regression and the dashed curves show overall non-linear trends. Polynomial trendline equations; CONT= $0.0047*VDI^2 - 1.4357*VDI + 146.78$, $R^2 = 0.76$, $p<0.001$; %FG= $0.0041VDI^2 - 0.7162VDI + 28.812$, $R^2 = 0.94$.

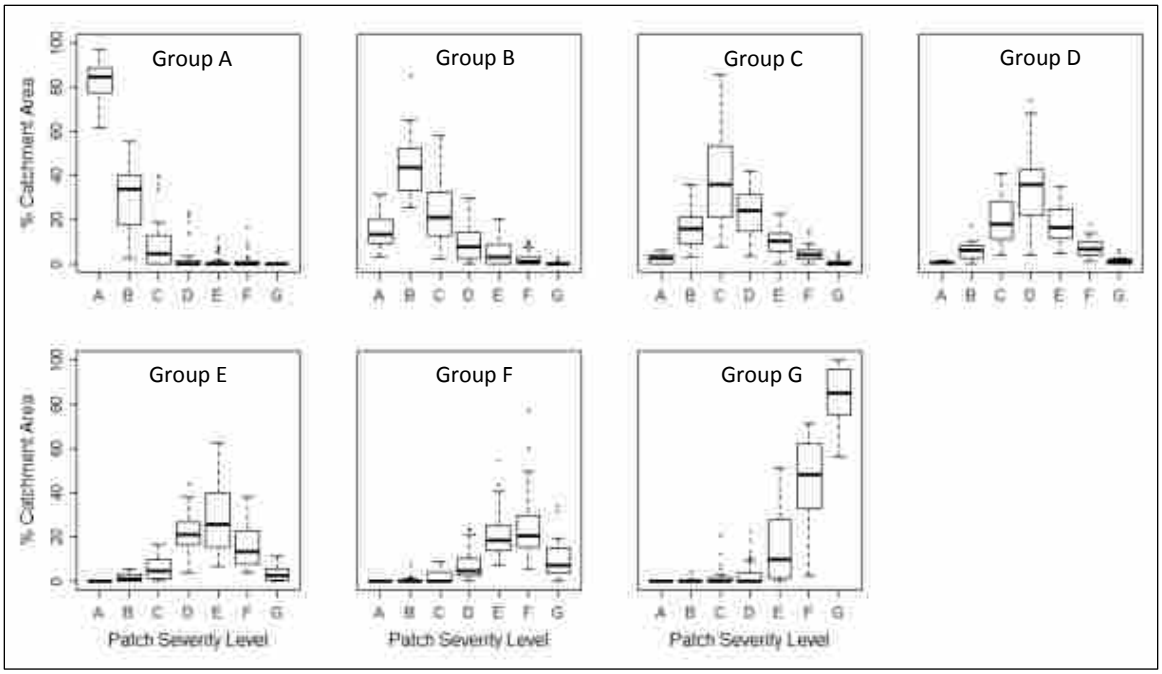

Figure 7: Subplots of the distributions of patch composition (PLAND) as percentage of catchment area by increasing fire severity levels.

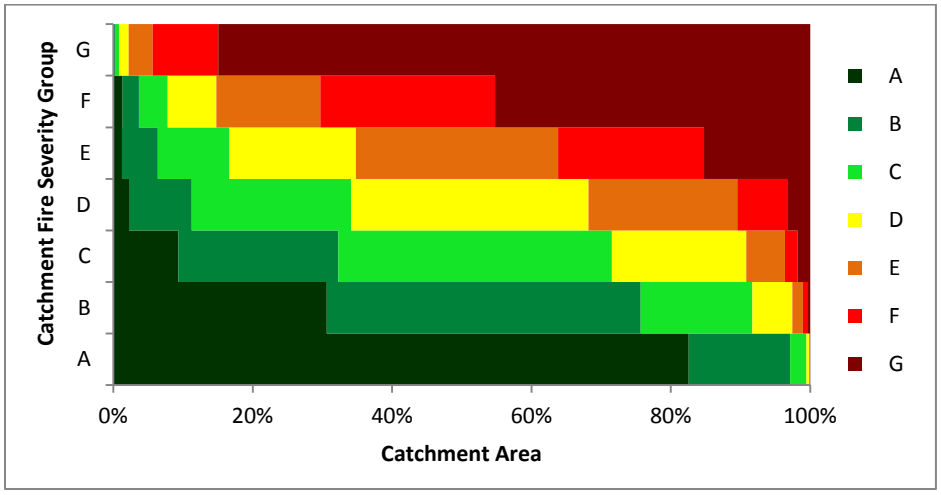

Figure 8: General distribution of fire severity levels within each fire severity group.

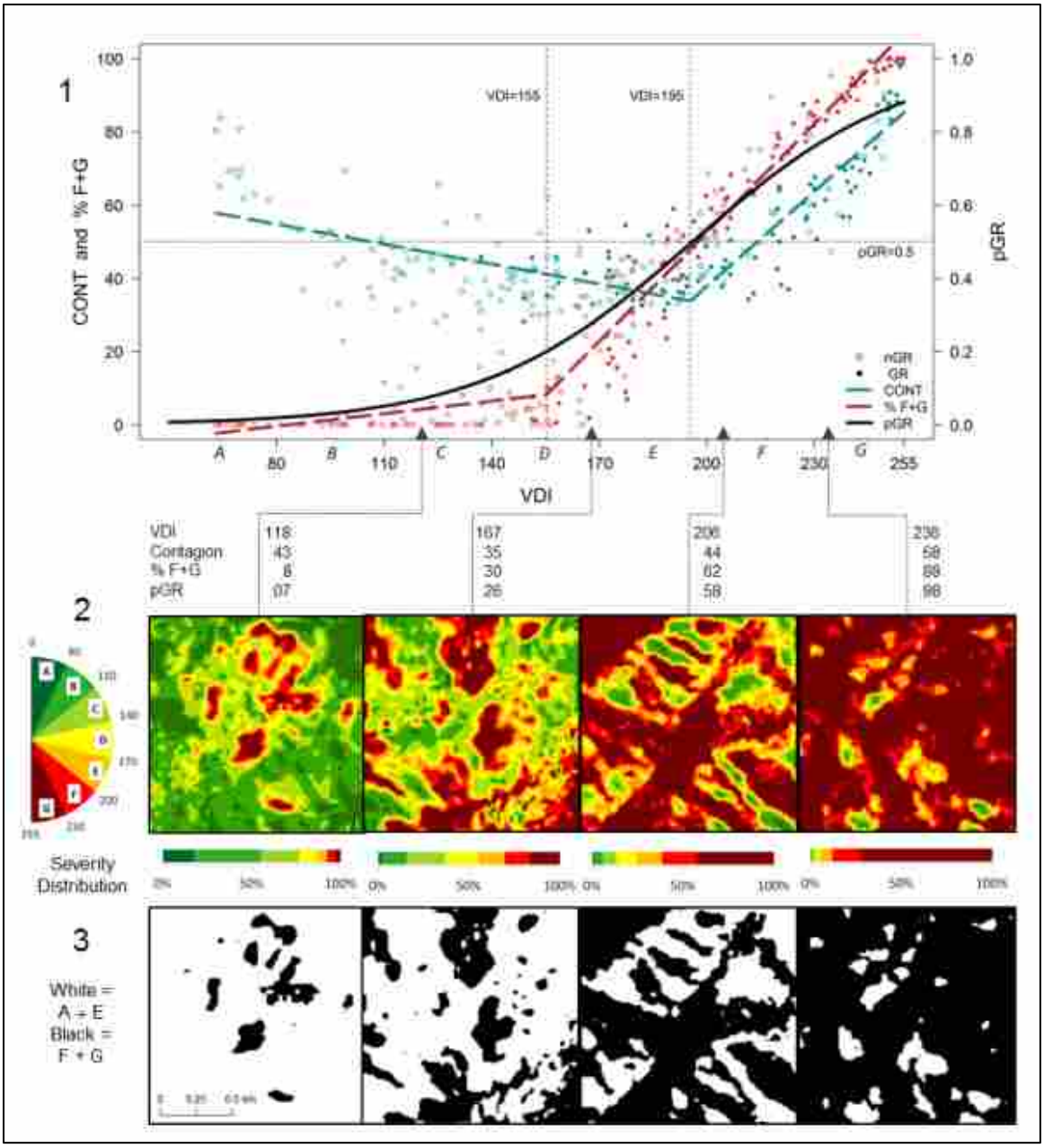

Figure 9: Summary of spatial structure of burn mosaics relative to fire severity (VDI) and the probability of gully rejuvenation. Panel 1: Comparison of trends of contagion, proportion of severely burned area (% F+G), and probability of GR over the range of fire severities. Panel 2: Four 22.5 ha burn mosaics randomly chosen to illustrate link between study metrics and landscape patterns within severity classes C-G. Panel 3: The black and white panels use the same areas to illustrate increasing consolidation of severely burned patches (% F+G) with increasing fire severity.

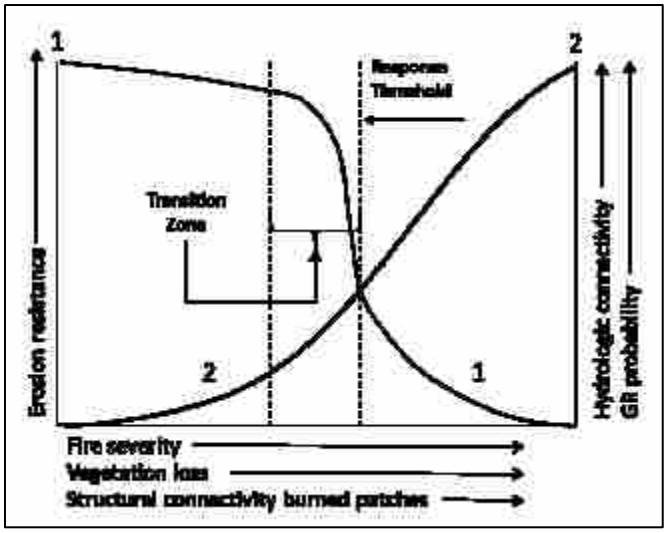

Figure 10: Conceptualization of erosion response threshold related to decreasing cover and increasing burn severity, size of severely burned patches, and increasing probability of GR. Overall plot and curve 1 are directly adapted from Davenport et al. (1998); curve 2 is GR probability curve derived from our observational data

CHAPTER 4: EFFECTS OF VEGETATION DISTURBANCE BY FIRE ON CHANNEL INITIATION THRESHOLDS[3]

Abstract

The disturbance or removal of vegetation by wildfire influences channel incision following intense rainfall events. Here we empirically examine relationships between the severity of vegetation disturbance and geomorphic controls on threshold conditions that lead to channel incision. We conducted post-fire field mapping and digital spatial analyses across 99 recently formed channel heads in the Rocky Mountains of Montana and Idaho to identify the relationship between remotely-sensed fire severity and vegetation disturbance and the source area and gradient conditions required for channel initiation. We found that the relationship between the size of source areas and source area steepness was described by an inverse power function, consistent with established theory, across the range of fire severity, but that the magnitude of the slope-area relationship was significantly correlated with increasing fire severity. Further, at higher levels of fire severity, source areas above channel heads had lower slopes and somewhat larger areas. The findings suggest that the onset of channel incision defined by location of channel heads is controlled by fire severity and that the threshold for channel initiation decreases as vegetation disturbance increases. We also found that, in a subset of catchments for which LiDAR data were available, total curvature explained channel head location across the range of fire severity, with a small but significant contribution

[3] The coauthors for the planned journal submission are Andrew Wilcox, Kelsey Jencso, and Scott Woods.

from source area steepness. Steepness remains more important at lower fire severity, however, and total curvature dominates where fire severity is most extreme. This suggests that forces of convergent flow are not fully expressed until a significant proportion of vegetation has been consumed such that flow resistance is minimized. Our findings, and the use of a continuous fire severity metric, contribute an ecohydrological and biogeomorphical template for studies of post-fire geomorphic responses and landscape evolution.

4.1 Introduction

Intense rainfall following wildfire often triggers gully rejuvenation in mountain landscapes, but the interactions between fire severity, landscape geometry, and the location of channel heads formed following fire are poorly understood. The term "gully rejuvenation" (GR) (Hyde et al., 2007, sensu Horton, 1945) captures the cyclical nature of gully formation and refill over time (Bull and Kirkby, 1997) driven by wildfire and other disturbance processes (Pierce et al., 2004). Debris flows resulting from gully rejuvenation can alter or threaten aquatic habitat (Gresswell, 1999), drinking water supplies, structures, infrastructure, and human safety. Debris flows following fire play a significant role in landform evolution (Benda et al., 2003; Roering and Gerber, 2005) and can supply the majority of sediment introduced into mountain stream systems (Pierce et al., 2004; Frechette and Meyer, 2009; Moody and Martin, 2009a). Climate change is expected to increase the magnitude and frequency of extreme wildfire events (Westerling et al., 2006), potentially increasing the probability of post-fire gully

rejuvenation. This increased probability intersects with growing recognition of the significance of gully formation under land-use change and degrading environmental conditions (Poesen et al., 2003).

The source area (SA), also termed the 0-order catchment (Tsukamoto et al., 1982) is a region of elevated susceptibility to channel initiation (Sidle et al., 1985) where the typical concave form creates a zone of converging flow (Willgoose et al., 1991), focusing runoff into the catchment hollow (Figure 1). Slope-area ($S:A_{SA}$) and curvature-area ($C:A_{SA}$) characteristics of SAs define primary controls on channel initiation thresholds (Stock and Dietrich, 2006; Yetemen et al., 2010). The slope and source area above channel heads often exhibit an inverse relationship (Montgomery and Dietrich, 1988; Tarboton et al., 1992; Tucker and Bras, 1998) ((Figure 1, Panels B and C) expressed in the form of a power function:

$$\boldsymbol{S = kA_{SA}^{-\theta}} \quad (1)$$

where S is slope or topographic steepness, A_{SA} is source area, a proxy for potential input of rainfall mass and energy, $\boldsymbol{k}$ is a constant that reflects soil and precipitation factors, and $\boldsymbol{\theta}$ is a slope scaling exponent that reflects hillslope form, transport properties, and erosional processes (Kirkby, 1971; Montgomery, 2001). Together *k* and $\boldsymbol{\theta}$ implicitly combine the effects of lithology, soils, climate, and vegetation on channel initiation processes (Yetemen et al., 2010). (Note: The nomenclature of *k* and $\boldsymbol{\theta}$ is expressed as *a* and *b*, respectively in other literature (Vandekerckhove et al., 1998)). The correlation of area to slope varies by locale and where correlations are weak other information beyond

topography must be assessed (Dietrich and Dunne, 1993; Vandekerckhove et al., 1998; Hancock and Evans, 2006). S:A_{SA} relationships have been studied extensively across geographic domains (e.g. Montgomery and Dietrich, 1994; Prosser and Abernethy, 1996; Vandaele et al., 1996; Hancock and Evans, 2006).

Curvature quantifies topographic convexity or concavity, where hillslope form either tends to concentrate or dissipate flow (Zevenbergen and Thorne, 1987; Schmidt et al., 2003; Gutiérrez-Jurado and Vivoni, 2013). Flow concentration leads to increased flow depth and thereby increased erosivity (Julien, 1998). A few studies have addressed curvature relative to channel initiation thresholds. The correlation of S:A_{SA} relationships above ephemeral gullies in Spain and Portugal were strengthened by adding planform curvature (Vandekerckhove et al., 1998). Calculation of curvature thresholds provided a quantitative method to identify hollows and channel heads in the Italian Alps (Tarolli and Dalla Fontana, 2009). A study based on field mapping of 253 channel heads and direct comparison of S:A_{SA} and C:A_{SA} relationships found that the strongest correlations of source area with topography varied between slope, planform, and profile curvature depending on physiographic provinces in the Eastern US (Julian et al., 2012).

Although vegetation disturbance may destabilize or change the traditionally conceived slope-area relationship and channelization thresholds, vegetation is typically not considered in these analyses. However, the degree of vegetation removal may impact the slope or area required for gully rejuvenation, and sediment yield likely increases with decreasing cover (Hooke, 2000). Kirkby (1995) posits that vegetation

strongly mediates how land surface changes modify landforms and geomorphic processes. Landforms tend to remain stable until acted on by tectonic forces, or vegetation loss from fire or other disturbance processes accelerates erosion activity (Horton, 1945; Collins and Bras, 2008). Fire destabilizes landscapes by reducing and removing vegetation, a substantial source of rainfall attenuation (canopy interception) and resistance to flow accumulation (infiltration excess) (Collins and Bras, 2010). Both mechanisms result in increased tractive forces and thus, increased erosion (Horton, 1945; Bull and Kirkby, 1997; Collins and Bras, 2008).

Land surfaces around gully heads are especially vulnerable to change in vegetative cover, and relatively minor changes in surface resistance substantially alter thresholds for channelization (Dietrich et al., 1992; Lesschen et al., 2007). Collins and Bras (2010) associate drainage density, a direct expression of channel incision processes, with climate-driven vegetation types and biophysical processes. Runoff and erosion processes are especially sensitive to vegetation disturbance in semi-arid landscapes (Davenport et al., 1998; Wilcox et al., 2003; Allen, 2007). In semi-arid regions, Dunne (1978) reported observing rainfall rates from high-intensity storms that readily exceeded infiltration capacities of soils and generated erosive overland flow, especially where combined with disturbed vegetation. In modeling experiments, Yetemen et al. (2010) found that land surface properties related to vegetation exerted strongest control on $S:A_{SA}$ and $C:A_{SA}$ relationships compared to soil properties and lithology.

1.3 Channel initiation following wildfire

S:A_{SA} and C:A_{SA} relationships for areas burned by wildfire have been previously evaluated in a number of different settings and with varying foci. Cannon et al. (2001) found channel initiation thresholds defined by a slope-area relationship, and that this relationship varied with underlying lithology (Cannon et al., 2003). Gabet and Bookter (2008) mapped nine of the same gullied catchments surveyed in this study and found evidence within the slope-area plots of channel initiation by Hortonian or infiltration-excess overland flow. Istanbulluoglu et al. (2003) surveyed gullies eroded following severe wildfire and derived shear stress estimates from slope-area relationships. In a subsequent modeling study, the binary occurrence of fire was used to study the influence of periodic disturbance by fire on landscape evolution (Istanbulluoglu and Bras, 2005b). The study concluded that removal of vegetation by fire caused a shift at the channel head in dominant erosion processes. Channel formation was driven by landslides from mass failure under vegetated conditions and erosion by concentrated runoff drove channel formation where vegetation was completely removed. Hancock and Evans (2006) suggest that lower channel initiation thresholds by S:A_{SA} relationships in their field study are due to chronically reduced vegetation caused by very frequent fires but they do not directly quantify or analyze fire effects. Wohl (2013) also treated the effects of fire as a binary occurrence and compared the source area and slope above 50 observed channel heads formed following wildfire to the source area and slope of channel heads in similar undisturbed areas previously reported by (Henkle et al., 2011). Channel heads following fire formed upslope from pre-fire locations below substantially smaller source areas while the steepness was not significantly different compared to

unburned areas. Moody and Kinner (2006) observed concave form in all source areas above gullies eroded following fire and suggested curvature may be an important control over channel initiation processes. They state that changes by fire to vegetation cover alter hydrologic processes via increased effective rainfall due to canopy loss and reduced hillslope roughness. They did not evaluate the effects of curvature or fire severity in their study.

The purpose of this work was to study the relationship between fire severity and threshold conditions for channel initiation relative to $S:A_{SA}$ and $C:A_{SA}$ relationships, and to use this information to evaluate how physical vegetation disturbance by fire alters hydrologic and geomorphic processes. We hypothesize that the level of fire severity affects the location of the channel head by reducing the threshold conditions that result in channel initiation. Specifically we expect that the combinations of source area and its steepness that control the location of the onset of channel incision will decrease as vegetation disturbance increases. We also expect that gully rejuvenation will occur with lower source area curvature where fire consumed more vegetation.

4.2 Study Areas and Regional Setting

We surveyed five areas in mountainous terrain of Montana and Idaho in the Northern Rocky Mountains, each of which has experienced recent post-fire gully rejuvenation (Figure 2, panel 1). Following the scheme of Moody and Martin (2009a), the Sleeping Child, Laird Creek and Cascade study areas experience a sub-Pacific precipitation regime, while the Rooks Creek and Warms Springs areas experience a

medium-intensity, Plains regime. Snowmelt runoff is the primary input of the regional hydrology and isolated high intensity, short duration storms are common during hot, low humidity summer months. Thin, friable and poorly developed sandy loam soils cover granitic and sedimentary parent materials (Reed Jr and Bush, 2005). Mixed conifer forests dominated by Douglas-fir (*Pseudotsuga menziesii*) populated the pre-fire landscape (USDOI Geological Survey, 2009); other species varied by study area. Wildfires burned the Sleeping Child and Laird Creek study areas in 2000. Severe erosion followed during summer 2001 and field work was completed from autumn 2001-2003. The Rooks Creek and Warm Springs areas burned during 2007 and the Cascade burned area during 2008. Rainfall triggered debris flows in these areas between June and July 2009. Field work in these areas was completed during autumn 2009-11.

4.3 Methods

4.3.1 Field mapping of gully heads and rainfall characteristics

We inventoried all first-order catchments in each study area and identified 99 channel heads (Figure 3); Cascade (CS, N=9), Laird Creek (LC, N=26), Rooks Creek (RC, N=9), Sleeping Child (SC, N=39), and Warm Springs (WS, N=16) (Figure 2**Error! eference source not found.**, panels 2-6). We mapped the location of 95 channel heads with a Trimble Juno SB global positioning system device (median horizontal precision of 2.9m). Four sites in Sleeping Creek were inaccessible and gully heads were mapped using georectified, 1:4200 scale air photos flown in 2001. We judged that channel initiation occurred where continuous incision (greater than 10m downslope) into the soil

B horizon originated at a channel head. Channels heads were consistently identifiable as abrupt, U-shaped (in plan view) transitions from distinct, shallow rills lined with fine, intact root hairs to incised channels 0.25 to 1-m deep sometimes scoured to bedrock (Figure 3 and Figure 4). This form is consistent with Hortonian or infiltration-excess overland flow that leads to the "finger" shaped channel head described by Dietrich and Dunne (1993, p.182) and the “stepped plunge pool” configuration described by Cannon et al. (2003). We interpreted the form observed at all channel head locations (Figure 3) as evidence of initiation by infiltration excess overland flow leading to progressive sediment bulking (Meyer and Wells, 1997; Coppus and Imeson, 2002; Cannon et al., 2008), the dominant cause of post-fire debris flows (Cannon et al., 2008). We found no evidence of saturation induced failure at any channel head location.

Three source areas were removed from the 99 observations. One source area in Rooks Creek was composed almost entirely of rock and therefore channel initiation was judged unrelated to fire. Gully rejuvenation originated from a catchment entirely covered by grasslands with few scattered trees pre-fire. Channel incision occurred very low in the catchment, immediately below a steep, bedrock controlled nick-point. The dominant initiating force for one gully in LC was judged to be fire-hose effect (Johnson, 1970) and representing a substantially different process. Identification of one channel head from air photos of Sleeping Child was judged too uncertain to be included in the analysis. An additional source area was removed from the Sleeping Child subset for curvature analysis because it fell partially outside of LiDAR coverage. The final

ensemble dataset consisted of 96 observations with 37 observations used for the Sleeping Child curvature analysis.

Rainfall intensity and distribution were assessed using local rain gage data and regional images from the Next Generation Radar (NEXRAD) weather system. We verified the temporal and spatial coincidence of high intensity storms with reported gully rejuvenation events (Table 1). The proximity of gages and NEXRAD stations to each study area varied substantially rendering rainfall intensity as the largest uncertainty of this analysis.

4.3.2 Morphometric analysis

Channel head locations were transferred into a geographic information system (GIS) for morphometric analysis of source area characteristics. Source areas were manually mapped guided by 10m digital elevation models and 1:24000 scale digital topographic maps (USDA, 2012). Delineation began at the channel head proceeding upslope perpendicular to the contour lines to the drainage divide. Attempts at source area delineation using automated methods failed to capture the subtle topography where channel heads were located.

Three metrics describing fire severity and morphology were compiled for all source areas: vegetation disturbance (described below), source area (SA, in hectares), and relief ratio (RR). The RR, a dimensionless characterization of the source area gradient, was calculated as the ratio between source area relief (elevation difference between channel head and highest point in catchment) and length of longest flow path

measured along the longest channel extended to the catchment divide. It is similar to measuring local channel gradient (Montgomery and Dietrich, 1994) in that RR captures valley slope and reflects convergent processes associated with channel incision (Tarboton et al., 1992) (e.g. as used in Collins and Bras, 2010; Legleiter et al., 2011). Cannon et al. (2001) used RR characterize source area slope in a study of thresholds for initiation of post-fire debris flows.

For a subset of 37 source areas for which LiDAR data were available, we also calculated planform (PLC), profile (PRC), and total curvature (TC) metrics (after Zevenbergen and Thorne (1987). Curvature is the second derivative of elevation and is defined in three forms: planform, profile, and total curvature. Planform curvature measures form across hillslopes along contour lines. Positive values indicate potential for convergence (accumulation) and negative values for divergence (dissipation) of runoff and erosion. Profile curvature measures the rate of change of slope in the downslope direction and reflects potential for incision by advective flow (positive values) or deposition (negative values). Total curvature integrates planform and profile curvature with respect to hillslope gradient or slope and incorporates potential flow acceleration and increasing flow volume (Gutiérrez-Jurado and Vivoni, 2013). The input elevation rasters were created from LiDAR data acquired for the majority of the Sleeping Child study area (horizontal accuracy of +/- 1.5cm, vertical accuracy of +/- 6cm (Watershed Sciences, 2010)). The elevation data were resampled using cubic convolution to 10m resolution as we judged this scale to better represent the scale of overland flow

processes, especially convergent and divergent flow. We recognized, as have others, that finer resolution elevation data captures micro relief that might mask broad scale surface processes (Tarolli and Tarboton, 2006; Jencso et al., 2009; Riveros-Iregui and McGlynn, 2009). The curvature metrics were exported as ASCII grids and summarized in the R statistical software package (R Core Team, 2013) to derive mean and median total, planform, and profile curvature for each mapped source area.

4.3.3 Mapping and quantifying fire severity

We defined fire severity as the degree of vegetation loss from wildfire (Keeley, 2009) and quantified it using the vegetation disturbance index (VDI). The VDI metric is a direct application of the full scale (0-255 integer scale) burned area reflectance classification (BARC 256) maps where increasing VDI values indicate increasing vegetation loss. The BARC 256 images (MTBS, 2012) are calculated using the differenced normalized burn ratio (dNBR) algorithm derived from 30m resolution Landsat satellite imagery (Key and Benson, 2006). A VDI is calculated in the GIS as the mean BARC 256 value for each source area. The VDI permits direct comparison of fire severity within and between areas and has been applied to predict the probability of post-fire gully rejuvenation (Hyde, 2013).

Fire severity data produced using the dNBR method accurately measure changes to forest canopy, including first layer of vegetation visible from above (Epting et al., 2005; Hudak et al., 2007; Chafer, 2008), especially in Western Montana where correlations between the satellite-derived image and vegetation loss were stronger

compared to other regions (Hudak et al., 2007). The 30-m native resolution of the BARC 256 image was interpolated using cubic convolution to 10-m resolution to match the 10m DEM data. Sensitivity analysis was conducted to determine the effect of rescaling the data. The VDI values were virtually identical between the 30m native and the 10m resampled data ($R^2 \geq 0.99$, $p < 0.0001$).

The VDI values were classified into seven classes to permit comparison between groups of source areas at different fire severity levels. Hyde (2013) determined that the probability of gully rejuvenations (P_{GR}) increases non-linearly with increasing fire effects as measured by the VDI scale (Figure 5). Attempting to avoid arbitrary class breaks, we examined the plot in Figure 5 and reviewed field observations for potentially meaningful VDI values. Classification of fire severity began by identifying at the probability crossover ($P_{GR} = 0.5$, VDI ≅ 200). Only one case of gully rejuvenation was observed where VDI was approximately less than 140. Seven equal interval fire severity classification levels (A-G) were defined at 30 unit increments based on these two points: A = <80; B = 80, <110; C = 110, < 140; D = 140, < 170; E = 170, <200; F = 200, <230; G = 230+ (Figure 2, panels 2-6).

4.3.4 Statistical analysis

All data were tested using R statistical software (R Core Team, 2013) for conformance with the assumptions of statistical tests to be used. As needed, individual metrics were transformed to satisfy normality assumptions (based on Lilliefors test (Lilliefors, 1967)) with a cutoff of p>0.10) using either logarithmic or the Box-Cox power

(BCP) transformation (Box and Cox, 1964) as indicated by the structure of the data. We tested subsets of metrics grouped by fire severity level for homogeneity of variance using the Levene test (Levene, 1960) with a cutoff of $p>0.10$. Analysis of outliers in the bivariate $S:A_{SA}$ relationship was conducted using Mahalanobis D^2 statistic (Mahalanobis, 1936) and evaluated using the $\boldsymbol{X}^2$ statistic.

Table 2 summarizes source area metrics overall and by fire severity group. Relief ratios were normally distributed (Lilliefors $D=0.08$, $p = 0.17$). Source area size required log transformation (after transformation Lilliefors $D=0.08$, $p = 0.17$). The fire severity metric was applied only to define fire severity groups, therefore the assumption of normality did not apply. The variance of RR and HA between severity groups was homogeneous (for RR, Levene's $F=0.34$, $p=0.78$; for HA, $F=0.98$, $p = 0.41$). No outliers were identified in RR:HA pairs (Mahalanobis D^2 test evaluated using a $\boldsymbol{X}^2$ test ($\boldsymbol{X}^2$ (DF=2, $N = 10$) $= 9.210$, $p<0.01$). The summary of SC data is presented in Table 3. The SA and curvature data required Box-Cox power transformations (Box and Cox, 1964) to satisfy assumptions of normal distribution. After transformations mean curvature values were more strongly correlated with SA than median values for all three metrics (mean to median: TC, r= -0.76 v. -0.49; PLC , r= -0.43 v. -0.38; and PRC, r=0.45 v. 0.15). Therefore we conducted our analysis using only mean values.

Separate analyses of fire severity and source area relationships were conducted for the ensemble data set and for the SC subset. The $S:A_{SA}$ relationships using all source areas were evaluated using scatter plots and generalized linear modeling (GLM). The

power of GLM models was assessed using D^2, where D^2 is calculated as 1-(residual deviance/null deviance) (Mittlböck and Schemper, 1996). It is interpreted as proportion of variance explained by the model and is numerically equivalent to R^2 calculated for a standard linear model. The $\boldsymbol{k}$ coefficient and the $\boldsymbol{\theta}$ exponent were determined using non-linear (weighted) least-squares regressions and compared between fire severity levels and study areas using regression analysis.

The conceptual design for assessing the effect of fire severity on the $S{:}A_{SA}$ is based on the hypothesis that $S{:}A_{SA}$ is a function of fire severity, where fire severity levels D-G are assigned by VDI ranges as illustrated in Figure and explained above. The effect of fire severity on the $S{:}A_{SA}$ relationship was tested using multivariate analysis of variance (MANOVA), a method selected for its capacity to test for significant group differences on linear combinations of dependent variables (Harlow, 2005). Following the procedures described in Harlow (2005), RR and A_{SA} were treated as co-varying dependent variables and fire severity level was the independent grouping variable. The relationship was first tested for macro-level effects and evaluated using Wilk's lambda ($\boldsymbol{\lambda}$) which quantifies the proportion of covariate behavior not explained by the response variables (Wilks, 1932). Follow-up tests then compared the differences in RR and area overall and between fire severity groups.

We used Pearson's correlation and GLM methods to analyze the role of curvature in $S{:}A_{SA}$ relationships in the Sleeping Child subset. Correlation tests were used to check for collinearity between transformed variables and comparative strength of

explanatory power between variables. GLMs were built using SA as the dependent variable and RR and the curvature metrics as the independent variables. We assessed the response of SA in all Sleeping Child source areas (N=37), between sources areas with the highest level of fire severity (level G, N=23), and all other Sleeping Child source areas at lower severity levels (levels D-F, N=14). The model with the strongest explanatory power for each of these three analysis was identified using D^2 and the Akaike information criterion (AIC) score (Akaike, 1974).

4.4 Results

4.4.1 S:A_{SA} Relationships by fire severity levels and study areas

The S:A_{SA} relationship derived from all source area data above channels incised following fire is described by an inverse power function, $S = 0.51A^{-0.20}$ ($D^2 = 0.35$, $p<0.001$ (Figure 6, panels 1 and 2; Table 4 and Table 5). At the lowest fire severity level, D (VDI = <170), SA and RR were not correlated ($r^2 = 0.027$, $p=0.42$). At the next level of severity and thereafter, levels E-G (VDI >170), the S:A_{SA} relationship maintains a consistent level of significant and moderately strong correlation ($D^2 = 0.39$ through 0.42). The significance of the S:A_{SA} relationships is lowest under lower fire severity and increases with increasing fire severity, whether data are grouped by fire severity level or study area. The plots by severity level show general trends of decreasing steepness of the source area and increasing source area size with increasing severity.

The influence of fire effects on the S:A_{SA} relationship is expressed in the value of θ (Table 4 , Figure 7) in the form of $\theta = f(VDI)$, where θ is the slope scaling exponent in

the S:A relationship. The change in θ is regular, linear, and strongly correlated with the mean fire severity value, including whether data are grouped by fire severity level (D^2 = 0.91, p = 0.05) or by study area (D^2 = 0.97, p = 0.002). There is no correlation between the k coefficient when data are grouped by severity level (D^2 = 0.37, p = 0.39) or by study area (D^2 = 0.47, p = 0.20). The strength of the θ:VDI relationship was tested over different fire severity class breaks and numbers of classes. The relationship generally held using 3-4 arbitrarily defined severity classes (D^2 ranged from 0.67 - 0.96) and was somewhat weaker using 5-6 arbitrarily defined severity classes (D^2 ranged from 0.62 - 0.80). Further, the slope of the linear relationship remained relatively consistent (ranging from -0 .0026 to -0.0031, mean = -0.0028, n= 8).

4.4.2 Effects of Fire Severity on S:A_{SA} Relationship

The level of fire severity significantly affects S:A_{SA} relationships and explains 20% of the variability of S:A_{SA} correlations (Table 6: Wilks λ = 0.80, p = 0.002). Fire severity level influences RR (ANOVA F= 6.19, p=0.001) more significantly than SA (ANOVA F= 3.46, p = 0.020). Mean RR decreases significantly ($p < 0.05$) (Table 6 and Figure) between the two lower severity levels (D - E) and the two upper severity levels (F - G). There is no significant difference in mean RR within the lower severity levels (D - E) or within the upper severity levels (F - G). Mean SA increases somewhat with increasing fire severity. The increase is only significant ($p < 0.05$) between the two lowest levels (D-E) and the highest (G). SA varies widely between fire severity levels compared to relatively consistent, lower variability of RR (Table).

4.4.3 Analysis of Curvature

Total curvature (TC) most strongly explains SA for all the Sleeping Child catchments (D^2=0.58, Table 7). Adding RR to TC provides unique information (AIC decreases) and improves explanatory power (D^2=0.64). PLC or PRC alone provide no explanatory power. Comparing between fire severity groups, RR significantly explains SA at lower fire severity levels (D-F). At the highest severity level (G), TC alone explains SA more strongly (D^2=0.65) than when combined with RR for all source areas. Adding RR under highest fire severity somewhat increases explanatory power but adds no new information, indicating that TC alone is the most important topographic control.

The S:A_{SA} and C:A_{SA} relationships for the SC source areas are inverse and non-linear (Figure 9 and Figure 10). Severely burned source areas (Level G) are generally larger, less steep and are less convex compared to areas less severely burned (Levels D-F) , however the differences in mean area, RR, and TC values between the fire severity groups (Figure 11, Table 7) are remarkable if not significant (p=0.54, 0.19, and 0.27, respectively). As fire severity increases the area tends to increase slightly while RR and TC decrease. As found within the entire dataset, the Sleeping Child source areas vary much more widely than RR or TC.

4.5 Discussion

4.5.1 Effects of fire severity on S:A_{SA} relationships

Increasing fire severity progressively lowers the slope-area threshold conditions for the location of channel initiation within a source area; in general, channel incision

will commence with smaller contributing areas and gentler gradients with increasing fire severity. We found inverse relationships between source area size and steepness (Figure 6 and Figure 9) that are consistent with previous studies (e.g. Montgomery and Dietrich, 1988; Vandekerckhove et al., 1998; Cannon et al., 2001; Hancock and Evans, 2006). However, adding fire severity as proxy for vegetation change improves explanatory power of these primary topographic controls on channel initiation conditions. The effect of fire severity is most evident on source area steepness; initiation of channel incision occurred at lower channel gradients in areas with higher fire severity. The large decrease in relief ratio observed as fire severity transitions from a moderate level of fire severity to the highest levels (VDI > 200) suggests a process threshold where biophysical changes from fire cause instabilities that lead to accelerated erosion. In contrast to our findings, Wohl (2013) reported that for channel heads formed following fire, source areas were substantially smaller and slopes were not significantly different. The comparison was made against a sample of source areas at similar elevations within the region and without considering slope-area variations within burned areas relative to scaled fire severity.

The regular, linear increase of the magnitude of the slope scaling exponent, θ, reinforces the significance of the effect of fire on the threshold $S:A_{SA}$ conditions under which channels will initiate in zero-order drainages (Figure 7). We propose that these changes in θ reflect the increasing structural changes to, and consumption of, vegetation that occurs with increasing fire severity. This overall reduction in vegetation then results

in reduction in rainfall interception and surface roughness. The highly variable continuity and structure of burn mosaics that can occur during wildfire (Kutiel et al., 1995; Parr and Andersen, 2006; Lentile et al., 2007), and as observed in our study areas (Figure 2), may also be reflected in changes in θ. Hyde (2013) presents a patch-pattern analysis that indicates an increasing spatial organization of burn severity mosaics with increasing fire severity. Increasing fire severity creates larger, more continuous patches of high severity burn, resulting in more connected hillslopes with increased structural connectivity and possibly increased hydrologic connectivity (Wilcox et al., 2003; Bracken et al., 2013). The increase in hydrologic connectivity may result in increasing overland flow depths and velocities, and subsequent increases in erosion are reflected by changes in the position of channel initiation within zero-order drainages.

We interpret the statistically weaker slope-area relationship at lower fire severity levels, the scatter in the plots over the range of fire severity (Figure 6), and initial low scaling exponent (

Table 4 and Figure 7) to reflect the expectation that multiple factors influence the slope-area relationship, including climate, soils, and geology, in addition to vegetation disturbance (Yetemen et al., 2010). We speculate that the importance of these other factors decrease as fire severity increases and that other local factors better explain channel incision under lower fire severity levels. One factor could be localized intense rainfall (Chaplot et al., 2005; Bracken et al., 2008). Local physical factors may also lower erosion thresholds, for example, locally steepened slopes near a channel head not captured in the generalized slope metric or impermeable conditions above the channel head such as extensive bedrock outcrops or rock-armored headwaters. Such conditions were commonly observed during our field surveys.

Our values for θ (-0.05 to -0.33) coincide with and are below the range (-0.25 to -0.60) reported by Vandaele et al. (1996) from their research and their summary of other studies. The reported studies span the western US, Europe, and Australia. Values from -0.4 to -0.6 originate from studies conducted by Montgomery and Dietrich (1988) in the US Pacific Northwest. They mapped channel heads resulting from local failure of saturated materials, a different process than evidence of initiation by progressive sediment bulking observed at our sites. The value for the scaling exponent at the highest level of fire severity in our study is similar to the value derived from source areas generating post-fire debris flows in Colorado (Cannon et al., 2001) (θ = -0.34). In Australia, a study of gully formation on lands judged undisturbed by human activity reported θ = -0.28 (Hancock and Evans, 2006). This value is interpreted to indicate low

channel initiation thresholds resulting from frequent fire. In Spain and Portugal, gully initiation studies in areas disturbed by extensive tillage reported values of θ = -0.13, Portugal -0.23, respectively (Vandekerckhove et al., 1998) . This similarity of values in our study suggests the scaling exponent may reflect similar physical processes associated with vegetation disturbance. Work remains to reconcile the variability of θ relative to the geographic and process domains of the many studies reporting this value.

We chose relief ratio to characterize source area steepness; inconsistent treatment of this measure in the literature may hinder insights into the process of interest. We contrast our values of θ with those reported by Gabet and Bookter (2008) for 9 gullies surveyed in both studies. They identified θ = -0.76 using local slope at gully head as their slope metric, more than double the value arrived at in our analysis based on the relief ratio. Their choice follows Montgomery and Dietrich (1988), who applied local slope in $S:A_{SA}$ analysis of channels initiation by saturation-induced failure. In this process mechanism, channels initiate where static driving forces on a saturated mass exceed resisting forces. We suggest that relief ratio better reflects the processes of channel incision by concentrated overland flow, since relief ratio implicitly captures the accumulated potential energy and potential tractive forces of accumulating overland flow leading to channel initiation.

The strong relationship between total curvature and source area size may indicate that channel initiation thresholds are more sensitive to the combination of converging flow (influenced by profile curvature) and increased flow velocities and

depths (influenced by planform curvature) than either factor alone. Total curvature, however, includes the spatially generalized downslope elevation gradient of the source area. This accounts for increasing tractive forces as flows converge and flow depth and velocity increases through the zone where channel initiation occurs. In addition, the higher explanatory power of relief ratio under lower fire severities and of total curvature at highest fire severity suggests that the accumulation of force by converging flow necessary to initiate channel incision is not fully reached until resisting forces from surface biomass are minimized, as would occur at the highest burn severities. In contrast to our study,Vandekerckhove et al. (1998) found that planform curvature rather than total curvature strengthened $S:A_{SA}$ correlations. However, they implied that the form of the catchment hollows in their study only reflected planform curvature; they did not explicitly measure curvature as we did in this study. Julian et al. (2012) found that strongest correlations between source area and topography above channel heads, steepness, total curvature, or profile curvature, varied by physiographic regions of their study areas in the Eastern US. Further work is required to understand the variability of dominant topographic controls by geographic setting.

4.5.2 Causal chain of biophysical processes

Fire results in structural changes to vegetation that alter hillslope hydrology and the subsequent erosional processes. The causal mechanisms for the effects of fire severity on the slope-area relationship can be approached from a biophysical or ecohydrological perspective (Collins and Bras, 2010), focusing on how basic structural changes to

vegetation alter hydrogeomorphic response (Figure 12). As fire consumes biomass, both canopy and surface cover decrease. When rainfall occurs, these losses translate to proportional decreases in interception within the canopy and on the forest floor (Dingman, 2002). A greater proportion of rainfall reaches the soil surface directly and more rapidly suggesting that rates of rainfall delivery may exceed infiltration capacity independent of changes to soil caused by combustion of surface and near surface organic materials (Larsen et al., 2009). The loss of surface vegetation, litter, and duff may lead to reduced surface roughness and reduced flow resistance. As infiltration-excess overland flow commences, the depth and velocity and thus erosive power of overland flow can build more rapidly where biomass is more completely consumed (Prosser et al., 1995; Bull and Kirkby, 1997) and result in significantly higher sediment yields compared to slopes with a higher percentage of residual ground cover following fire (Benavides-Solorio and MacDonald, 2001).

4.6 Conclusions

Based on field mapping of the locations of channel heads at the transition from zero- to first-order drainages and measurement of fire severity using remote sensed imagery, we find that vegetation change from fire systematically lowers the slope and area threshold conditions required for channel incision. Additionally, increasing fire severity lowers the upslope channel gradient at which channel incision can occur, and decreases the necessary size of the source area, a reflection of the magnitude of flow contribution, above the point of channel incision. Our findings and the use of a

continuous fire severity metric contribute an ecohydrological and biogeomorphical template for transferring localized observations of vegetation disturbance to broader studies of landscape evolution and provide efficient and consistent methods to assess the potential for gully rejuvenation and debris flows following wildfire.

Further work is necessary to quantify process-based linkages between the VDI fire severity metric and additional hydrologic and geomorphic factors. Specifically, VDI needs to be linked to continuous structural changes in canopy and ground surface cover and related processes, including interception, effective rainfall rate, surface roughness, and flow resistance. These process linkages are similar to biological linkages between the same image source for the VDI metric and fire effects on vegetation (Miller and Thode, 2007). Relative to hazard prediction, this work demonstrates an efficient means to rapidly assess potential hydrogeomorphic consequences of fire effects over broad spatial scales and permits efficient comparison between impacted catchments and regions.

Our finding of a direct, scaled relationship between fire severity, source area, catchment morphology, and channel initiation location may be relevant for more generalized studies of the vegetation controls of threshold conditions for channel initiation (Istanbulluoglu and Bras, 2005b), the influence of vegetation disturbance on landscape evolution (Collins et al., 2004), and related development of geomorphic transport laws (Dietrich et al., 2003). Further, the successful use of the VDI metric responds to the need for a continuous metric to quantify vegetation change relative to

other landscape factors measured on continuous scales (Kremens and Smith, 2010). For example, an application of the continuous fire disturbance metric could be used to extend the work of Istanbulluoglu et al. (2004) beyond fire as a binary landscape condition to a gradient of disturbance in landscapes over time, perhaps over shorter time scales, in response to variable fire effects. We propose that the use of full-scale measures of vegetation change may be applied to broader studies of the vegetation disturbance by any source and accelerated gully erosion. Considering the concern about the effects of climate change on gully processes and general land surface processes (Poesen et al., 2003), such applications may be especially relevant.

Tables

Table 1: Summary of rainfall event data for each study area for known gully events

Study Area	Fire Year	Gully Event(s)	RAIN GAGE Max Intensity mm h^{-1}	NEXRAD Max 3hr Ttl Ppt mm
CS	2008	29 July 2009	28.7	32.8
LC	2000	15, 20, 21 July 2001	8.0-14.0	5.1-31.8
RC	2007	June 2009 Multiple	10.2	1.2-5.1
SC	2000	15, 20, 21 July 2001	4.0-17.0	12.7-19.1
WS	2007	June 2009 Multiple	10.2	2.5-12.7

Table 2: Summary of metrics for all source areas and by fire severity level

Variable	Level	N	Mean	Median	Min	Max	SD	COV
VDI	All	96	208	204	124	255	35.27	0.17
	D	16	154	160	124	169	13.19	0.09
	E	23	185	183	172	199	8.06	0.04
	F	23	213	214	200	229	11.29	0.05
	G	34	246	249	230	255	7.77	0.03
RR	All		0.38	0.39	0.15	0.62	0.12	0.31
	D		0.41	0.39	0.17	0.61	0.11	0.28
	E		0.45	0.44	0.27	0.62	0.09	0.20
	F		0.33	0.38	0.17	0.47	0.11	0.32
	G		0.34	0.36	0.15	0.60	0.12	0.34
SA ha	All		6.93	4.34	0.57	38.83	7.33	1.06
	D		5.33	3.27	0.57	16.90	5.17	0.97
	E		4.26	3.28	0.73	11.94	2.79	0.65
	F		8.65	3.73	0.90	38.69	10.52	1.22
	G		8.32	5.68	1.94	38.83	7.29	0.88

Table 3: Summary of metrics for SC source areas before transformation

Metric	Data	Mean	Median	Min	Max	SD	COV
VDI	All	229	244	139	255	33	0.14
	nG	194	193	139	229	28	0.14
	G	250	253	230	255	6.30	0.03
SA (ha)	All	7.66	4.49	2.13	38.84	8.73	1.14
	nG	6.48	3.63	2.13	38.68	9.36	1.45
	G	8.38	4.57	2.18	38.84	8.46	1.01
RR	All	0.40	0.40	0.18	0.61	0.10	0.26
	nG	0.43	0.43	0.21	0.61	0.09	0.21
	G	0.38	0.39	0.18	0.60	0.11	0.29
TC	All	0.48	0.25	-0.10	1.66	0.48	1.01
	nG	0.58	0.43	-0.04	1.22	0.41	0.70
	G	0.41	0.22	-0.10	1.66	0.52	1.26
PLC	All	0.07	-0.09	-0.50	1.08	0.41	5.79
	nG	0.58	0.43	-0.04	1.22	0.41	0.70
	G	0.05	-0.11	-0.50	1.08	0.43	9.21
PRC	All	-0.41	-0.37	-1.12	-0.09	0.24	-0.58
	nG	0.58	0.43	-0.04	1.22	0.41	0.70
	G	-0.37	-0.31	-1.12	-0.09	0.24	-0.65

Table 4: Results of non-linear (weighted) least-squares regressions for S=*f*(A) for all data and for each fire severity level and study area with mean fire severity level (VDI), scaling coefficient, *k*, and exponent, θ for each group.

	Group	N	VDI	Scaling Values	Estimate	Std.Err	t-value	p value
All Source areas		96	208	***k***	0.508	0.024	21.532	<0.001
				θ	-0.200	0.031	-6.515	<0.001
Fire Severity Level	D	16	154	***k***	0.444	0.049	9.099	<0.001
				θ	-0.062	0.074	-0.830	0.421
	E	23	185	***k***	0.569	0.031	18.543	<0.001
				θ	-0.199	0.043	-4.652	<0.001
	F	23	213	***k***	0.452	0.042	10.772	<0.001
				θ	-0.199	0.060	-3.295	0.003
	G	34	246	***k***	0.611	0.079	7.771	<0.001
				θ	-0.320	0.075	-4.252	<0.001
Study Area	CS	9	161	***k***	0.312	0.094	3.319	0.013
				θ	0.096	0.168	0.575	0.583
	LC	25	222	***k***	0.439	0.057	7.688	<0.001
				θ	-0.263	0.074	-3.559	0.002
	RC	8	183	***k***	0.383	0.051	7.457	<0.001
				θ	-0.014	0.072	-0.196	0.851
	SC	38	228	***k***	0.569	0.045	12.667	<0.001
				θ	-0.225	0.050	-4.494	<0.001
	WS	16	178	***k***	0.509	0.023	22.090	<0.001
				θ	-0.006	0.047	-0.120	0.906

Table 5: Results of GLM regressions with transformed area (log (A_{SA})10 HA) data for all data and by fire severity level.

Severity Level	Coefficients	Estimate	Std.err	t-values	p-value	Null deviance	Residual deviance	D^2
All	Int.	0.50	0.02	25.14	0.000	1.30	0.84	0.35
	log10 HA	-0.18	0.03	-7.10	0.000			
D	Int.	0.44	0.05	9.28	0.000	0.20	0.19	0.05
	log10 HA	-0.06	0.07	-0.85	0.411			
E	Int.	0.56	0.03	19.32	0.000	0.19	0.10	0.48
	log10 HA	-0.21	0.05	-4.39	0.000			
F	Int.	0.44	0.03	13.39	0.000	0.25	0.15	0.42
	log10 HA	-0.16	0.04	-3.92	0.001			
G	Int.	0.54	0.05	11.66	0.000	0.44	0.27	0.38
	log10 HA	-0.24	0.05	-4.47	0.000			

Table 6: Results of MANOVA tests: 1. Macro-level test using Wilks λ, 2. ANOVA tests evaluating overall effect of fire severity on each variable, and 3.Tests of significance of difference between means of area and RR between fire severity levels.

1. MANOVA Test: $S:A_{SA} = f$ Fire Severity Level

	Df	**Wilks**	**approx F**	**num.DF**	**den.DF**	**p value**
Level	3	0.80	3.57	6	182	0.002
Residuals	92					

2. ANOVA Tests: Significant differences between severity levels

Area (log10 ha)

	Df	Sum Sq	Mean Sq	F Value	**P value**
Level	3	1.35	0.45	3.46	0.020
Residuals	92	11.99	0.13		

RR

	Df	Sum Sq	Mean Sq	F Value	**P value**
Level	3	0.22	0.07	6.19	0.001
Residuals	92	1.08	0.01		

3. Pairwise t-tests (Pooled SD): **Specific differences between severity levels** (p values)

	Area (log10 ha)				**RR**		
No adjust	**D**	**E**	**F**		**D**	**E**	**F**
E	0.939	-	-	**E**	0.272	-	-
F	0.185	0.122	-	**F**	0.031	0.000	-
G	0.017	0.006	0.270	**G**	0.048	0.001	0.694

Table 7: Results of GLM models with explanatory power of RR and curvature metrics relative to source area in Sleeping Child study area. The three sections are subdivided into single and two variable models. The strongest model based on AIC score is emphasized in each section. Intercept values omitted for sake of clarity.

Variable	Estimate	Std. error	t-val	p-val	Null dev.	Resid. dev.	D^2	AIC
All Source areas (N=37)								
Single variable models								
RR	-0.41	0.08	-5.36	0.000	0.14	0.08	0.45	-116.54
TC	-0.31	0.04	-7.00	0.000	0.14	0.06	0.58	-126.78
PLC	-0.08	0.03	-2.86	0.007	0.14	0.12	0.19	-102.12
PRC	0.12	0.04	2.96	0.005	0.14	0.11	0.20	-102.65
Two variable models								
RR	**-0.19**	**0.08**	**-2.29**	**0.028**	**0.14**	**0.05**	**0.64**	**-130.09**
TC	**-0.23**	**0.05**	**-4.22**	**0.000**				
RR	-0.36	0.08	-4.41	0.000	0.14	0.07	0.48	-116.86
PLC	-0.04	0.02	-1.49	0.147				
RR	-0.36	0.08	-4.35	0.000	0.14	0.07	0.49	-117.05
PRC	0.06	0.04	1.54	0.132				
Fire Severity Levels D-F (N=14)								
Single variable models								
RR	**-0.52**	**0.13**	**-3.84**	**0.002**	**0.05**	**0.02**	**0.55**	**-43.95**
TC	-0.30	0.10	-2.83	0.015	0.05	0.03	0.40	-39.89
PLC	-0.04	0.05	-0.80	0.438	0.05	0.05	0.05	-33.44
PRC	0.14	0.07	1.91	0.080	0.05	0.04	0.23	-36.44
Two variable models								
RR	-0.40	0.18	-2.25	0.046	0.05	0.02	0.59	-43.20
TC	-0.12	0.12	-1.01	0.332				
RR	-0.53	0.15	-3.52	0.005	0.05	0.02	0.55	-41.99
PLC	0.01	0.04	0.18	0.858				
RR	-0.47	0.16	-2.90	0.015	0.05	0.02	0.57	-42.37
PRC	0.04	0.07	0.59	0.571				
Fire Severity Levels G (N=23)								
Single variable models								
RR	-0.35	0.10	-3.55	0.002	0.08	0.05	0.37	-68.95
TC	**-0.31**	**0.05**	**-6.30**	**0.000**	**0.08**	**0.03**	**0.65**	**-82.54**
PLC	-0.10	0.03	-3.00	0.007	0.08	0.06	0.30	-66.36
PRC	0.10	0.05	1.82	0.083	0.08	0.07	0.14	-61.51
Two variable models								
RR	-0.11	0.09	-1.20	0.244	0.08	0.03	0.68	-82.14
TC	-0.26	0.06	-4.33	0.000				
RR	-0.26	0.10	-2.65	0.015	0.08	0.04	0.48	-71.27
PLC	-0.06	0.03	-2.03	0.056				
RR	-0.31	0.10	-3.05	0.006	0.08	0.05	0.41	-68.29
PRC	0.05	0.05	1.09	0.287				

Figures

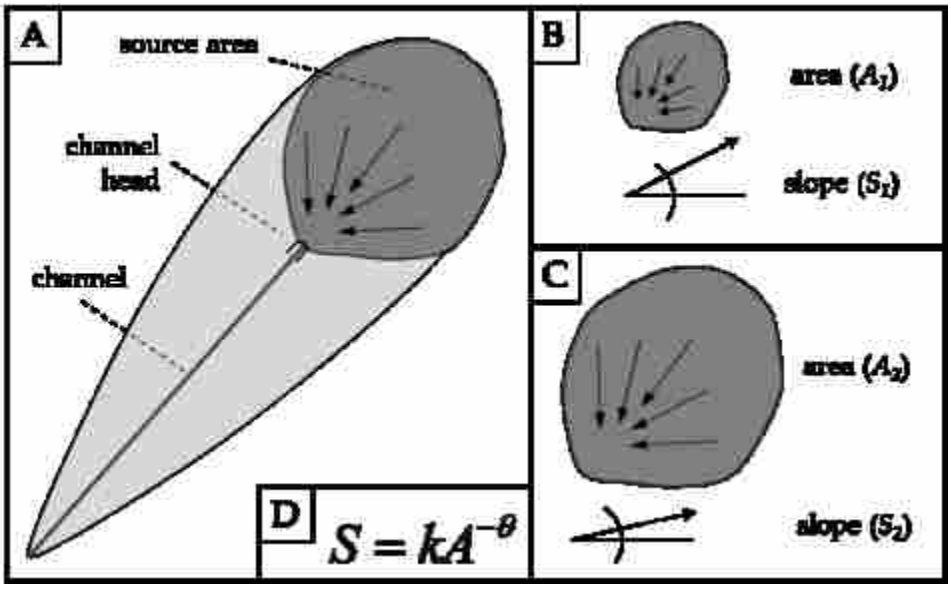

Figure 1: Conceptual model of zero and first-order catchment, source area, channel head location and channel. Panel A – Full catchment showing source area with converging flow above a channel head. Panels B and C – A relatively small source area (A_1) above a channel head has a steeper slope (S_1) than a relatively larger source area (A_2, S_2). The inverse relationship between area (A_i) and slope (S_i) is defined by a power function (Panel D). Illustration after Willgoose et al. (1991).

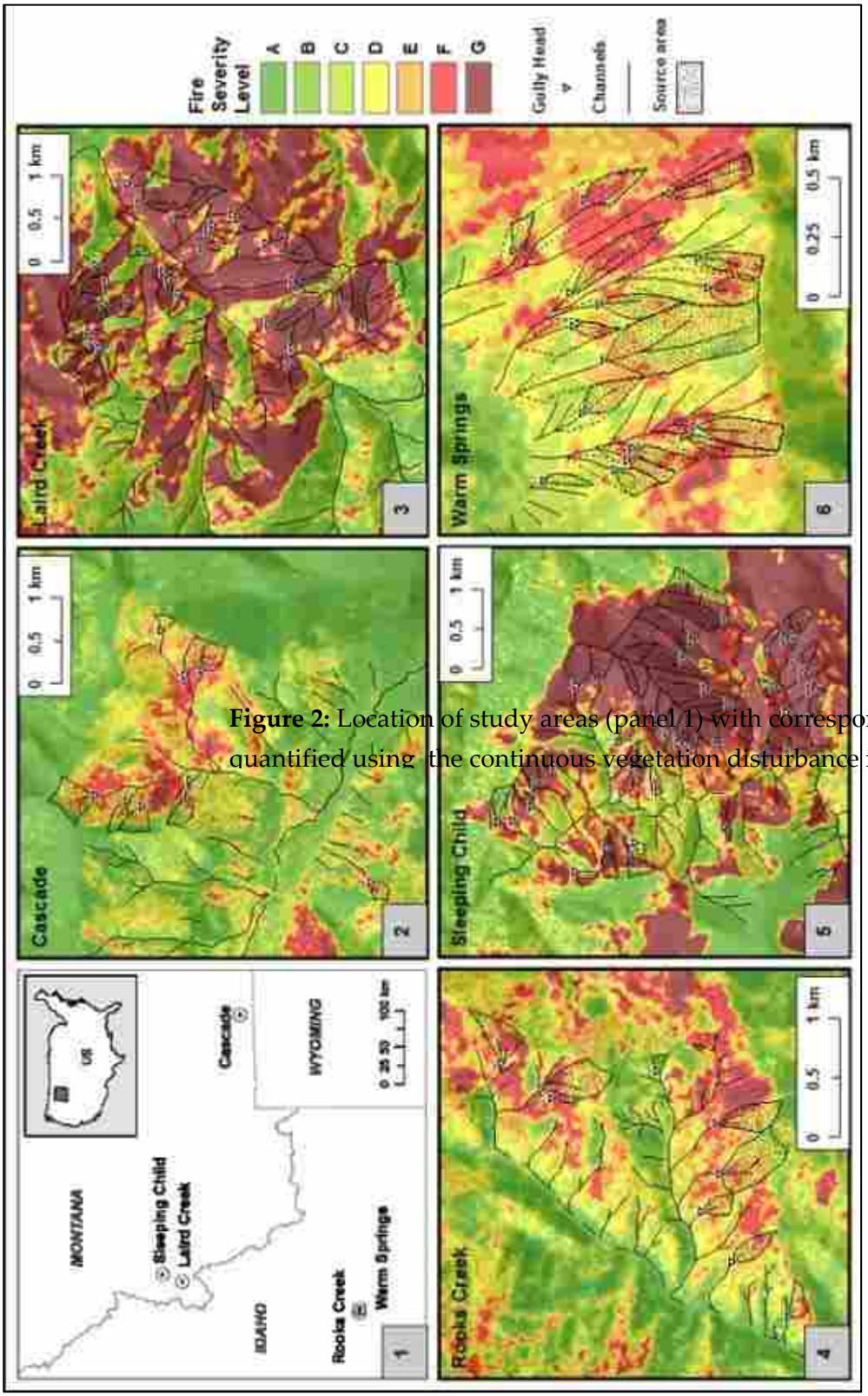

Figure 2: Location of study areas (panel 1) with corresponding gully heads and sou
quantified using the continuous vegetation disturbance index (VDI) and stratified i

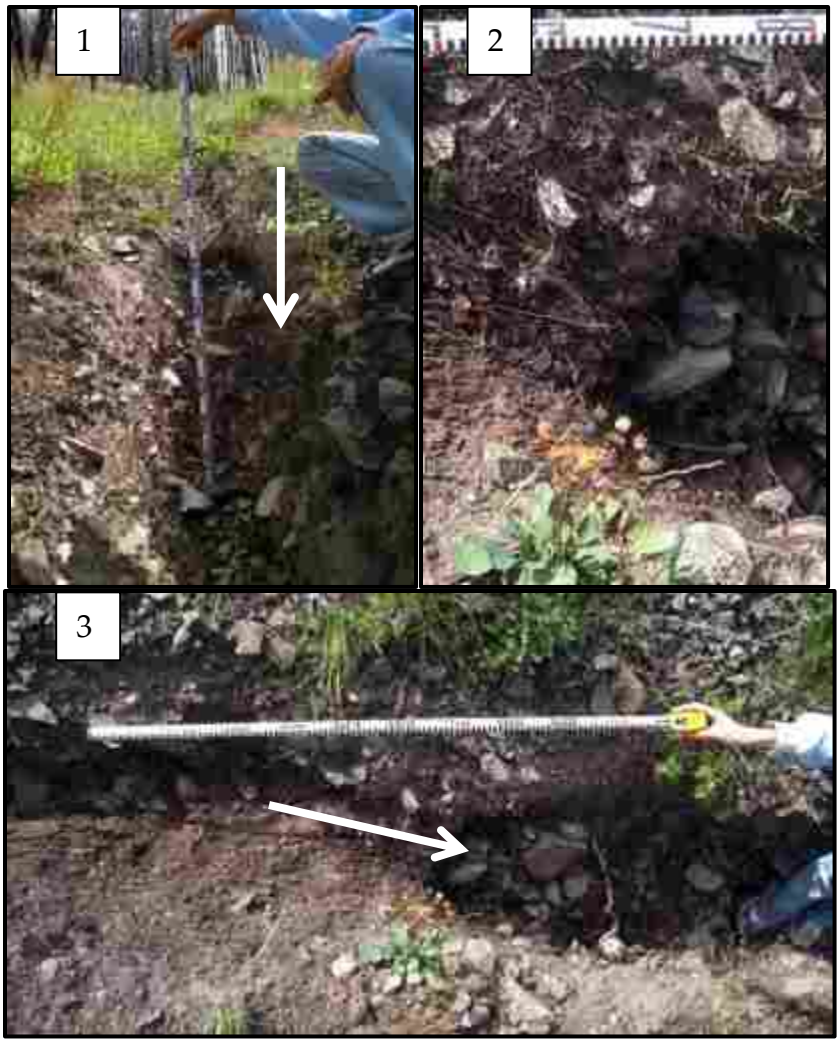

Figure 3: Typical channel head form where gully rejuvenation occurred following wildfire. Panel 1 – Upslope view of abrupt incision into colluvial fill. Panel 2 – Channel head directly from above with fine root hairs lining the rill above the channel incision and only few, coarse roots visible below. Panel 3 – Wider overhead view of the abrupt transition from the rill form into the incised channel form. Arrows indicate flow direction. The abrupt morphology provides visual evidence of a process transition and thus, an erosion response threshold.

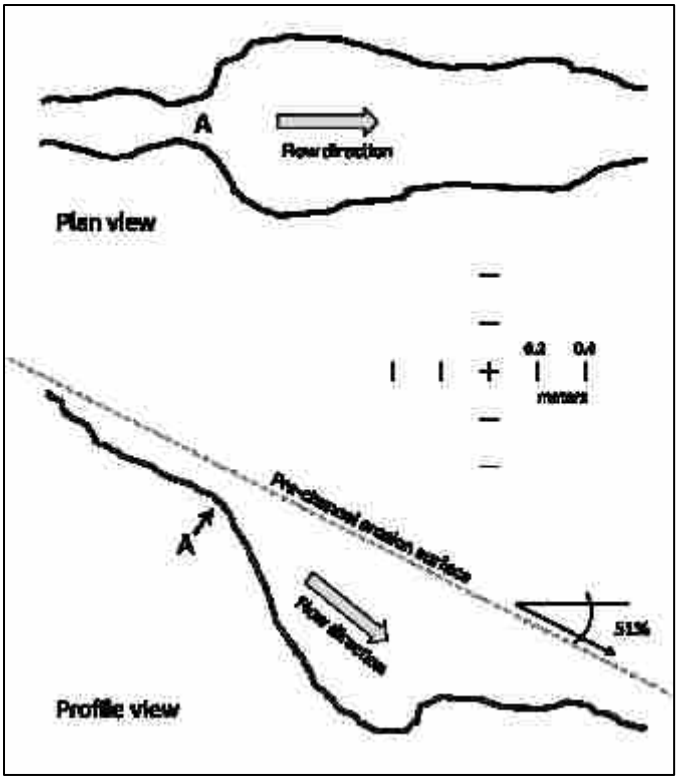

Figure 4: Scaled rendering of the channel head as photographed in Figure 3. Location "A" marks the abrupt transition of a shallow rill to a channel downcut into colluvial fill. The form is consistent with channel initiation by overland flow as described in Dietrich and Dunne (1993).

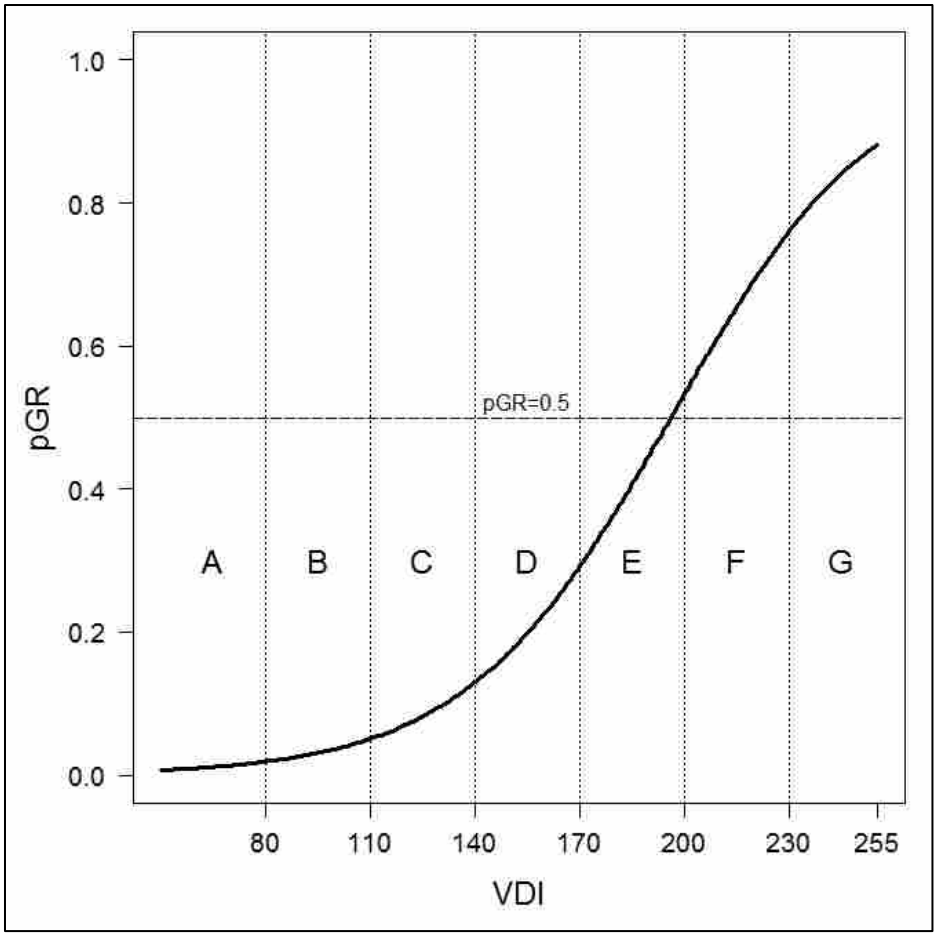

Figure 5: Probability of gully rejuvenation (No GR v GR) following wildfire as a function of fire severity measured by the vegetation disturbance index (VDI). Fire severity levels, A-G, are illustrated as defined in section 3.3.

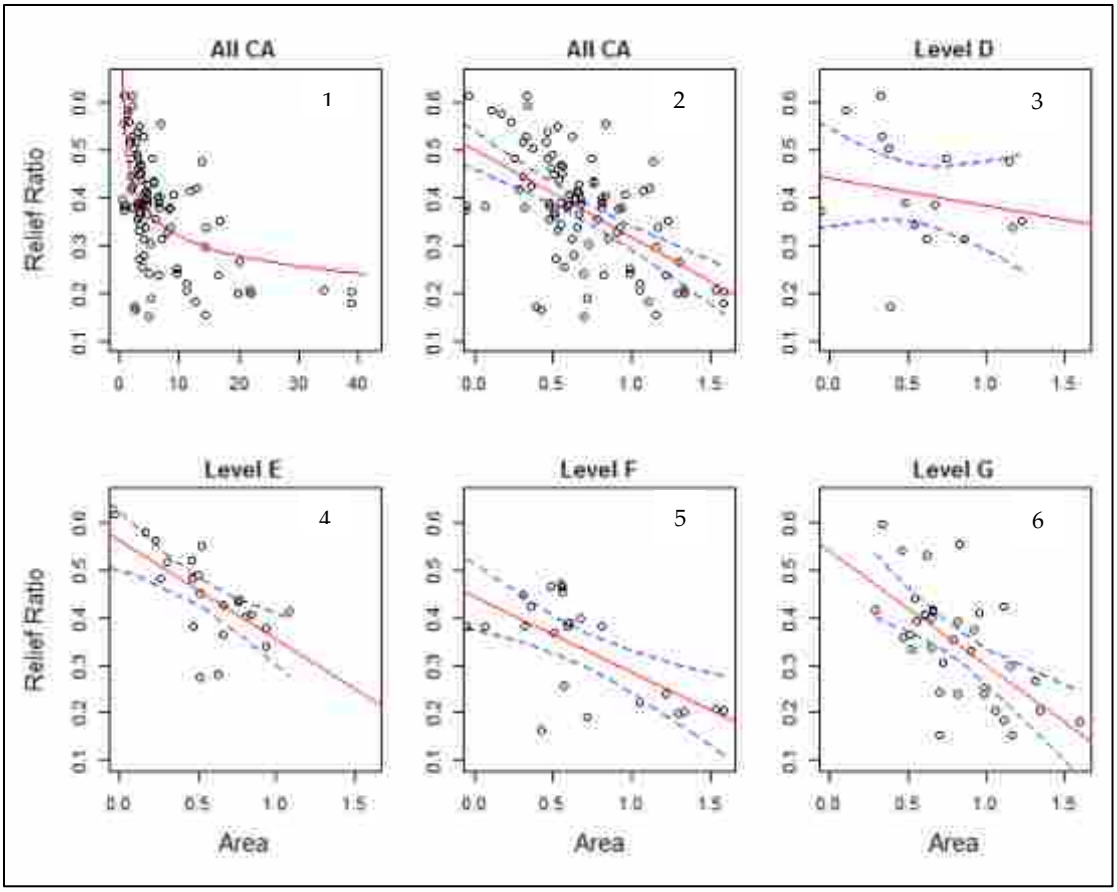

Figure 6: Plots of S:A_{SA} relationships by fire severity level using RR to measure the slope component. Panel 1 includes untransformed data from all source areas and shows the non-linear inverse relationship. Panels 2-6 plot S:A_{SA} relationships using transformed area data for all source areas and by increasing levels of fire severity (Level D-G). Solid red line is fitted regression equation and dashed blue lines delineate 95% confidence interval. Refer to Table 5 for the coefficients of the equation, $S = kA^{-\theta}$ for each plot.

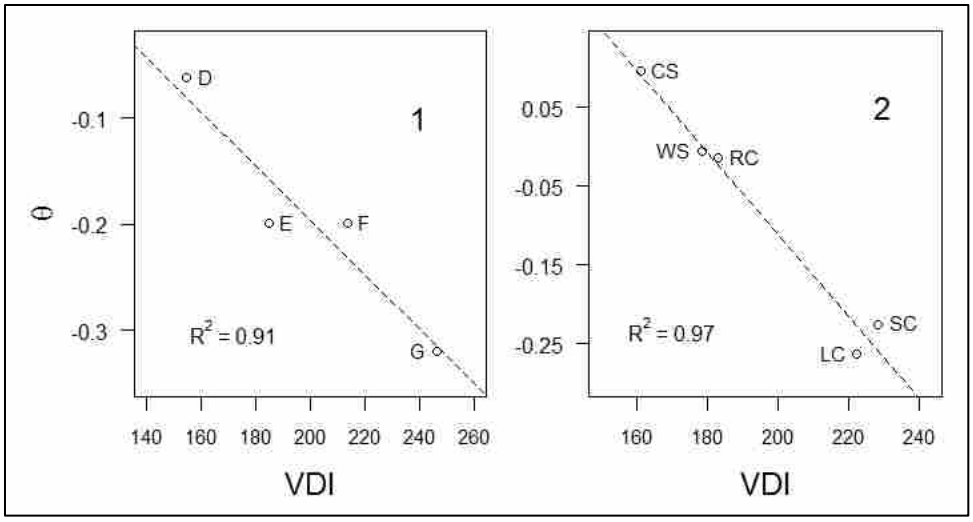

Figure 7: Plot of Theta (θ) as function of mean VDI for all source areas within the four fire severity levels (Panel 1) and by source areas group by study area (Panel 2). The plots shows a regular, linear correlation of θ = f (VDI).

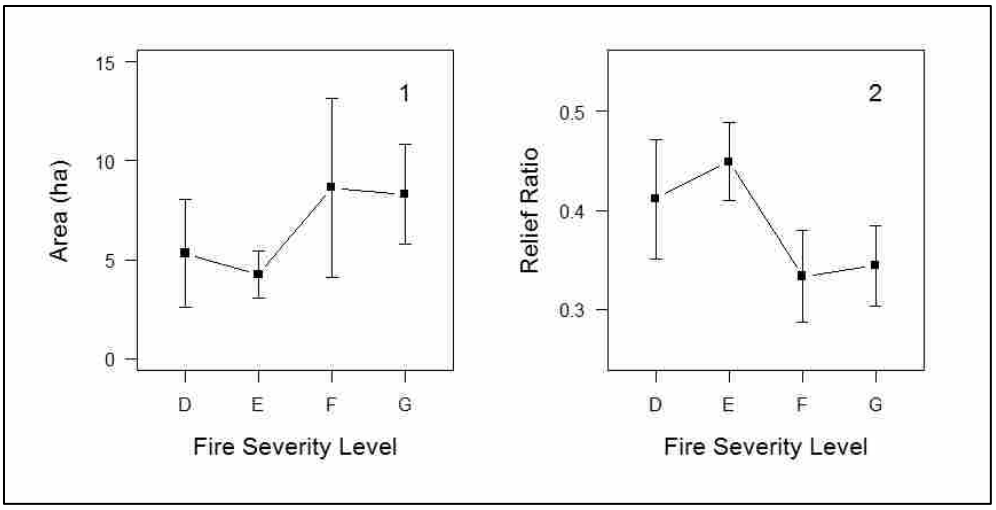

Figure 8: Changes in mean source area (panel 1) and slope (panel 2) with increasing levels of fire severity. Vertical lines represent 95% confidence intervals. Mean source area is significantly different only between levels E and G. Mean slope is significantly different between levels E – F and E – G.

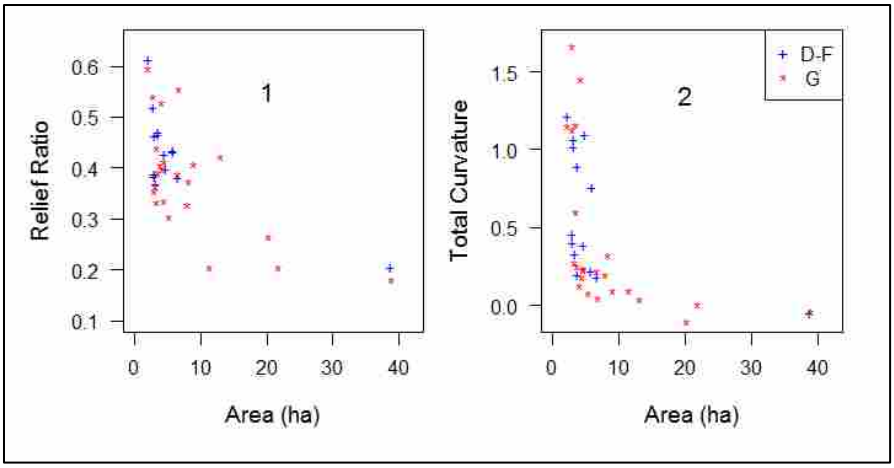

Figure 9: Source area as a function of RR and mean TC for all SC source areas, for lower fire severity levels (D-F), and for the highest fire severity level (G) using untransformed data. RR varies more than TC at the highest severity levels.

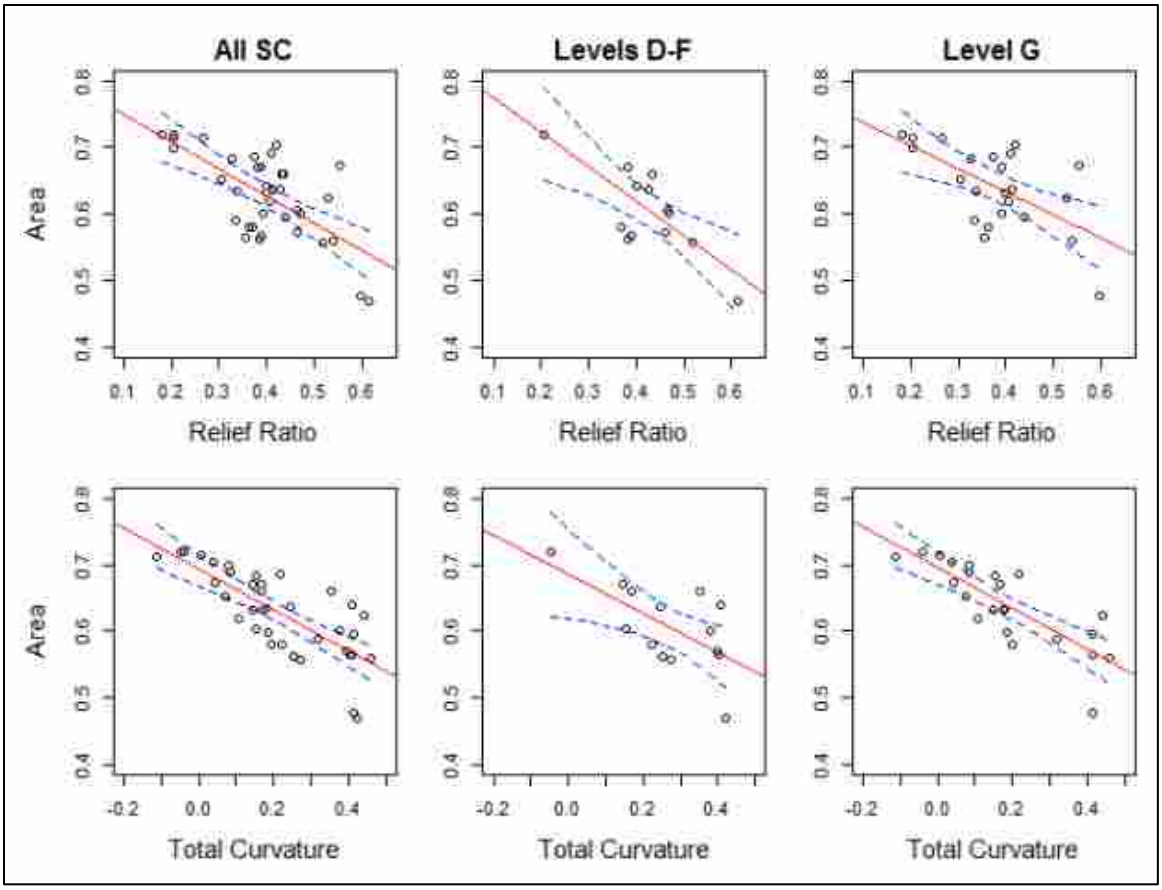

Figure 10: Source area as a function of RR and mean TC for all SC source areas, for lower fire severity levels (D-F), and for the highest fire severity level (G). Solid red line is fitted regression equation and dashed blue lines delineate 95% confidence interval. Area and curvature values are transformed using the Box-Cox power function.

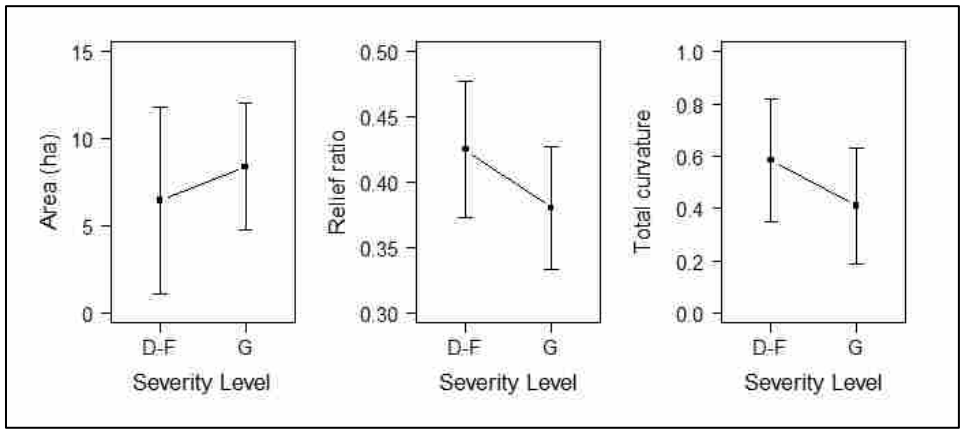

Figure 11: Means with error bars of source area (ha), relief ratio, and total curvature with increasing fire severity using SC data.

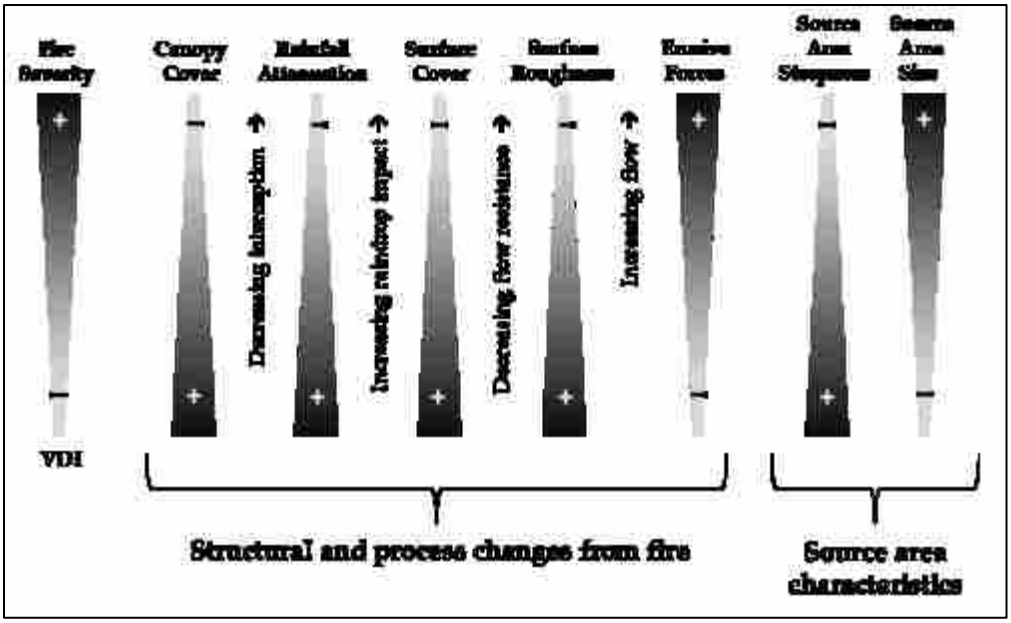

Figure 12: Causal chain of relationships between fire severity, resulting structural and process changes caused by fire, and source area characteristics. With increasing fire severity canopy and surface cover decrease with corresponding decreases in rainfall attenuation, both delivery rate and impact force, and surface roughness. Erosive forces increase and thus lower S:A_{SA} threshold for conditions that lead to channel initiation.

CHAPTER 5: CONCLUSIONS

5.1 Overview

The results of the three lines of investigation support the conclusion that vegetation disturbance by fire exerts first-order controls on post-fire runoff and erosion processes and the threshold conditions required for gully rejuvenation. This work provides observed and empirical evidence for the elemental importance of vegetation controls over erosion (Kirkby, 1995; Yetemen et al., 2010) and the emerging understanding that vegetation consumption and loss of cover by fire may significantly explain accelerated runoff and erosion following fire.

As a primary interpretation of vegetation controls, intact vegetation interrupts hydrologic connectivity through two primary mechanisms. Canopy cover intercepts rainfall, modulates effective rainfall delivery, and reduces rainfall intensity at the ground surface (Hanshaw et al., 2009; Stoof et al., 2012). Undisturbed vegetation resists the accumulation of mass and energy from rainfall inputs and overland flow and thereby reduces erosivity and force accumulation (Kutiel et al., 1995; Lavee et al., 1995; Bergkamp, 1998) and shear stress from overland flow is inversely proportional to the density of vegetative cover (Istanbulluoglu and Bras, 2005b). Therefore, vegetation loss fosters rapid accumulation of rainfall and overland flow(Collins and Bras, 2010) and the increase of erosive forces. Wildfire may create large continuous patches virtually devoid of surface vegetation and thereby create landscape structural continuity that enhances potential for hydrologic connectivity. Source area curvature results in converging force

vectors that amplify with vegetation loss. Under constant slope and increasing fire severity critical shear stress would be reached over shorter distances and across smaller source areas. In conjunction with topographic controls in catchment source areas (Dietrich and Dunne, 1993; Vandekerckhove et al., 1998; Lesschen et al., 2007) the reduced surface roughness of severely burned areas lowers thresholds of channel incision and increases the probability of GR with increasing fire severity.

5.2 Summary by Investigation

In the first investigation, vegetation disturbance by fire significantly explained the occurrence of GR with much less influence of catchment shape and pre-fire vegetation cover. Other geologic and local conditions observed during field surveys and verified in the GIS strongly influence GR and also need to be considered in post-fire assessments of severe erosion potential. The binary logistic regression analysis produced classification models with significant power to discriminate between catchments where GR did and did not occur based on vegetation disturbance alone and over the full range of study areas. This phase of the research set the foundation to suggest that major erosion will not occur until fire consumes above ground biomass and that spatial arrangement of burned patches may be important.

The second chapter also demonstrated that remote sensed measures of fire severity as implemented through the VDI provide effective means to integrate this spatially continuous measure of vegetation change with other landscape metrics. The application of VDI answers the identified need for integrating such use of satellite

imagery with other landscape metrics (Kremens and Smith, 2010; Reinhardt et al., 2010) and may prove useful in broader geospatial studies of the full spectrum of fire effects (Hyde et al., 2012), the role of vegetation in landform processes (Istanbulluoglu and Bras, 2005b; Tucker and Hancock, 2010; Yetemen et al., 2010), and in addressing fundamental questions of cross-scale interactions of biophysical controls on erosion processes (Dietrich and Perron, 2006; Istanbulluoglu, 2009; Marston, 2010; Reinhardt et al., 2010; Jencso and McGlynn, 2011; Wainwright et al., 2011) on geomorphic transport laws (Dietrich et al., 2003). I anticipate the VDI metric can be readily applied as the new generation of airborne sensors of fire severity is deployed (Dickinson et al., 2013).

Patch pattern analysis of burn mosaics in the second investigation revealed the development of large continuous patches of severely burned area with increasing fire severity. The increase of catchment area covered by patches of severe burn correlated strongly and with increasing probability of GR. Trends in changes of spatial structure were non-linear. Statistical analysis revealed a threshold of erosion response (VDI=195) defined by the spatial structure of burn mosaics. A transition zone of high patch fragmentation precedes the threshold after which patches of progressively larger severely burned areas were observed. Visual analysis of burn mosaics revealed that transitions between patch types continuously graded from one fire severity level to the next and severely burned areas at overall low fire severity existed as small fragmented islands. As fire severity increased large paths emerged, then merged with other severely

burned areas via connected bridges until severely burned areas formed a landscape matrix surrounding isolated patches of lower severity burn.

The burn mosaic analysis suggests that progressive loss of vegetation due to wildfire leads to critical thresholds of hydrologic connectivity after which runoff and erosion accelerate. The empirical evidence from the second phase of the study is consistent with theories of non-linear system response with increasing landscape disturbance and in the context of pattern-process relationships and wildfire (Carlson and Doyle, 1999; Peters et al., 2004; Moritz et al., 2005; Peters et al., 2007). The analysis specifically supports and extends prior work coupling increasing vegetation disturbance with nonlinear increases in erosion and lowering of erosion thresholds (Davenport et al., 1998; Allen, 2007). This study provides empirical evidence of the link between spatial patterns of vegetation disturbance by fire to channel initiation thresholds and supports the idea that increased fire severity and the increasing connected topology of severely burned patches leads to hydrologic connectivity of overland flow pathways when precipitation occurs.

The findings of the third investigation were consistent with the established theory that the size of source areas above channel heads is inversely proportional to slope steepness where channel incision occurred with and without association of fire (Montgomery and Dietrich, 1988; Tarboton et al., 1992; Tucker and Bras, 1998; Cannon et al., 2001; Hancock and Evans, 2006). The slope-area relationship generally held across the range of fire severity, except at lowest severity levels. However, the magnitude of the

slope-area relationship correlated with increasing fire severity. Slope steepness decreased and source areas somewhat increased with increasing fire severity. The findings suggest that the onset of channel incision as defined by the location of channel heads is strongly controlled by fire severity and that the threshold for channel initiation decreases as vegetation disturbance increases. Reduction in total curvature associated with increased fire severity was more significant than the reduction in slope steepness. This suggests that forces of convergent flow are not fully expressed until a significant proportion of vegetation has been consumed such that flow resistance is minimized.

The results of the source area study suggest that changes in the slope-area relationship associated with fire severity reflect the structural changes to, and consumption of, vegetation. The highly variable continuity and structure of burn mosaics that can occur during wildfire as documented in Chapter 3 and observed by others (Kutiel et al., 1995; Parr and Andersen, 2006; Lentile et al., 2007) may also be reflected in slope-area changes. Weak slope-area relationship at lower fire severity levels and the variability of slope-area rations overall likely reflect that multiple factors influence the slope area relationship, including climate, soils, and geology, in addition to vegetation disturbance (Yetemen et al., 2010). That total curvature, versus planform or profile curvature significantly explains source area size may indicate that channel initiation thresholds are more sensitive to the combination of converging flow (influenced by profile curvature) and increased flow velocities and depths (influenced by planform curvature) than either factor alone.

5.3 Implications and research needs

Direct vegetation controls on post-fire erosion have not been rigorously tested beyond a few foundational experiments (Kutiel et al., 1995; Lavee et al., 1995; Hanshaw et al., 2009; Larsen et al., 2009; Stoof et al., 2012). Work is needed to link measures of vegetation disturbance via satellite and other remote sensing platforms images to physical processes controlling runoff generation and flow accumulation. Empirical studies are needed to measure changes in effective rainfall relative to canopy loss over the range of fire severity and in geographically representative fire domains. Similar work is needed to measure residual biomass on the ground surface and empirical links to dynamics of overland flow. Such studies could improve process-based models of runoff and erosion relative to land cover disturbance and land-use change.

Further work is needed to evaluate interactions of burn mosaics, topographic forms, and bio-physical changes to understand broad-scale energy dynamics of flow accumulation and influences of geomorphic processes. Initially, this could be accomplished through dynamic modeling experiments draping burn mosaics over high-resolution digital terrain models (such as derived from LiDAR). Multiple factors including patch pattern sequences could be controlled to evaluate runoff accumulation and response thresholds.

REFERENCES

Abrahams, A.D., Parsons, A.J., Wainwright, J., 1994. Resistance to overland flow on semiarid grassland and shrubland hillslopes, Walnut Gulch, southern Arizona. Journal of Hydrology, 156(1–4), 431-446.

Akaike, H., 1974. A new look at the statistical model identification. Automatic Control, IEEE Transactions on, 19(6), 716-723.

Allen, C.D., 2007. Interactions across spatial scales among forest dieback, fire, and erosion in northern New Mexico landscapes. Ecosystems, 10, 797-808.

Arnau-Rosalén, E., Calvo-Cases, A., Boix-Fayos, C., Lavee, H., Sarah, P., 2008. Analysis of soil surface component patterns affecting runoff generation. An example of methods applied to Mediterranean hillslopes in Alicante (Spain). Geomorphology, 101, 595-606.

Arno, S.F., 2000. Fire in Western Forest Ecosystems. In: J.K. Brown, J.K. Smith (Eds.), Wildland Fire in Ecosystems: Effects of Fire on Flora. U.S. Department of Agriculture, Forest Service, Rocky Mountain Research Station, Ogden, UT, pp. 257.

Bautista, S., Mayor, A.G., Bourakhouadar, J., Bellot, J., 2007. Plant spatial pattern predicts hillslope runoff and erosion in a semiarid Mediterranean landscape. Ecosystems, 10(6), 987-998.

Beeson, P.C., Martens, S.N., Breshears, D.D., 2001. Simulating overland flow following wildfire: Mapping vulnerability to landscape disturbance. Hydrological Processes, 15(2917–2930).

Benavides-Solorio, J., MacDonald, L.H., 2001. Post-fire runoff and erosion from simulated rainfall on small plots, Colorado Front Range. Hydrological Processes, 15(15), 2931-2952.

Benda, L., Andras, K., Miller, D., Bigelow, P., 2004. Confluence effects in rivers: interactions of basin scale, network geometry, and disturbance regimes. Water Resources Research, 40(5), W05402.

Benda, L., Miller, D., Bigelow, P., Andras, K., 2003. Effects of post-wildfire erosion on channel environments, Boise River, Idaho. Forest Ecology and Management, 178, 105-119.

Bergkamp, G., 1998. A hierarchical view of the interactions of runoff and infiltration with vegetation and microtopography in semiarid shrublands. CATENA, 33, 201-220.

Boer, M., Puigdefábregas, J., 2005. Effects of spatially structured vegetation patterns on hillslope erosion in a semiarid Mediterranean environment: a simulation study. Earth Surface Processes and Landforms, 30, 149–167.

Boer, M.M., Sadler, R.J., Wittkuhn, R.S., McCaw, L., Grierson, P.F., 2009. Long-term impacts of prescribed burning on regional extent and incidence of wildfires--Evidence from 50 years of active fire management in SW Australian forests. Forest Ecology and Management, 259(1), 132-142.

Box, G.E., Cox, D.R., 1964. An analysis of transformations. Journal of the Royal Statistical Society. Series B (Methodological), 211-252.

Bracken, L.J., Cox, N., Shannon, J., 2008. The relationship between rainfall inputs and flood generation in south–east Spain. Hydrological Processes, 22(5), 683-696.

Bracken, L.J., Croke, J., 2007. The concept of hydrological connectivity and its contribution to understanding runoff-dominated geomorphic systems. Hydrological Processes, 21, 1749-1763.

Bracken, L.J., Wainwright, J., Ali, G.A., Tetzlaff, D., Smith, M.W., Reaney, S.M., Roy, A.G., 2013. Concepts of hydrological connectivity: Research approaches, pathways and future agendas. Earth-Science Reviews(0).

Bradley, A.P., 1997. The use of the area under the ROC curve in the evaluation of machine learning algorithms. Pattern recognition, 30(7), 1145-1159.

Bull, L., Kirkby, M., 1997. Gully processes and modelling. Progress in Physical Geography, 21(3), 354-374.

Burton, T.A., 2005. Fish and stream habitat risks from uncharacteristic wildfire: Observations from 17 years of fire-related disturbances on the Boise National Forest, Idaho. Forest Ecology and Management, 211, 140-149.

Calkin, D.E., Hyde, K.D., Robichaud, P.R., Jones, J.G., Ashmun, L.E., Dan, L., 2007. Assessing post-fire values-at-risk with a new calculation tool. RMRS-GTR-205, USDA Forest Service, Rocky Mountain Research Station, Fort Collins, CO.

Calkin, D.E., Rieck, J.D., Hyde, K.D., Kaiden, J.D., 2011. Built structure identification in wildland fire decision support. International Journal of Wildland Fire, 20, 78-90.

Cammeraat, L.H., 2004. Scale dependent thresholds in hydrological and erosion response of a semi-arid catchment in southeast Spain. Agricultural Ecosystems and Environment, 104, 317-332.

Cannon, S.H., Gartner, J.E., Parrett, C., Parise, C., 2003. Wildfire-related debris-flow generation through episodic progressive sediment-bulking processes, western-USA. In: D. Rickenmann, C. Chen (Eds.), Debris-Flow Hazards Mitigation: Mechanics, Prediction, and Assessment. Millpress, Rotterdam, pp. 71-82.

Cannon, S.H., Gartner, J.E., Rupert, M.G., Michael, J.A., Rea, A.H., Parrett, C., 2010. Predicting the probability and volume of postwildfire debris flows in the intermountain western United States. GSA Bulletin, 122, 127-144; doi: 110.1130/B26459.26451.

Cannon, S.H., Gartner, J.E., Wilson, R.C., Bowers, J.C., Laber, J.L., 2008. Storm rainfall conditions for floods and debris flows from recently burned areas in southwestern Colorado and southern California. Geomorphology, 96, 250–269.

Cannon, S.H., Kirkham, R.M., Parise, M., 2001. Wildfire-related debris-flow initiation processes, Storm King Mountain, CO. Geomorphology, 39, 171-188.

Carlson, J.M., Doyle, J., 1999. Highly optimized tolerance: A mechanism for power laws in designed systems. Physical Review E, 60(2), 1412-1427.

Cawson, J., Sheridan, G., Smith, H., Lane, P., 2012. Surface runoff and erosion after prescribed burning and the effect of different fire regimes in forests and shrublands: a review. International Journal of Wildland Fire.

Cerda, A., Robichaud, P.R., 2009. Fire Effects on Soil Infiltration. In: A. Cerda, P.R. Robichaud (Eds.), Fire Effecs on Soils and Restoration Strategies. Science Publishers, Enfield, NH, pp. 81-104.

Chafer, C.J., 2008. A comparison of fire severity measures: An Australian example and implications for predicting major areas of soil erosion. CATENA, 74, 235-245.

Chaplot, V., Saleh, A., Jaynes, D.B., 2005. Effect of the accuracy of spatial rainfall information on the modeling of water, sediment, and NO3-N loads at the watershed level. Journal of Hydrology, 312(1-4), 223-234.

Coe, J.A., Kinner, D.A., Godt, J.W., 2008. Initiation conditions for debris flows generated by runoff at Chalk Cliffs, central Colorado. Geomorphology, 96(3-4), 270-297.

Collins, B.M., Kelly, M., Wagtendonk, J.W.v., Stephens, S.L., 2007. Spatial patterns of large natural fires in Sierra Nevada wilderness areas. Landscape Ecology, 22, 545-557.

Collins, D., Bras, R., 2008. Climatic control of sediment yield in dry lands following climate and land cover change. Water Resources Research, 44(10), W10405.

Collins, D., Bras, R., 2010. Climatic and ecological controls of equilibrium drainage density, relief, and channel concavity in dry lands. Water Resources Research, 46(4), W04508.

Collins, D.B.G., Bras, R.L., Tucker, G.E., 2004. Modeling the effects of vegetation-erosion coupling on landscape evolution. Journal of Geophysical Research, 109(F03004), doi:10.1029/2003JF000028.

Conedera, M., Peter, L., Marxer, P., Forster, F., Rickenmann, D., Re, L., 2003. Consequences of forest fires on the hydrogeological response of mountain catchments: a case study of the Riale Buffaga, Ticino, Switzerland. Earth Surface Processes and Landforms, 28(2), 117-129.

Coppus, R., Imeson, A.C., 2002. Extreme events controlling erosion and sediment transport in a semi-arid sub-Andean valley. Earth Surface Processes and Landforms, 27, 1365-1375.

Cushman, S.A., McGarigal, K., Neel, M.C., 2008. Parsimony in landscape metrics: Strength, universality, and consistency. Ecological Indicators, 8, 691-703.

Darboux, F., Davy, P., Gascuel-Odoux, C., Huang, C., 2002. Evolution of soil surface roughness and flowpath connectivity in overland flow experiments. Catena, 46(2), 125-139.

Davenport, D.W., Breshears, D.D., Wilcox, B.P., Allen, C.D., 1998. Viewpoint: Sustainability of pinon-juniper ecosystems-a unifying perspective of soil erosion thresholds Journal of Range Management, 51(2), 231-240.

De Santis, A., Chuvieco, E., Vaughan, P.J., 2009. Short-term assessment of burn severity using the inversion of PROSPECT and GeoSail models. Remote Sensing of Environment, 113(1), 126-136.

DeMaris, A., 2002. Explained variance in logistic regression a Monte Carlo study of proposed measures. Sociological Methods & Research, 31(1), 27-74.

Dickinson, M.B., Hudak, A.T., Hyde, K.D., Suciu, L., 2013. Fire Research Applications: Integrating data and models to understand and predict resource effects of

wildland fires, Autonomous Modular Sensor (AMS) Airborne Science Applications Use Workshop. NASA, NASA-Ames Research Center, CA.
Dietrich, W.E., Bellugi, D.G., Sklar, L.S., Stock, J.D., Heimsath, A.M., Roering, J.J., 2003. Geomorphic Transport Laws for Predicting Landscape Form and Dynamics. In: P.R. Wilcock, R.M. Iverson (Eds.), Prediction in Geomorphology. Geophysical Monograph 135. American Geophysical Union, Washington, D.C., pp. 103-132.
Dietrich, W.E., Dunne, T., 1993. The Channel Head. In: K. Beven, M. Kirkby (Eds.), Channel Network Hydrology. John Wiley, New York, pp. 175-219.
Dietrich, W.E., Perron, J.T., 2006. The search for a topographic signature of life. Nature, 439(7075), 411-418.
Dietrich, W.E., Wilson, C.J., Montgomery, D.R., McKean, J., Bauer, R., 1992. Erosion thresholds and land surface morphology. Geology, 20, 675-679.
Dingman, S.L., 2002. Physical Hydrology. Waveland Press, Long Grove, IL.
Doerr, S.H., Shakesby, R.A., MacDonald, L.H., 2009. Soil Water Repellency: A Key Factor in Post-Fire Erosion. In: A. Cerda, P.R. Robichaud (Eds.), Fire Effects on Soils and Restoration Strategies. Land Reconstruction and Management. Science Publishers, Enfield, HN, pp. 197-223.
Dunne, T., 1978. Field studies of hillslope flow processes. In: M. Kirkby (Ed.), Hillslope hydrology. John Wiley & Sons, Chichester, pp. 227-293.
Dunne, T., Dietrich, W., 1980. Experimental study of Horton overland flow on tropical hillslopes, 1, Soil conditions, infiltration and frequency of runoff. Z. Geomorphol. Suppl, 35, 60-80.
Dunne, T., Zhang, W., Aubry, B.F., 1991. Effects of Rainfall, Vegetation, and Microtopography on Infiltration and Runoff. Water Resources Research, 27(9), 2271-2285.
Ebel, B.A., Moody, J.A., Martin, D.A., 2012. Hydrologic conditions controlling runoff generation immediately after wildfire. Water Resources Research, 48.
Epting, J., Verbyla, D., Sorbel, B., 2005. Evaluation of remotely sensed indices for assessing burn severity in interior Alaska using Landsat TM and ETM+. Remote Sensing of Environment, 96, 328-339.
Eustace, A., Pringle, M., Denham, R., 2011. A risk map for gully locations in central Queensland, Australia. European Journal of Soil Science, 62(3), 431-441.
Folke, C., 2006. Resilience: The emergence of a perspective for social-ecological systems analyses. Global Environmental Change, 16(3), 253-267.
Frechette, J.D., Meyer, G.A., 2009. Holocene fire-related alluvial-fan deposition and climate in ponderosa pine and mixed-conifer forests, Sacramento Mountains, New Mexico, USA. The Holocene, 19(4), 639-651.
Gabet, E.J., Bookter, A., 2008. A morphometric analysis of gullies scoured by post-fire progressively bulked debris flows in southwest Montana, USA. Geomorphology, 96, 298-309.
Gartner, J.E., Cannon, S.H., Santi, P.M., Dewolfe, V.G., 2008. Empirical models to predict the volumes of debris flows generated by recently burned basins in the Western U.S. Geomorphology, 96, 339-354.

Giordanengo, J.H., Frasier, G.W., Trlica, M.J., 2003. Hydrologic and sediment responses to vegetation and soil disturbances. Journal of Range Management, 56, 152-158.
Gresswell, R.E., 1999. Fire and aquatic ecosystems in forested biomes of North America. Transactions of the American Fisheries Society, 128, 193-221.
Gustafson, E.J., 1998. Quantifying Landscape Spatial Pattern: What Is the State of the Art? Ecosystems, 1, 143-156.
Gutiérrez-Jurado, H.A., Vivoni, E.R., 2013. Ecogeomorphic expressions of an aspect-controlled semiarid basin: I. Topographic analyses with high-resolution data sets. Ecohydrology, 6, 8-23.
Gutierrez, A.G., Schnabel, S., Felicisimo, A.M., 2009. Modelling the occurrence of gullies in rangelands of southwest Spain. Earth Surface Processes and Landforms, 34(14), 1894-1902.
Hancock, G., Evans, K., 2010. Gully, channel and hillslope erosion–an assessment for a traditionally managed catchment. Earth Surface Processes and Landforms.
Hancock, G.R., Evans, K.G., 2006. Gully position, characteristics and geomorphic thresholds in an undisturbed catchment in northern Australia. Hydrological Processes, 20, 2935-2951.
Hanshaw, M.N., Schmidt, K.M., Stock, J.D., 2009. The role of vegetation canopy on post-fire debris-flow rainfall intensity-duration thresholds, GSA Annual Meeting. Geological Society of America, Portland, OR, pp. p.495.
Harlow, L.L., 2005. The Essence of Multivariate Thinking: Basic themes and methods. Lawrence Erlbaum, Mahwah, NJ.
Harvey, A.M., 2007. Geomorphic instability and change Introduction: Implications of temporal and spatial scales. Geomorphology, 84, 153-158.
Hayes, J.J., Robeson, S.M., 2009. Spatial Variability of Landscape Pattern Change Following a Ponderosa Pine Wildfire in Northeastern New Mexico, USA. Physical Geography, 30(5), 410-429.
Henkle, J.E., Wohl, E., Beckman, N., 2011. Locations of channel heads in the semiarid Colorado Front Range, USA. Geomorphology, 129(3), 309-319.
Holden, Z.A., Morgan, P., Evans, J.S., 2009. A predictive model of burn severity based on 20-year satellite-inferred burn severity data in a large southwestern US wilderness area. Forest Ecology and Management, 258, 2399-2406.
Hooke, R.L., 2000. Toward a uniform theory of clastic sediment yield in fluvial systems. Geological Society of America Bulletin, 112(12), 1778-1786.
Horton, R.E., 1933. The role of infiltration in the hydrologic cycle. Transactions, American Geophysical Union, 14, 446-460.
Horton, R.E., 1945. Erosional development of streams and drainage basins; Hydrophysical approach to their quantitative morphology. Geological Society of America Bulletin, 56, 275-370.
Hosmer, D.W., Lemeshow, S., 2000. Applied Logistic Regression. John Wiley and Sons, New York.
Hudak, A.T., Morgan, P., Bobbitt, M.J., Smith, A.M.S., Lewis, S.A., Lentile, L.B., Robichaud, P.R., Clark, J.T., McKinley, R.A., 2007. The Relationship of

Multispectral Satellite Imagery to Immediate Fire Effects. Fire Ecology, 3(1), 64-90.
Hyde, K., Dickinson, M.B., Bohrer, G., Calkin, D., Evers, L., Gilbertson-Day, J., Nicolet, T., Ryan, K., Tague, C., 2012. Research and development supporting risk-based wildfire effects prediction for fuels and fire management: status and needs. International Journal of Wildland Fire, 22(1), 37-50.
Hyde, K., Woods, S.W., Donahue, J., 2007. Predicting gully rejuvenation after wildfire using remotely sensed burn severity data. Geomorphology, 86(3-4), 496-511.
Hyde, K.D., 2013. Control by Vegetation Disturbance on Gully Rejuvenation Following Wildfire. Doctor of Philosophy Dissertation, The University of Montana, Missoula, MT.
Istanbulluoglu, E., 2009. An Eco-hydro-geomorphic Perspective to Modeling the Role of Climate in Catchment Evolution. Geography Compass, 3(3), 1151-1175.
Istanbulluoglu, E., Bras, R.L., 2005a. Vegetation-modulated landscape evolution: Effects of vegetation on landscape processes, drainage density, and topography. Journal of Geophysical Research, 110(F02012), doi:10.1029/2004JF000249.
Istanbulluoglu, E., Bras, R.L., 2005b. Vegetation-modulated landscape evolution: Effects of vegetation on landscape processes, drainage density, and topography. Journal of Geophysical Research, 110, 19: F02012.
Istanbulluoglu, E., Tarboton, D.G., Pack, R.T., Luce, C.H., 2003. A sediment transport model for incision of gullies on steep topography. Water Resources Research, 39(4), 1103, doi:1110.1029/2002WR001467.
Istanbulluoglu, E., Tarboton, D.G., Pack, R.T., Luce, C.H., 2004. Modeling of the interactions between forest vegetation, disturbances, and sediment yields. Journal of Geophysical Research, 109, F01009.
James, A.L., Roulet, N.T., 2007. Investigating hydrologic connectivity and its association with threshold change in runoff response in a temperate forested watershed. Hydrological Processes, 21, 3391–3408.
Jencso, K.G., McGlynn, B.L., 2011. Hierarchical controls on runoff generation: Topographically driven hydrologic connectivity, geology, and vegetation. Water Resources Research, 47(11), W11527.
Jencso, K.G., McGlynn, B.L., Gooseff, M.N., Wondzell, S.M., Bencala, K.E., Marshall, L.A., 2009. Hydrologic connectivity between landscapes and streams: Transferring reach-and plot-scale understanding to the catchment scale. Water Resour. Res, 45.
Jenkins, S.E., Sieg, C.H., Anderson, D.E., Kaufman, D.S., Pearthree, P.A., 2011. Late Holocene geomorphic record of fire in ponderosa pine and mixed-conifer forests, Kendrick Mountain, northern Arizona, USA. International Journal of Wildland Fire, 20(1), 125-141.
Johnson, A.M., 1970. Physical Processes in Geology. Freeman, Cooper & Company, San Francisco.

Julian, J.P., Elmore, A., Guinn, S., 2012. Channel head locations in forested watersheds across the mid-Atlantic United States: A physiographic analysis. Geomorphology.

Julien, P.Y., 1998. Erosion and Sedimentation. Cambridge University Press, Cambridge.

Keeley, J.E., 2009. Fire intensity, fire severity and burn severity: a brief review and suggested usage. International Journal of Wildland Fire, 18, 116-126.

Key, C.H., Benson, N.C., 2001. The Normalized Burn Ratio (NBR): A Landsat TM Radiometric Measure of Burn Severity. http://nrmsc.usgs.gov/research/ndbr.htm.

Key, C.H., Benson, N.C., 2006. Landscape assessment: Ground measure of severity, the Composite Burn Index; and remote sensing of severity, the Normalized Burn Ratio. General Technical Report RMRS-GTR-164-CD, USDA Forest Service, Rocky Mountain Research Station, Fort Collins, CO.

Kirkby, M., 1971. Hillslope process-response models based on the continuity equation. Inst. Br. Geogr. Spec. Publ, 3, 15-30.

Kirkby, M., 1995. Modelling the links between vegetation and landforms. Geomorphology, 13(1), 319-335.

Kirkby, M., Bracken, L., Reaney, S., 2002. The influence of land use, soils and topography on the delivery of hillslope runoff to channels in SE Spain. Earth Surface Processes and Landforms, 27(13), 1459-1473.

Kremens, R.L., Smith, A., 2010. Fire metrology: current and future directions in physics-based measurements. The Journal of the Association for Fire Ecology, 6(1), 13.

Kremens, R.L., Smith, A.M.S., Dickinson, M.B., 2010. Fire Metrology: Current and Future Directions in Physics-Based Measurements. Fire Ecology, 6(1), 13-35.

Kupfer, J.A., 2012. Landscape ecology and biogeography: Rethinking landscape metrics in a post-FRAGSTATS landscape. Progress in physical geography, 36(3), 400-420.

Kutiel, P., Lavee, H., Segev, M., Benyamini, Y., 1995. The effect of fire-induced surface heterogeneity on rainfall-runoff-erosion relationships in an eastern Mediterranean ecosystem, Israel. CATENA, 25, 77-87.

Larsen, I.J., MacDonald, L.H., Brown, E., Rough, D., Welsh, M.J., 2009. Causes of Post-Fire Runoff and Erosion: Water Repellency, Cover, or Soil Sealing? Soil Sci. Soc. Am. J., 73, 1393-1407.

Larsen, I.J., Pederson, J.L., Schmidt, J.C., 2006. Geologic versus wildfire controls on hillslope processes and debris flow initiation in the Green River canyons of Dinosaur National Monument. Geomorphology, 81(1-2), 114-127.

Lavee, H., Kutiel, P., Segev, M., Benyamini, Y., 1995. Effect of surface roughness on runoff and erosion in a Mediterranean ecosystem: the role of fire. Geomorphology, 11, 227-234.

Legleiter, C., Harrison, L., Dunne, T., 2011. Effect of point bar development on the local force balance governing flow in a simple, meandering gravel bed river. Journal of Geophysical Research, 116(F1), F01005.

Lentile, L.B., Morgan, P., Hudak, A.T., Bobbitt, M.J., Lewis, S.A., Smith, A.M.S., Robichaud, P.R., 2007. Post-fire burn severity and vegetation response following eight large wildfires across the Western United States. Fire Ecology, 3(1), 91-108.

Lentile, L.B., Smith, F.W., Shepperd, W.D., 2006. Influence of topography and forest structure on patterns of mixed severity fire in ponderosa pine forests of the South Dakota Black Hills, USA. International Journal of Wildland Fire, 15(4), 557-566.
Lesschen, J.P., Cammeraat, L.H., Kooijman, A.M., Wesemael, B.v., 2008. Development of spatial heterogeneity in vegetation and soil properties after land abandonment in a semi-arid ecosystem. Journal of Arid Environments, 72, 2082-2092.
Lesschen, J.P., Kok, K., Verburg, P.H., Cammeraat, L.H., 2007. Identification of vulnerable areas for gully erosion under different scenarios of land abandonment in Southeast Spain. CATENA, 71, 110-121.
Lesschen, J.P., Schoorl, J.M., Cammeraat, L.H., 2009. Modelling runoff and erosion for a semi-arid catchment using a multi-scale approach based on hydrological connectivity. Geomorphology, 109, 174-183.
Levene, H., 1960. Robust tests for equality of variances. In: I. Olkin (Ed.), Contributions to probability and statistics: Essays in honor of Harold Hotelling. Stanford University Press, Palo Alto, CA, pp. 278-292.
Lexartza-Artza, I., Wainwright, J., 2009. Hydrological connectivity: Linking concepts with practical implications. CATENA, 79(2), 146-152.
Lilliefors, H.W., 1967. On the Kolmogorov-Smirnov test for normality with mean and variance unknown. Journal of the American Statistical Association, 62(318), 399-402.
Lozano, F.J., SuÃ¡rez-Seoane, S., De Luis, E., 2010. Effects of wildfires on environmental variability: a comparative analysis using different spectral indices, patch metrics and thematic resolutions. Landscape Ecology, 25(5), 697-710.
Luca , F., Conforti, M., Robustelli, G., 2011. Comparison of GIS-based gullying susceptibility mapping using bivariate and multivariate statistics: Northern Calabria, South Italy. Geomorphology, 134(3-4), 297-308.
Ludwig, J.A., Wilcox, B.P., Breshears, D.D., Tongway, D.J., Imeson, A.C., 2005. Vegetation patches and runoff-erosion as interacting ecohydrological processes in semiarid landscapes. Ecology, 86(2), 288-297.
Mahalanobis, P.C., 1936. On the generalized distance in statistics, Proceedings of the National Institute of Sciences of India. New Delhi, pp. 49-55.
Marques, M.A., Mora, E., 1992. The influence of aspect on runoff and soil loss in a Mediterranean burnt forest. Catena, 19, 333-344.
Marston, R.A., 2010. Geomorphology and vegetation on hillslopes: Interactions, dependencies, and feedback loops. Geomorphology, 116, 206-217.
Matthews, B.W., 1975. Comparison of the predicted and observed secondary structure of T4 phage lysozyme. Biochimica et Biophysica Acta (BBA)-Protein Structure, 405(2), 442-451.
McDaniel, J., 2007. WFDSS: Taking Decision Support into the 21st Century, Wildfire Lessons Learned Center. National Advanced Fire and Resource Institute, Tucson.
McGarigal, K., Cushman, S.A., Ene, E., 2012. FRAGSTATS v4: Spatial Pattern Analysis Program for Categorical Maps. University of Massachusetts, Amherst, MA, pp. Computer software program.

McKelvey, R.D., Zavoina, W., 1975. A statistical model for the analysis of ordinal level dependent variables. Journal of mathematical sociology, 4(1), 103-120.
Meyer, G.A., Pierce, J.L., Wood, S.H., Jull, A.J.T., 2001. Fire, storms, and erosional events in the Idaho batholith. Hydrological Processes, 15, 3025-3038.
Meyer, G.A., Wells, S.G., 1997. Fire-related sedimentation events on alluvial fans, Yellowstone National Park, U.S.A. Journal of Sedimentary Research, 67(5), 776-791.
Miller, J.D., Thode, A.E., 2007. Quantifying burn severity in a heterogeneous landscape with a relative version of the delta Normalized Burn Ratio (dNBR). Remote Sensing of Environment, 109, 66-80.
Mittlböck, M., Schemper, M., 1996. Explained variation for logistic regression. Statistics in medicine, 15(19), 1987-1997.
Montgomery, D.R., 2001. Slope distributions, threshold hillslopes, and steady-state topography. American Journal of Science, 301(4-5), 432-454.
Montgomery, D.R., Dietrich, W.E., 1988. Where do channels begin? Nature, 336, 232-234.
Montgomery, D.R., Dietrich, W.E., 1994. Landscape Dissection and Drainage Area-Slope Thresholds. In: M.J. Kirkby (Ed.), Process Models and Theoretical Geomorphology. John Wiley & Sons, Chichester, pp. 221-246.
Montgomery, D.R., Dietrich, W.E., Torres, R., Anderson, S.P., Heffner, J.T., Loague, K., 1997. Hydrologic response of a steep, unchanneled valley to natural and applied rainfall. Water Resources Research, 33(1), 91-109.
Moody, J.A., Kinner, D.A., 2006. Spatial structures of stream and hillslope drainage networks following gully erosion after wildfire. Earth Surface Processes and Landforms, 31(3), 319-337.
Moody, J.A., Kinner, D.A., Úbeda, X., 2009. Linking hydraulic properties of fire-affected soils to infiltration and water repellency. Journal of Hydrology, 379, 291-303.
Moody, J.A., Martin, D., 2009a. Synthesis of sediment yields after wildland fire in different rainfall regimes in the western United States. International Journal of Wildland Fire, 18, 96-115.
Moody, J.A., Martin, D.A., 2002. Geomorphic Consequences of Wildfire, Abstracts with Proceedings - Annual Meeting of the Geological Society of America. Geological Society of America, Denver, CO.
Moody, J.A., Martin, D.A., 2009b. Forest Fire Effects on Geomorphic Processes. In: A. Cerda, P.R. Robichaud (Eds.), Fire Effecs on Soils and Restoration Strategies. Science Publishers, Enfield, NH, pp. 41-80.
Moody, J.A., Martin, D.A., Haire, S.L., Kinner, D.A., 2007. Linking runoff response to burn severity after a wildfire. Hydrological Processes, 22, 2063–2074.
Moritz, M.A., Morais, M.E., Summerell, L.A., Carlson, J.M., Doyle, J., 2005. Wildfires, complexity, and highly optimized tolerance. Proceedings of the National Academy of Sciences, 102(50), 17912-17917.
MTBS, 2012. Monitoring Trends in Burn Severity.

Murray, A.B., Knaapen, M.A.F., Tal, M., Kirwan, M.L., 2008. Biomorphodynamics: Physical-biological feedbacks that shape landscapes. Water Resour. Res., 44(11), W11301.

NOAA, 2012. Weather and Climate Toolkit. National Oceanic and Atmospheric Administration.

Odion, D.C., Frost, E.J., Strittholt, J.R., Jiang, H., Dellasala, D.A., Moritz, M.A., 2004. Patterns of Fire Severity and Forest Conditions in the Western Klamath Mountains, California. Conservation Biology, 18(4), 927-936.

Parise, M., Cannon, S., 2011. Wildfire impacts on the processes that generate debris flows in burned watersheds. Natural Hazards, 1-11.

Parr, C.L., Andersen, A.N., 2006. Patch Mosaic Burning for Biodiversity Conservation: a Critique of the Pyrodiversity Paradigm. Conservation Biology, 20(6), 1610-1619.

Parsons, A., Robichaud, P.R., Lewis, S.A., Napper, C., Clark, J.T., 2010. Field guide for mapping post-fire soil burn severity. RMRS-GTR-243, USDA Forest Service, Rocky Mountain Research Station, Fort Collins, CO.

Peters, D.P.C., Bestelmeyer, B.T., Turner, M.G., 2007. Cross–scale interactions and changing pattern–process relationships: consequences for system dynamics. Ecosystems, 10, 790-796.

Peters, D.P.C., Pielke, R.A., Sr., Bestelmeyer, B.T., Allen, C.D., Munson-McGee, S., Havstad, K.M., 2004. Cross-scale interactions, nonlinearities, and forecasting catastrophic events. Proceedings of the National Academy of Sciences, 101(42), 15130–15135.

Phillips, J.D., 2003. Sources of nonlinearity and complexity in geomorphic systems. Progress in Physical Geography, 27(1), 1-23.

Pierce, J.L., Meyer, G.A., Jull, A.J.T., 2004. Fire-induced erosion and millennial scale climate change in northern ponderosa pine forests. Nature, 432, 87-90.

Poesen, J., Nachtergaele, J., Verstraeten, G., Valentin, C., 2003. Gully erosion and environmental change: importance and research needs. CATENA, 50, 91-133.

Pringle, C., 2003. What is hydrologic connectivity and why is it ecologically important? Hydrological Processes, 17, 2685–2689.

Prosser, I.P., Abernethy, B., 1996. Predicting the topographic limits to a gully network using a digital terrain model and process thresholds. Water Resources Research, 32(7), 2289-2298.

Prosser, I.P., Dietrich, W.E., Stevenson, J., 1995. Flow resistance and sediment transport by concentrated overland flow in a grassland valley. Geomorphology, 13, 71-86.

Prosser, I.P., Williams, L., 1998. The effect of wildfire on runff and erosion in native Eucalyptus forest. Hydrological Processes, 12, 251-265.

Puigdefábregas, J., 2005. The role of vegetation patterns in structuring runoff and sediment fluxes in drylands. Earth Surface Processes and Landforms, 30, 133-147.

R Core Team, 2013. R: A language and environment for statistical computing. R Foundation for Statistical Computing, Vienna, Austria.

Reed Jr, J.C., Bush, C.A., 2005. Generalized Geologic Map of the Conterminous United States, The National Atlas. U.S. Geological Survey, Denver, CO.

Reinhardt, L., Jerolmack, D., Cardinale, B.J., Vanacker, V., Wright, J., 2010. Dynamic interactions of life and its landscape: feedbacks at the interface of geomorphology and ecology. Earth Surface Processes and Landforms, 35, 78-101.
Riveros-Iregui, D.A., McGlynn, B.L., 2009. Landscape structure control on soil CO2 efflux variability in complex terrain: Scaling from point observations to watershed scale fluxes. Journal of Geophysical Research, 114(G2), G02010.
Roering, J.J., Gerber, M., 2005. Fire and the evolution of steep, soil-mantled landscapes. Geology, 33(5), 349-352.
Rossiter, D., Loza, A., 2011. Technical Note: Analyzing land cover change with logistic regression in R, University of Twente, Enschede, NL.
RSAC, 2009. Burned Area Reflectance Classification. USDA Forest Service, Salt Lake City, UT. Available at: http://activefiremaps.fs.fed.us/baer/download.php. Accessed: 1 February 2013.
Santi, P.M., deWolfe, V.G., Higgins, J.D., Cannon, S.H., Gartner, J.E., 2008. Sources of debris flow material in burned areas. Geomorphology, 96, 310-321.
Schmidt, J., Evans, I.S., Brinkmann, J., 2003. Comparison of polynomial models for land surface curvature calculation. International Journal of Geographical Information Science, 17(8), 797-814.
Shakesby, R., 2011. Post-wildfire soil erosion in the Mediterranean: Review and future research directions. Earth-Science Reviews, 105(3), 71-100.
Shakesby, R.A., Doerr, S.H., 2006. Wildfire as a hydrological and geomorphological agent. Earth-Science Reviews, 74(3-4), 269-307.
Sidle, R.C., Pearce, A.J., O'Loughlin, C.L., 1985. Hill slope stability and land use, 11. American geophysical union.
Smith, A.M.S., Lentile, L.B., Hudak, A.T., Morgan, P., 2007. Evaluation of linear spectral unmixing and dNBR for predicting post-fire recovery in a North American ponderosa pine forest International Journal of Remote Sensing, 28, 5159 - 5166.
Smith, J.A., Seo, D.J., Baeck, M.L., Hudlow, M.D., 1996. An intercomparison study of NEXRAD precipitation estimates. Water Resources Research, 32(7), 2035-2045.
Smucker, K.M., Hutto, R.L., Steele, B.M., 2005. Changes in bird abundance after wildfire: importance of fire severity and time since fire. Ecological Applications, 15(5), 1535-1549.
Stock, J.D., Dietrich, W.E., 2006. Erosion of steepland valleys by debris flows. GSA Bulletin, 118(9/10), 1125-1148.
Stoof, C., Vervoort, R., Iwema, J., Van Den Elsen, E., Ferreira, A., Ritsema, C., 2012. Hydrological response of a small catchment burned by experimental fire. Hydrology and Earth System Sciences, 16(2), 267.
Strahler, A.N., 1957. Quantitative analysis of watershed geomorphology. Trans. Am. Geophys. Union, 38, 913-920.
Swanson, F.J., 1978. Fire and Geomorphic Processes. In: H.A. Mooney, T.M. Bonnicksen, N.L. Christensen, J.E. Lotan, W.A. Reiners (Eds.), Fire Regimes and Ecosystem Properties. US Department of Agriculture, Honolulu, Hawaii, pp. 401-420.

Tarboton, D.G., Bras, R.L., Rodriguez-Iturbe, I., 1992. A physical basis for drainage density. Geomorphology, 5(1-2), 59-76.
Tarolli, P., Dalla Fontana, G., 2009. Hillslope-to-valley transition morphology: New opportunities from high resolution DTMs. Geomorphology, 113(1), 47-56.
Tarolli, P., Tarboton, D., 2006. A new method for determination of most likely landslide initiation points and the evaluation of digital terrain model scale in terrain stability mapping. Hydrology and Earth System Sciences Discussions, 10(5), 663-677.
Tiranti, D., Bonetto, S., Mandrone, G., 2008. Quantitative basin characterisation to refine debris-flow triggering criteria and processes: an example from the Italian Western Alps. Landslides, 5(1), 45-57.
Toms, J.D., Lesperance, M.L., 2003. Piecewise regression: a tool for identifying ecological thresholds. Ecology, 84(8), 2034-2041.
Tsukamoto, Y., Ohta, T., Noguchi, H., 1982. Hydrological and geomorphological studies of debris slides on forested hillslopes in Japan. IAHS Publ, 137, 89-98.
Tucker, G.E., Bras, R.L., 1998. Hillslope processes, drainage density, and landscape morphology. Water Resources Research, 34(10), 2751-2764.
Tucker, G.E., Hancock, G.R., 2010. Modelling landscape evolution. Earth Surface Processes and Landforms, 35, 28-50.
Turnbull, L., Wainwright, J., Brazier, R., 2008. A conceptual framework for understanding semi-arid land degradation: Ecohydrological interactions across multiple-space and time scales. Ecohydrology, 1(1), 23-34.
Turner, M.G., 1989. Landscape Ecology: The Effect of Pattern on Process. Annual Review of Ecological Systems, 20, 171-197.
Turner, M.G., 2005. Landscape ecology: what is the state of the science? Annual Review of Ecology, Evolution, and Systematics, 319-344.
Turner, M.G., Hargrove, W.W., Gardner, R.H., Romme, W.H., 1994. Effects of fire on landscape heterogeneity in Yellowstone National Park, Wyoming Journal of Vegetation Science, 5, 731-742
USDA, 2012. Geospatial Data Gateway.
USDA NRCS Soil Survey Staff, Web Soil Survey.
USDOI Geological Survey, 2009. The National Map LANDFIRE, Available at: http://www.landfire.gov/. Accessed 15 Nov 2011.
Vandaele, K., Poesen, J., Govers, G., Wesemael, B.v., 1996. Geomorphic threshold conditions for ephemeral gully incision. Geomorphology, 16, 161-173.
Vandekerckhove, L., Poesen, J., Oostwoud-Wijdenes, D., Figueiredo, T.d., 1998. Topographical thresholds for ephemeral gully initiation in intensively cultivated areas of the Mediterranean. CATENA, 33, 271–292.
Vivoni, E.R., 2012. Spatial patterns, processes and predictions in ecohydrology: integrating technologies to meet the challenge. Ecohydrology, 5(3), 235-241.
Wainwright, J., Mathys, N., Esteves, M., 2006. Gully erosion in mountain areas: processes, measurement, modelling and regionalization. Earth Surface Processes and Landforms, 31, 133-134.

Wainwright, J., Turnbull, L., Ibrahim, T.G., Lexartza-Artza, I., Thornton, S.F., Brazier, R.E., 2011. Linking environmental regimes, space and time: Interpretations of structural and functional connectivity. Geomorphology, 126, 387-404.

Watershed Sciences, 2010. LiDAR Remote Sensing Data Collection: USFS: Bitterroot National Forest, Montana, Watershed Sciences, Corvallis OR.

Westerling, A.L., Hidalgo, H.G., Cayan, D.R., Swetnam, T.W., 2006. Warming and Earlier Spring Increase Western U.S. Forest Wildfire Activity. Science, 313, 940-943.

Wieczorek, G.F., McWreath, H.C., Davenport, C., 2001. Remote rainfall sensing for landslide hazard analysis. US Geological Survey Open-File Report, 01-339.

Wigmosta, M.S., Vail, L.W., Lettenmaier, D.P., 1994. A distributed hydrology-vegetation model for complex terrain. Water Resources Research, 30(6), 1665-1679.

Wilcox, B.P., Breshears, D.D., Allen, C.D., 2003. Ecohydrology of a Resource-Conserving Semiarid Woodland: Effects of Scale and Disturbance. Ecological Monographs, 73(2), 233-239.

Wilks, S.S., 1932. Certain generalizations in the analysis of variance. Biometrika, 471-494.

Willgoose, G., Bras, R.L., Rodriguez-Iturbe, I., 1991. A Coupled Channel Network Growth and Hillslope Evolution Model 1. Theory. Water Resources Research, 27(7), 1671-1684.

Wisner, B., Blaikie, P., Cannon, T., Davis, I., 2004. At risk: natural hazards, people's vulnerability and disasters. Routledge, New York.

Wohl, E., 2013. Migration of channel heads following wildfire in the Colorado Front Range, USA. Earth Surface Processes and Landforms, n/a-n/a.

Wondzell, S.M., King, J., G., 2003. Postfire erosional processes in the Pacific Northwest and Rocky Mountain regions. Forest Ecology and Management, 178, 75–87.

Woods, S.W., Balfour, V.N., 2008. The effect of ash on runoff and erosion after a severe forest wildfire, Montana, USA. International Journal of Wildland Fire, 17, 535–548.

Woods, S.W., Balfour, V.N., 2010. The effects of soil texture and ash thickness on the post-fire hydrological response from ash-covered soils. Journal of Hydrology, 393, 274-286.

Woods, S.W., Birkas, A., Ahl, R., 2007. Spatial variability of soil hydrophobicity after wildfires in Montana and Colorado. Geomorphology, 86(3-4), 465-479.

Worsley, K., 1983. Testing for a two-phase multiple regression. Technometrics, 25(1), 35-42.

WRCC, 2013. PRISM Precipitation Maps: 1961-90. Western Regional Climate Center Reno, NV.

Yetemen, O., Istanbulluoglu, E., Vivoni, E.R., 2010. The implications of geology, soils, and vegetation on landscape morphology: Inferences from semi-arid basins with complex vegetation patterns in Central New Mexico, USA. Geomorphology, 116, 246-263.

Zelt, R.B., Wohl, E.E., 2004. Channel and woody debris characteristics in adjacent burned and unburned watersheds a decade after wildfire, Park County, Wyoming. Geomorphology, 57, 217–233.
Zevenbergen, L.W., Thorne, C.R., 1987. Quantitative analysis of land surface topography. Earth Surface Processes and Landforms, 12, 47-56.

APPENDICES

A.1 Dominant species by study area, including proportions greater than 5% values

Dominant Species	Cascade	Laird Creek	Rooks Creek	Sleeping Child	Warm Springs
Aspen *(Populus tremuloides)*	-	-	12%	-	18%
Interior Douglas-Fir *(Pseudotsuga menziesii)*	13%	63%	69%	68%	76%
Whitebark Pine *(Pinus albicaulis)*	45%	-	-	-	-
Lodgepole Pine *(Pinus contorta)*	31%	-	-	15%	-
Interior Ponderosa Pine *(Pinus ponderosa)*	-	8%	-	-	-
Engelmann Spruce-Subalpine Fir *(Picea engelmannii/Abies lasiocarpa)*	5%	17%	-	14%	-
Mountain Big Sagebrush *(Artemisia tridentata)*	-	-	10%	-	-

(USDOI Geological Survey, 2009)

A.2 Analysis of covariance of study metrics used in Chapter 2

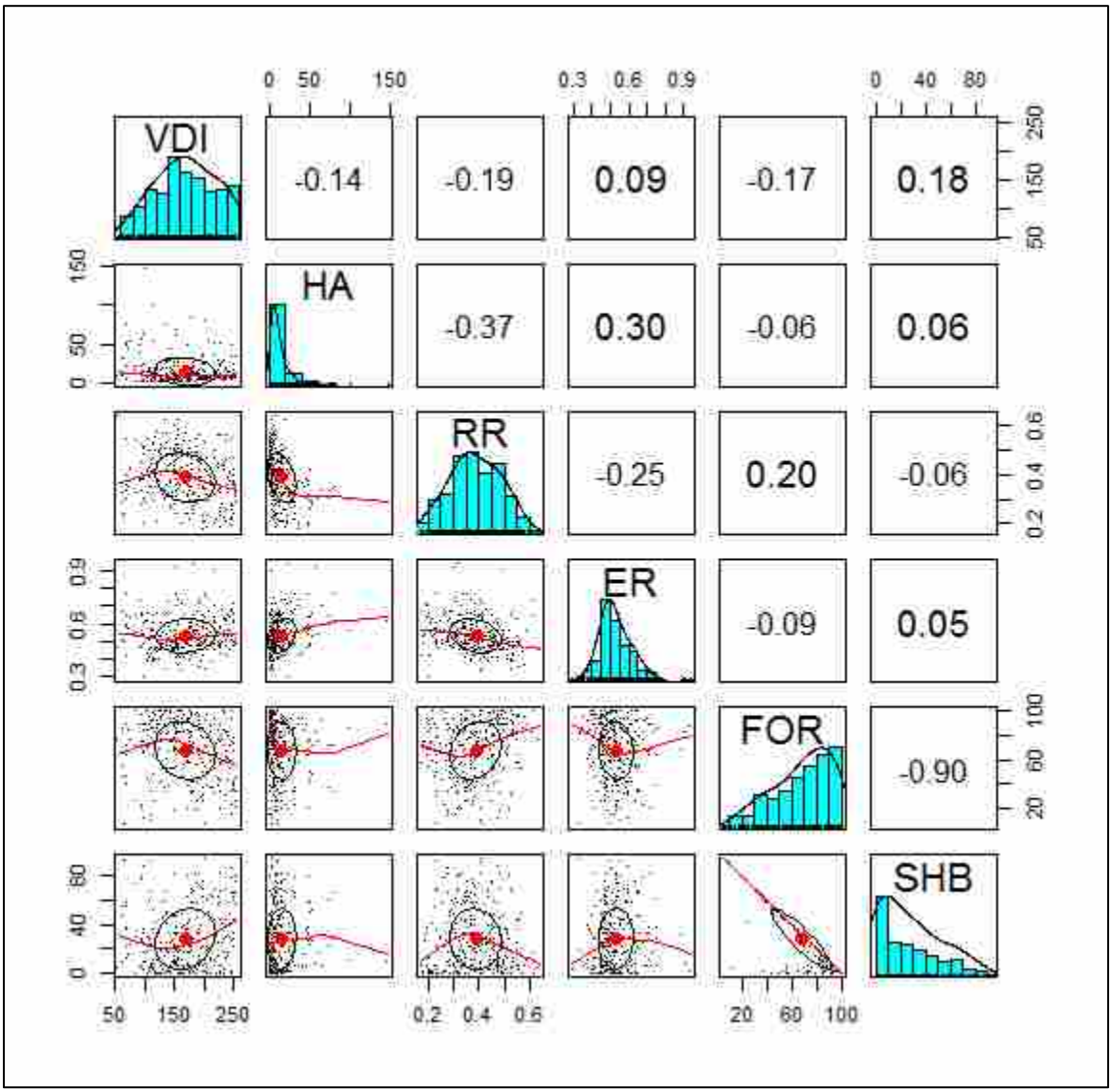

A.3 Detailed summary of variables used in Chapter 2 for all catchments and by study area

Study Area	Metric	Area ha	Relief Ratio	Elongation Ratio	Forest %	Shrub %	Herb %	Other %	VDI
All Study Areas n=269	Min	0.3	0.17	0.29	6.0	0.0	0.0	0.0	**55**
	Mean	14.7	0.39	0.53	68.0	28.3	3.2	0.4	**169**
	Median	8.1	0.38	0.52	72.0	23.0	0.0	0.0	**170**
	Max	147.3	0.64	0.94	100.0	94.0	61.0	20.0	**255**
	Range	146.9	0.46	0.65	94.0	94.0	61.0	20.0	**200**
	s.d	18.0	0.10	0.10	23.8	24.9	10.1	1.9	**51123**
	COV	1.22	0.26	0.18	0.35	0.88	3.13	4.80	**0.30**
Cascade n=35	Min	3.9	0.24	0.33	19.0	0.0	0.0	0.0	**55**
	Mean	25.1	0.42	0.50	77.5	19.2	0.8	2.5	**131**
	Median	13.3	0.41	0.47	83.0	12.0	0.0	0.0	**127**
	Max	147.3	0.64	0.91	100.0	81.0	9.0	20.0	**196**
	Range	143.4	0.40	0.58	81.0	81.0	9.0	20.0	**141**
	s.d	30.2	0.09	0.12	18.3	19.8	2.0	4.5	**33**
	COV	1.20	0.22	0.24	0.24	1.03	2.58	1.81	**0.25**
Laird Creek n=76	Min	2.0	0.17	0.29	14.0	0.0	0.0	0.0	**64**
	Mean	22.0	0.30	0.56	64.2	24.3	11.0	0.1	**172**
	Median	15.3	0.32	0.55	68.5	11.5	2.0	0.0	**187**
	Max	82.1	0.45	0.94	100.0	86.0	61.0	1.0	**250**
	Range	80.1	0.27	0.65	86.0	86.0	61.0	1.0	**185**
	s.d	20.1	0.07	0.10	24.5	26.9	16.7	0.2	**59**
	COV	0.91	0.22	0.17	0.38	1.11	1.52	4.27	**0.34**
Rooks Creek n=44	Min	1.0	0.20	0.39	12.0	0.0	0.0	0.0	**95**
	Mean	7.2	0.38	0.53	66.5	33.4	0.0	0.0	**157**
	Median	5.0	0.37	0.52	69.0	31.0	0.0	0.0	**162**
	Max	30.0	0.55	0.90	100.0	88.0	1.0	1.0	**220**
	Range	29.0	0.35	0.51	88.0	88.0	1.0	1.0	**124**
	s.d	6.7	0.08	0.09	20.9	20.9	0.2	0.2	**36**
	COV	0.94	0.20	0.17	0.31	0.62	4.64	6.63	**0.23**
Sleeping Child n=77	Min	3.5	0.20	0.34	6.0	0.0	0.0	0.0	**63**
	Mean	12.6	0.41	0.55	58.6	41.3	0.1	0.0	**195**
	Median	9.6	0.42	0.53	60.0	40.0	0.0	0.0	**203**
	Max	49.1	0.62	0.73	100.0	94.0	3.0	1.0	**255**
	Range	45.6	0.42	0.39	94.0	94.0	3.0	1.0	**192**
	s.d	9.8	0.10	0.08	24.2	24.2	0.4	0.2	**51**
	COV	0.78	0.25	0.15	0.41	0.59	4.78	6.16	**0.26**
Warm Springs n=37	Min	0.3	0.40	0.34	46.0	0.0	0.0	0.0	**87**
	Mean	3.1	0.49	0.48	87.7	12.1	0.0	0.2	**157**
	Median	2.6	0.50	0.47	93.0	7.0	0.0	0.0	**157**
	Max	20.0	0.58	0.66	100.0	48.0	0.0	5.0	**218**
	Range	19.7	0.18	0.32	54.0	48.0	0.0	5.0	**130**
	s.d	3.3	0.04	0.07	14.3	13.7	0.0	1.0	**28**
	COV	1.07	0.09	0.15	0.16	1.14		3.92	**0.18**

A.4 Plots of cumulative distribution of catchment VDI values all catchments and by study area